Yerevan Physics Institute

Hayk Poghosyan

Computational and analytical studies of classical and quantum spin lattice systems

PhD Thesis

01.04.02 - Theoretical Physics

Adviser: Prof. Nerses Ananikian

Yerevan-2018

Contents

0.1 Introduction

The theory of dynamical systems, besides its intrinsic theoretical relevance, recently had a significant impact on a wide range of disciplines from physics to ecology and economics, providing methodological tools which are currently employed in financial and economic forecasting, environmental modeling, medical diagnosis, industrial equipment diagnosis and so on. An important physical setting in which such dynamical techniques are profitably applied is equilibrium statistical mechanics of lattice models, more specifically in the investigation of physical properties of low-dimensional classic and quantum spin systems in an external magnetic field. The Ising model was invented by the physicist Wilhelm Lenz(1920) [1], and solved by his student Ernst Ising. The one-dimensional model which was solved by Ising has no phase transition. The Ising model was further researched by Peierls, Onsager, Yang and many others. The model has also been successfully studied with the Monte Carlo method. The Heisenberg model was discovered by Werner Heisenberg and, nearly simultaneously, by P. A. M. Dirac, in 1926. Further work over the following decade established the Heisenberg model, due to its versatility, to be the fundamental object of study of the theory of magnetism. Since then, much work in theoretical statistical mechanics, solid state physics, and mathematical physics alike has been concentrated on understanding this model. Despite this effort, the Heisenberg model remains largely intractable, its predicted energy levels and eigenfunctions poorly understood, especially in a three-dimensional setting. The first step towards solving the Heisenberg model was the diagonalization by Hans Bethe in 1931 of the one-dimensional Heisenberg XXX model. Using an extension of the Bethe ansatz, Rodney Baxter solved the more general one-dimensional XYZ model in 1971. This solution, however, as well as approaches to the two-dimensional and three-dimensional Heisenberg models [2–5], is exceedingly complicated. The Heisenberg model can be used to describe magnetically ordered solids, in which internal magnetic interactions cause individual magnetic ions to possess nonzero magnetic moments below some critical temperature. Physical properties of low-dimensional quantum spin systems have attracted much attention over the last few decades. For the first time K. Hida [6] in a pioneering work has shown the appearance of magnetization plateau in

trimerized Heisenberg model. The magnetization plateaus play an important role in understanding a large family of nontrivial quantum phenomena in spin systems, both in experimental physics and in theory [7–15]. The magnetization plateau phenomena is greatly connected with entanglement. The understanding of correlated quantum systems, phase transitions, and collective quantum phenomena has an important role in the study of entanglement [16–18]. The concept of entanglement, and indeed the coining of the word itself, dates back to the origins of quantum mechanics [19]. Entanglement is considered to play a key role for understanding of strongly correlated quantum systems, quantum phase transitions and collective quantum phenomena in particular many-body spin and fermionic lattice models [16–18, 20–22]. With the advent of quantum information theory, entanglement was recognized as a resource, enabling tasks like quantum cryptography [23], quantum teleportation [24] or measurement based on quantum computation [25]. Together with the rapid experimental progress on quantum control, this leads to a rapidly growing interest in entanglement theory and many nowadays experiments aim at the generation of entanglement. Moreover, a recent experimental observation showed a possibility of entangling macroscopic millimeter sized diamonds at room temperature [26].

Geometrically frustrated spin systems exhibit fascinating new phases of matter, a rich variety of unusual ground states and thermal properties as a result of zero and finite temperature phase transitions respectively [27]. Among the most notable features of these systems one could mention an existence of the magnetization plateau in a low-temperature magnetization curve, a striking plateau of Lyapunov exponents, temperature dependences of susceptibility and specific heat. The magnetization plateaus play a great role in understanding of a large family of nontrivial quantum phenomena in one- and two-dimensional spin systems [15, 28]. One can obtain magnetization plateaus with multiple-spin exchange interaction using the dynamic and transfer-matrix methods. As attractive materials among geometrically frustrated spin systems, one should mention the metal-containing complexes (compounds). A distinguishable feature of this family of materials is that the coupling between the sites of their lattices can be described by an alternating sequence of Ising-type and Heisenberg-type interactions. This makes the corresponding models exactly solvable, using both transfer-matrix and/or recurrence relation techniques.

Another important part in this dissertation are pseudo random number generators(PRNG). PRNGs

have a wide variety of uses in both commercial and scientific problems. The demanded quality of PRNGs varies depending on its application. One of the main uses of PRNGs in science is its use in Monte Carlo simulations which have high requirements on the applied PRNG. K-system PRNGs have been proven to have high quality and low computational costs. Monte Carlo Simulations are widely used in the study of Ising model. Another essential part of the dissertation are Cellular automata and the Abelian sandpile model. Cellular automata are used in a number of spheres starting from computer processors, cryptography to forest fires.

This dissertation is organized in the following way.

The dissertation consists of 6 chapters. In chapter 1 we review the material necessary to present our results which are given in chapters 2-6. The first chapter start with a short introduction of statistical mechanics with a strong emphasis on the Ising model. Chapter 1 also includes a description of the basics of Cellular Automata and the Abelian Sandpile model, an introduction to K-system PRNGs and Monte Carlo simulations.

In chapter 1 we collect and review the basics of Statistical mechanics. In section 1.1 we review and define the concepts of partition function, free energy and their relation. We also define the average of an observable quantity in the language of Statistical mechanics and show that the equation of internal energy can be easy derived from these concept. In section 1.2 we give the basic definition of the general Ising model, in form of its Hamiltonian. In section 1.3 we review the idea of free energy and give its definition as a thermodynamical limit. We also give the definition of specific heat. In section 1.4 we give the definition of magnetization as an average of magnetic moment per site and review some of its properties. We also give the definition of susceptibility. Section 1.5 is a short intruduction to correlations. In section 1.6 we consider the nearest-neighbor Ising model and discuss some of its interesting properties. In chapter 1.2 we discuss and review the one-dimensional Ising model. Section 1.2 also acts as a theoretical background for the Chapter 3 and 4. In Section 2.1 we describe the model and give the general form of its free energy and magnetization. We also discuss the transfer matrix method which has a essential role in exact solutions of Ising and/or Heisenberg models. Next in section 2.2 we talk about the correlations between two spins, here we also take advantage of the transfer matrix method. And at last but not least in 2.3 section of chapter 1 we discuss the models

critical behavior near $T = 0$. In section 3 we study the Ising model on Bethe Lattice. In the first part of the section we discuss the Bethe lattice and Cayley tree. We give a convenient definition of the Bethe lattice as a sub lattice of the Cayley tree. Next we show that the Bethe lattice has seemingly infinite dimensionality. In the next section we describe the recurrence relations technique. As the transfer matrix method it is also an essential tool in the study of Ising and Heisenberg models. Next we show the form of the partition function and magnetization when using the recurrence relations method. The set of recurrence relation for the Ising model on Bethe lattice has only one element and its form is comparatively simple. In the following section we take a closer look at the magnetization. We express it as a function of H. We also discuss its behavior depending on the critical point. In the next section we study the free energy of the Cayley tree and from it derived free energy of Bethe lattice.

In Chapter 4 we give an introduction to the Abelian sandpile model. This model was presented by Per Bak, Chao Tang and Kurt Wiesenfeld in a 1987 paper [29]. It is the first dynamical model shown to have self-organized criticality. Dynamical systems have self-organized criticality if they manifest a critical point as an attractor. Their macroscopic behavior thus displays the spatial and/or temporal scale-invariance characteristic of the critical point of a phase transition, but without the need to tune control parameters to a precise value, because the system, effectively, tunes itself as it evolves towards criticality. The concept self-organized criticality has been applied in a variety of disciplines including physical cosmology, evolutionary biology and ecology, bio-inspired computing and optimization (mathematics), economics, sociology, neurobiology and others. The model can be thought of as a Cellular automata. The concept of cellular automata was first introduced by John von Neumann in the 1940s. In section 4.1 we give the definition of Cellular automata and discuss some of its more important properties. In chapter 4.2 we study frontal cellular automata and Abelian sandpile model. We give the deffinition of frontal cellular automata and discuss its advantages over frontal cellular automata. We also justify our choice of using frontal cellular automata. Next we give the definition of the sandpile model. We also introduce a couple of concepts which simply and enhance our understanding of the sandpile model. And atlast but not least we give the criteria which makes a sandpile model Abelian and discuss some pivotal lemmas of the subject.

In Chapter 5 we give an introduction to pseudo random number generators and especially the K-system generators. There are two methods of random number generation first the so called true random number generators and second pseudo random generators. True number generators first measure some physical phenomena then transform the output of the measurement to counter some possible biases. Of course the physical phenomena is chosen to be as random as possible. The most popular phenomena include atmospheric noise, thermal noise, and other external electromagnetic and quantum phenomena. One of the apparent weakness of such method is its speed. Most true random generators have much slower speed compared to pseudo random generators which makes them uncontentious if a large set of random numbers are required. Another shortcoming of true random generator is their unreliability, i.e. if we generate random numbers with the help of cosmic background radiance it will return different data depending on the radiance of the sun. The second group of random number generators are pseudo random generators or ells called deterministic random bit generator. Pseudo random generators are essential an algorithm which takes a seed and returns a sequence of numbers. Of course this sequence depends on the seed and is not truly random as the sequences generated by true random generators. Nevertheless there are pseudo random generators which generate sequences very close too true random. An advantage of pseudo number generators os its reproducibility, i.e. by knowing the seed we can reproduce the sequence of numbers. Pseudo random generators are mostly used in simulations such as the Monte Carlo method and cryptography. Devising a pseudo number generator with quality output is not a trivial problem. Especially in cryptography and some Monte Carlo simulations have a very high requirements on the pdeudo random generator. In general, careful mathematical analysis is required to have any confidence that a pseudo random generator generates numbers that are sufficiently close to true random to suit the intended use. In section 5.1 we discuss the Monte Carlo method. Next we give the definition of the Metropolis algorithm. We also show the application of metropolis algorithm for the Ising model. After we give the definition of the so called K-system generators. Next we show some results connected to the K-system generators.

Chapter 2 is based on the paper [30]. In this paper we consider the appearance of superstable cycles in the dynamical approach to the antiferromagnetic and ferromagnetic spin-1 Ising and Ising-Heisenberg models on diamond chains, and their connection with magnetization plateaus. The rational mappings,

which provide the statistical properties of the model, are derived by using recurrence relations technique. We consider stability properties of the mapping, providing evidences of a connection between magnetization plateaus and dynamical properties, as the behavior of Lyapunov exponents. The newfound correspondence between superstable point and zero magnetic plateau in spin-1 models on a diamond chain has been tested for a range of parameters.

Chapter 3 is based on the paper [31]. The geometrically magnetic frustrations and quantum thermal entanglement of antiferromagnetic metal-containing compounds are considered on a diamond chain. We researched the magnetic and thermal properties of the symmetric Hubbard dimers with delocalized interstitial spins and the quantum entanglement states. It is presented magnetization plateaus and negativity in spin-1 Ising-Heisenberg model using transfer matrix technique. Applying the dynamic system approach we study the magnetic curves, Lyapunov exponents and superstable point in the two-dimensional mapping for the partition function of spin-1 classical and Ising-Heisenberg models at $T \to 0$ on a diamond chain.

Chapter 4 is based on the paper [32]. In this paper we consider the appearance of superstable points and cycles in the dynamical approach to the antiferromagnetic and ferromagnetic spin-1 Ising on diamond-like decorated Bethe lattice, also their connection with magnetization plateaus. The calculations of Lyapunov exponents, magnetisation and quadrupole moment are done via recursion relation technique.

Chapter 5 is based on the paper [33]. In this paper we investigate the interrelation between the distribution of stochastic fluctuations of independent random variables in probability theory and the distribution of time averages in deterministic Anosov C-systems. On the one hand, in probability theory, our interest dwells on three basic topics: the laws of large numbers, the central limit theorem and the law of the iterated logarithm for sequences of real-valued random variables. On the other hand we have chaotic, uniformly hyperbolic Anosov C-systems defined on tori which have mixing of all orders and nonzero Kolmogorov entropy. These extraordinary ergodic properties of deterministic Anosov C-systems ensure that the above classical limit theorems for sums of independent random variables in probability theory are fulfilled by the time averages for the sequences generated by the C-systems. The MIXMAX generator of pseudorandom numbers represents the C-system for which

the classical limit theorems are fulfilled.

Chapter 6 is based on the paper [34].The paper provides frontal cellular automata algorithms for abelian sandpile models [35–37]. Also in this paper we calculate the height probabilities on a 2D lattice with fractal boundaries. Fractals have been subject of study in a variety of fields. One of the more interesting features of fractals is its way of scaling. If we take a polygon and double its edge length its are becomes four times its original area i.e the area is multiplied by ${2_e}^{2_d}$ where 2_e is the times the edge length is being multiplied and 2_d is the dimension in which the polygon is residing. In the same manner if we take a sphere and multiply its radius by two its volume becomes eight times the original i.e. the volume is being multiplied by ${2_r}^{3_d}$ where 2_r is the factor with which we multiply the radius and 3_d is the dimension of sphere. But if a fractal's one-dimensional lengths are all doubled, the spatial content of the fractal scales by a power that is not necessarily an integer. This power is called the fractal dimension of the fractal, and it usually exceeds the fractal's topological dimension. Fractal patterns which exhibit diverse degrees of self-similarity have been the focus of rendering or study in images, structures and sounds and have been observed in nature, technology, art, architecture and law. The graphs of most chaotic processes are fractal which makes them especially interesting to study from the perspective of Chaos theory.

Chapter 1

Preliminary ideas and concepts

1.1 Basics of Statistical mechanics

1.1.1 Partition function

A partition function describes the statistical properties of a system in thermodynamic equilibrium [38–40]. The partition function is one of the fundamental functions in statistical mechanics which allows the calculation of thermodynamic functions such as magnetization from the microscopic forces between the elements of the system. The partition function is given by the following formula:

$$Z = \sum_{n} e^{-\frac{E(n)}{k_B T}} \tag{1.1}$$

where k_B denotes the Boltzmann constant and $E(n)$ admits all allowed states of the system. Another fundamental variable in statistical mechanics is the free energy. The free energy is the most important quantity at fixed temperature. It is also the quantity that is most directly related to the partition function Z:

$$F = -k_B T \ln Z \tag{1.2}$$

The probability of the system being at state n is given by:

$$Z^{-1}e^{-\frac{E(n)}{k_BT}} \tag{1.3}$$

The observed average thermodynamic value of any observable A i.e. the magnetization or total energy which has the value $A(n)$ at state n is

$$\langle A\rangle = Z^{-1}\sum_n A(n)e^{-\frac{E(n)}{k_BT}} \tag{1.4}$$

Notably the internal energy [41, 42] is

$$U = \langle E\rangle = Z^{-1}\sum_n E(n)e^{-\frac{E(n)}{k_BT}} \tag{1.5}$$

By using the definitions of partition function and free energy the above equation can be written i the following form

$$U = k_BT^2\frac{\partial}{\partial T}\ln Z = -T^2\frac{\partial}{\partial T}(F/T) \tag{1.6}$$

which complies with thermodynamics. So if our system is at equilibrium the goal of statistical mechanics is to calculate the partition function. This enables us to calculate F which in itself allows us to obtain by differentiation the thermodynamic properties of the system.

But of course the size of any macroscopic system makes the above procedure for most cases unmanageable. Therefore one is forced to uses one or both of the following methods:

A. Replace the real system with some kind of model which is an idealization of the former one. In a Mathematical language this is equal to specifying the states n and the energy Hamiltonian function $E(n)$.

B. Evaluate the partition function by using some approximations.

1.1.2 Ising model

The Ising model [43–50], named after the physicist Ernst Ising [1,51,52], is a mathematical model of ferromagnetism [53,54] in statistical mechanics. The Ising model can be thought of as a model of a magnet. The model consists of discrete variables that represent magnetic dipole moments of atomic spins that can be in one of two states (+1 or -1). The spin σ_i is considered to be up when it takes the value +1 and down when it has the value of -1. Frequently these values are written just + or -. The spins lay on a graph which in most cases is a lattice also each spin is allowed to interact with its neighbors. As a simplified model of reality the model allows the identification of phase transitions. Lets give the formal Mathematical definition of the Ising model.

Lets consider a set of lattice sites Λ, each with a set of adjacent sites (e.g. a graph) forming a d-dimensional lattice. For each lattice site $k \in \Lambda$ there is a discrete variable σ_k such that $\sigma_k \in \{+1,-1\}$, representing the site's spin. A spin configuration, $\sigma = (\sigma_k)_{k\in\Lambda}$ is an assignment of spin value to each lattice site.

$$\sigma = \{\sigma_1, \sigma_2, \ldots, \sigma_N, \} \tag{1.7}$$

A general Hamiltonian function for the Ising model will have the following form:

$$H(\sigma) = -\sum_{\langle i,j\rangle} J_{ij}\sigma_i\sigma_j - \mu\sum_j h_j\sigma_j \tag{1.8}$$

where J_{ij} is an interaction term for two adjacent sites $i, j \in \Lambda$. And h_j is the external magnetic fields interacting with the j-th site. Positive J correspond to ferromagnetism and negative J-s to antiferromagnetism. $\langle ij\rangle$ denotes two nearest neighbor sites i and j. μ is the magnetic moment. In a ferromagnetic Ising model, spins desire to be aligned: the configurations in which adjacent spins are of the same sign have higher probability. In an antiferromagnetic model, adjacent spins tend to have opposite signs.

The Boltzmann distribution describes the configuration probability, with inverse temperature $\beta \geq 0$ it

has the following form:

$$P_\beta(\sigma) = \frac{e^{-\beta H(\sigma)}}{Z_\beta} \tag{1.9}$$

where $\beta = (k_B T)^{-1}$ and Z_β is the normalization constant which is given by

$$Z_\beta = \sum_\sigma e^{-\beta H(\sigma)} \tag{1.10}$$

which is the partition function.

1.1.3 Free Energy and Specific Heat

In physical large systems we expect the free energy to be proportional to the size of the system. That means the thermodynamical limit

$$f(H,T) = -k_B T \lim_{N\to\infty} N^{-1} \ln Z_N(H,T) \tag{1.11}$$

should exist, where f is the free energy per site.

We expect the limit in the above equation to be independent of the way it is taken. For example we assume that whether the length, breadth and height of the crystal go to infinity together or or one after another doesn't matter as long they go to infinity eventual.

By using the equation of internal energy from thermodynamics and the above equation we get

$$u(H,T) = -T^2 \frac{\partial}{\partial T}(f(H,T)/T) \tag{1.12}$$

The definition of specific heat is given by the following equation

$$C(H,T) = \frac{\partial}{\partial T} u(H,T) \tag{1.13}$$

Lets define two critical exponents α and α' by asserting that near T_c the zero-field specific heat diverges as a power-law, i. e.

$$C(0,T) \sim t^{-\alpha} \qquad as \quad t \to 0^+ \tag{1.14}$$

$$C(0,T) \sim (-t)^{-\alpha'} \qquad as \quad t \to 0^- \tag{1.15}$$

where t is

$$t = (T - T_c)/T_c \tag{1.16}$$

The problem with this definition is that $C(0,T)$ may remain finite as t goes to zero through positive (or negative) values, even though it is not an analytic function $t = 0$. For example $C(0,T)$ may have a simple jump discontinuity at $t = 0$, as in the mean-field model.

In most cases to get an exponent which characterizes such behavior it is simpler to use the following technique.

We define $f_+(0,T)$ $f_-(0,T)$ as the zero-field free energy functions for $T > T_c$ and $T < T_c$ respectively. Analytically continue these functions into the complex T plate and define the 'singular part' of the free energy to be

$$f_s(0,T) = f_+(0,T) - f_-(0,T) \tag{1.17}$$

Near the point $T = T_c$ the value of this function vanishes as a power law, so α can be defined by

$$f_s(0,T) \sim t^{2-\alpha} \qquad as \quad t \to 0 \tag{1.18}$$

This definition is equivalent to the above definitions of α and α' when $\alpha' = \alpha$ for the case when $u(0,T)$ is continuous and $C(0,T)$ diverges both above and below T_c.

It used to be thought that the only possible singularity in $f(0,T)$ was a jump-discontinuity in some derivative of f. If the first $r-1$ derivatives where continuous but the r-th derivative discontinuous, then it was said that the system had a "transition of order r". In particular, a discontinuity in u (i.e. latent heat) is called first-order transition.

While it is now known that this classification is not exhaustive, such behavior is included in the above case: a transition of order r corresponds to $2-\alpha = r$. In particular, $\alpha = 1$ for a first order transition. From the definition of specific heat per site the the above definition implies that $u(0,T)$ contains a term proportional to $t^{1-\alpha}$. Since $u(0,T)$ is usually bounded, it follows that

$$\alpha \leq 1 \tag{1.19}$$

The exponent α may be negative.

1.1.4 Magnetization

The average of the magnetic moment per site is the magnetization. Using the general equation for any observed average we get:

$$\begin{aligned} M(H,T) &= N^{-1}\langle \sigma_1 + \cdots + \sigma_N \rangle \\ &= N^{-1} Z_N^{-1} \sum_{\sigma} (\sigma_1 + \cdots + \sigma_N) \\ &\times \exp\left[-(E_0(\sigma) - H\sum_i \sigma_i)/k_B T \right] \end{aligned} \tag{1.20}$$

By using the definition of the partition function and free energy the following equation can be obtained:

$$M(H,T) = -\frac{\partial}{\partial H} f(H,T) \tag{1.21}$$

Its obvious that the summand in partition function doesn't change when we negate H and σ also Z_N and f are even functions depending of H so it can be concluded that M is an odd function, i.e.

$$M(-H,T) = -M(H,T) \tag{1.22}$$

from the definition of M one can see that it lies in the interval

$$-1 \leq M(H,T) \leq 1 \tag{1.23}$$

By differentiating the equalization of M with respect to H and using the equation of spontaneous magnetization and the average of an expected value the equation for susceptibility is

$$\chi = \frac{\partial \mathcal{M}}{\partial H} = (Nk_BT)^{-1}(\langle \mathcal{M}^2 \rangle - \langle \mathcal{M} \rangle^2) \tag{1.24}$$

where

$$\mathcal{M} = \sum_i \sigma_i \tag{1.25}$$

Considering the fact that the average of a constant and the constant are equal one can write the equation for susceptibility in the following way.

$$\chi = (Nk_BT)^{-1}\langle (\mathcal{M} - \langle \mathcal{M} \rangle)^2 \rangle \tag{1.26}$$

From the above equation follows that the susceptibility is the average of a non-negative quantity, so

$$\chi = \frac{\partial \mathcal{M}}{\partial H} \geq 0 \tag{1.27}$$

From this follows that the magnetization is an odd monotonic increasing function of H, which lays in the interval $[-1,1]$.

1.1.5 Correlations

Between the spins i and j the correlations are

$$g_{ij} = \langle \sigma_i \sigma_j \rangle - \langle \sigma_i \rangle \langle \sigma_j \rangle \tag{1.28}$$

Assuming $E(\sigma)$ is translation invariant which is true in most cases, then the average $\langle \sigma_i \rangle$ is constant for all sites i so from this and the definition of magnetization follows

$$\langle \sigma_i \rangle = \langle \sigma_j \rangle = M(H,T) \tag{1.29}$$

Another important fact is that the correlation g_{ij} will depend only on the vector distance r_{ij} between sites i and j i.e.

$$g_{ij} = g(r) \tag{1.30}$$

where $g(r)$ is the correlation function. We expect the correlation function $g(r)$ to decay exponentially to zero as r becomes large wen we move away from T_c. In more mathematical terms, if k is s0me fixed unit vector it is expected

$$g(xk) \sim x^{-\tau} e^{-x/\xi} \qquad as \quad x \to \infty \tag{1.31}$$

where ξ is the correlation length taken in the direction k and τ is some number.

We expect the correlation length to become infinite at T_c, which is also a function of H and T. A hallmark of a critical point can be regarded the property of an infinite correlation length. In particular it is expected that

$$\begin{aligned} \xi(0,T) &\sim t^{-\nu} \qquad as \quad t \to 0^+ \\ &\sim (-t)^{-\nu'} \quad as \quad t \to 0^- \end{aligned} \tag{1.32}$$

where ν and ν' are the correlation length critical exponents.

The fact that ξ also depends on the direction k is somewhat discouraging. However it is expected that the dependence will disappear near T_c and the large-distance correlations to become isotropic. Therefore the critical exponents ν and ν' should not depend on the direction in which ξ is defined.

The correlation function $g(r)$ near the critical point itself still exists which decays as a power law instead of decaying exponentially.

$$g(r) \sim r^{-d+2-\eta} \tag{1.33}$$

where η is a critical exponent.

In scaling theory, these properties are simple corollaries of the correlation scaling hypothesis, which is near T_c for $r \sim \xi$.

$$g(r) \sim r^{-d+2-\eta} D(r/\xi, t|H|^{-1/\beta\delta}) \tag{1.34}$$

We can express the χ susceptibility in terms of $g(r)$. To achieve this we need to sum the correlation between two spins g_{ij} over all sites. From the definition of χ we can get the following equation

$$\chi = (Nk_BT)^{-1} \sum_i \sum_j g_{ij} \tag{1.35}$$

For a translation-invariant system,

$$\sum_j g_{ij} = \sum_j g(r_{ij}) = \text{independent of } i \tag{1.36}$$

therefore

$$\chi = (k_BT)^{-1} \sum_j g(r_{0j}) \tag{1.37}$$

where 0 is some fixed site in the lattice. The function $g(r)$ is an isotropic bounded slowly varying function depending on r near the point T_c therefore we can replace the summation by an integral getting

$$\chi \sim \int_0^\infty g(r) r^{d-1} dr \tag{1.38}$$

by replacing $r = x\xi$ and using the above equation it follows that neat T_c

$$\chi \sim \xi^{2-\eta} \tag{1.39}$$

Now teh scaling relations follow from the equality of γ and γ' and the definitions of γ, γ', ν, ν'.

1.1.6 Nearest-Neighbor Ising model

In the previous sections the equations are true for any even Hamiltonian $E_0(\sigma)$ which is only subject to the implicit assumptions of existence ferromagnetic critical point and eq. 1.11 thermodynamical limit.

The most basic of such Hamiltonians is one which has only nearest neighbors interaction, i.e,

$$E_0(\sigma) = -J \sum_{(i,j)} \sigma_i \sigma_j \tag{1.40}$$

here the sum goes over all nearest-neighbors pairs of spins in the graph. If we choose $J > 0$ then the system is ferromagnetic that means when all spins point the same way the system is in the lowest energy state.

The above model has been subject of great interest and has been thoroughly studied, a great deal is know even for the cases when an exact solution has not been found such as in three dimensions or in two dimensions when an external field is present. For example it is possible at high or low temperatures to develop valid expansions.

The partition function will have the following form

$$Z_N = \sum_{\sigma} \exp\left[K \sum_{(i,j)} \sigma_i \sigma_j + h \sum_i \sigma_i\right] \tag{1.41}$$

where

$$K = J/k_B T \tag{1.42}$$

$$h = H/k_B T$$

therefore we can think of Z_N as a function depending on h and K. So the magnetization per sit will be

$$M = \frac{\partial}{\partial h} \lim_{N\to\infty} N^{-1} \ln Z_N(h,K) \tag{1.43}$$

We expect the magnetization to have a critical point at $H = 0$ for some positive value T_c of T.

Lets consider a square lattice (the following argument is true for any multi-dimensional lattice). The right hand side of the partition function equation is possible to expand in powers of K, giving

$$Z_N = (2\cosh h)^N (1 + 2NKt^2 + NK^2((2N-7)t^4 + 6t^2 + 1) + O(K^3)) \tag{1.44}$$

where

$$t = \tanh h \tag{1.45}$$

Using this expansion in the magnetization equation gives

$$M = \tanh h\{1 + 4\,\mathrm{sech}^2 h(K + (3 - 7t^2)K^2 + O(K^3))\} \tag{1.46}$$

Note that all terms in the above equation are odd analytic bounded functions depending on h. By assuming that for sufficiently small K the expansion converges. The expansion at $H = 0$ is continuous

and

$$M_0(T) = M(0,T) = 0, \quad T \text{ is sufficiently large} \tag{1.47}$$

As for when the temperature is low then K is large and the right hand side of the partition function can be expanded in powers of

$$u = \exp(-4K) \tag{1.48}$$

The first term to Z is with all spins up (or down) of the expansion. The succeeding terms to contribute to Z are N terms with one pin up and the rest down (or reversed); the following are a group of $2N$ states which have two adjacent spins up (or down); and so on. This will result

$$\begin{aligned} Z_N &= \exp(2NK+Nh)\{1+Nu^2e^{-2h} \\ &+ 2Nu^3e^{-4h}+\frac{1}{2}N(N-5)u^4e^{-4h} \\ &+ 6Nu^4e^{-6h}+Nu^4e^{-8}+\mathbf{O}(u^5)\} \\ &+ e^{2NK-Nh}\{1+Nu^2e^{2h} \\ &+ 2Nu^3e^{4h}+\frac{1}{2}N(N-5)u^4e^{4h} \\ &+ 6Nu^4e^{6h}+Nu^4e^{8h}+O(u^5)\} \end{aligned} \tag{1.49}$$

In the above expression the first term in curly brackets comes from states which have almost all spins up, as for the states with almost all spins down their contribution is the second term in curly brackets. The previous equation can also be written in the following form

$$Z_N = e^{N\psi(h,K)} + e^{N\psi(-h,K)} \tag{1.50}$$

where

$$\begin{aligned}\psi(h,K) &= 2K+h+u^2e^{-2h} \\ &+ 2u^3e^{-4h}+u^4(-e^{-4h}+6e^{-6h}+e^{-8h}) \\ &+ O(u^5)\end{aligned} \tag{1.51}$$

If N is sufficiently large for any order in u-expansion $\psi(h,K)$ doesn't depend on N.

In the partition function when $h>0$ then $e^{N\psi(h,K)}$ becomes larger then $e^{N\psi(-h,K)}$. In the limit of N large we can write the magnetization in the following form

$$\begin{aligned}M &= \frac{\partial}{\partial h}\psi(h,K) = 1-2u^2e^{-2h}-8u^3e^{-4h} \\ &- u^4(-10e^{-4h}+36e^{-6h}+8e^{-8h})-O(u^5) \quad \text{if } h>0\end{aligned} \tag{1.52}$$

therefore the spontaneous magnetization will be

$$M_0(T) = \lim_{h\to 0^+} M = 1-2u^2-8u^3-34u^4-O(u^5) \tag{1.53}$$

If the temperature is sufficiently low which is the same u being sufficiently small and the expansions converge then M_0 will be positive if u is small. Using the fact that $M(H,T)$ is an odd function depending on H one can obtain the fact that $M(H,T)$ has a discontinuity at $H=0$.

Therefore for sufficiently large T $M_0(t)$ is identically zero but for sufficiently small T it is positive. It will change from zero to non-zero at some intermediate temperature T_0 also at point T_0 it must be a non-analytic function depending on T. Therefore at $H=0$, $T=T_c$ there must be a critical point where the thermodynamical functions became non-analytic. For a closer look at correlations see [55,55–58].

1.2 One dimensional Ising model

1.2.1 Free Energy and Magnetization

The Ising model [59] has been proposed in 1920 and solved for the one-dimensional case at 1925. The solution is obtained whit transfer matrix technique. This model does not exhibit phase transitions [60–65] at any non-zero temperature. At $H = T = 0$ it has a critical point.

Lets consider an Ising model on a one-dimensional lattice which has N sites whith the labels $j = 1, 2, \ldots, N$. The energy is given by the following expression

$$E(\sigma) = -J \sum_{j=1}^{N} \sigma_j \sigma_{j+1} - H \sum_{j=1}^{N} \sigma_j \tag{1.54}$$

we connect the first site σ_1 and the last site σ_N so σ_{N+1} is regarded as σ_1. This is the same as imposing periodic boundary conditions on the system. This step ensures that the system is translationally invariant and all sites are equivalent. In particular

$$\langle \sigma_1 \rangle = \langle \sigma_2 \rangle = \cdots = \langle \sigma_N \rangle \tag{1.55}$$

the magnetization per site will have the following form

$$M(H,T) = \langle \sigma_1 \rangle \tag{1.56}$$

where instead of 1 we could have taken any site. For any translationally invariant system this reasoning holds.

The partition function of this system will have the following form

$$Z_N = \sum_{\sigma} \exp \left[-K \sum_{j=1}^{N} \sigma_j \sigma_{j+1} - h \sum_{j=1}^{N} \sigma_j \right] \tag{1.57}$$

where

$$K = J/k_BT, \quad h = H/k_BT \tag{1.58}$$

The exponential in partition function is possible to factored into terms in which every one depends only on two neighboring spins resulting

$$\begin{aligned} Z_N = \quad & \sum_\sigma \quad V(\sigma_1,\sigma_2)V(\sigma_2,\sigma_3)V(\sigma_3,\sigma_4)\dots \\ & \dots \quad V(\sigma_{N-1},\sigma_N)V(\sigma_N,\sigma_1) \end{aligned} \tag{1.59}$$

where

$$V(\sigma,\sigma') = \exp\left[K(\sigma\sigma') + \frac{1}{2}h(\sigma+\sigma')\right] \tag{1.60}$$

There are several ways to choose V for example: we can multiply it with $\exp[a(\sigma-\sigma')]$ (where a can be any number) and the partition function wont change. We choose V in the above form because it guaranties that

$$V(\sigma,\sigma') = V(\sigma',\sigma) \tag{1.61}$$

this symmetry will be useful in later calculations.

Now lets look at the right hand side of partition function, we shall view $V(\sigma,\sigma')$ as elements of a two-by-two matrix

$$V = \begin{pmatrix} V(+,+) & V(+,-) \\ V(-,+) & V(-,-) \end{pmatrix} = \begin{pmatrix} e^{K+h} & e^{-K} \\ e^{-K} & e^{K-h} \end{pmatrix} \tag{1.62}$$

In the partition function the summation over $\sigma_2, \sigma_3, \ldots, \sigma_N$ sites will be interpreted as matrix multiplication as for the summation over σ_1 as the taking of a trace

$$Z_N = \text{Trace}\, V^N \tag{1.63}$$

Matrix V is called the transfer matrix.

We denote the eigenvectors of V as x_1, x_2 and λ_1, λ_2 their corresponding eigenvalues. Then

$$V x_j = \lambda_j x_j, \quad j = 1,2 \tag{1.64}$$

Lets define a 2×2 matrix consisting of column vectors x_1, x_2 we name this matrix P

$$P = (x_1, x_2) \tag{1.65}$$

so

$$VP = P \begin{pmatrix} \lambda_1 & 0 \\ 0 & \lambda_2 \end{pmatrix} \tag{1.66}$$

We can choose x_1 and x_2 orthogonal and linearly independent because V a symmetric matrix. P is non-singular.Multiplying the right side of the above equation we get

$$V = P \begin{pmatrix} \lambda_1 & 0 \\ 0 & \lambda_2 \end{pmatrix} P^{-1} \tag{1.67}$$

By using this equation in the partition function we get

$$Z_N = \text{Trace} \begin{pmatrix} \lambda_1 & 0 \\ 0 & \lambda_2 \end{pmatrix}^N = \lambda_1^N + \lambda_2^N \tag{1.68}$$

we suppose the larger of the two eigenvalues is λ_1 so

$$N^{-1}\ln Z_N = \ln\lambda_1 + N^{-1}\ln\left[1+(\lambda_1/\lambda_2)^N\right] \tag{1.69}$$

since $\lambda_1 > \lambda_2$ as N tends to infinity $N^{-1}\ln\left[1+(\lambda_1/\lambda_2)^N\right]$ will tend to zero. So the free energy per site as $N\to\infty$ will be

$$\begin{aligned} f(H,T) &= -k_BT\lim_{N\to\infty} N^{-1}\ln Z_N = -k_BT\ln Z_N \\ &= -k_BT\ln\left[e^K\cosh h + (e^{2K}\sinh^2 h + e^{-2K})^{1/2}\right] \end{aligned} \tag{1.70}$$

We can obtain the magnetization per site by differentiating the above equation with h

$$M(H,T) = \frac{e^K\sinh h}{\left[e^{2K}\sinh^2 h + e^{-2K}\right]^{1/2}} \tag{1.71}$$

For all positive T and real H the free energy is an analytic function.Also depending on H the magnetization is an analytic function. Therefore for any positive temperature the system does not exhibit phase transitions.

1.2.2 Correlations

The probability of the system being in the state $\sigma \equiv \{\sigma_1,\ldots,\sigma_N\}$ is

$$Z_N^{-1}V(\sigma_1,\sigma_2)V(\sigma_2,\sigma_3)V(\sigma_3,\sigma_4)\ldots V(\sigma_N,\sigma_1) \tag{1.72}$$

Therefore the average value of lets say $\sigma_1\sigma_3$ is equal to

$$\langle\sigma_1\sigma_3\rangle Z_N^{-1}\sum_{\sigma}\sigma_1 V(\sigma_1,\sigma_2)V(\sigma_2,\sigma_3)\sigma_3 V(\sigma_3,\sigma_4)\ldots V(\sigma_N,\sigma_1) \tag{1.73}$$

The same thing can be written in the language of matrices:

$$S = \begin{pmatrix} 1 & 0 \\ 0 & -1 \end{pmatrix} \tag{1.74}$$

S is a diagonal matrix and its elements are

$$S(\sigma, \sigma') = \sigma\delta(\sigma, \sigma') \tag{1.75}$$

The right hand side of the equation of two spins average can be written as

$$Z_N^{-1} \,\mathrm{Trace}\, SVVSV \ldots V \tag{1.76}$$

therefore

$$\langle \sigma_1 \sigma_3 \rangle = Z_N^{-1} \,\mathrm{Trace}\, SV^2 SV^{N-2} \tag{1.77}$$

and if $0 \leq j - i \leq N$

$$\langle \sigma_i \sigma_j \rangle = Z_N^{-1} \,\mathrm{Trace}\, SV^{j-i} SV^{N+i-j} \tag{1.78}$$

$$\langle \sigma_i \rangle = Z_N^{-1} \,\mathrm{Trace}\, SV^N \tag{1.79}$$

From the above equations one can easily confirm that the system is translational invariant.

Lets define an angle ϕ by the following equation

$$\cot 2\phi = e^{2K} \sinh h, \quad 0 < \phi < \frac{\pi}{2} \tag{1.80}$$

It is possible to choose P to be an orthogonal matrix

$$P = \begin{pmatrix} \cos\phi & -\sin\phi \\ \sin\phi & \cos\phi \end{pmatrix} \tag{1.81}$$

By keeping $i-j$ fixed and taking N to infinity the average value of $\sigma_i\sigma_j$ will be

$$\langle\sigma_i\sigma_j\rangle = \cos^2 2\phi + \sin^2 2\phi(\frac{\lambda_2}{\lambda_1})^{j-i} \tag{1.82}$$

similarly the average of σ_i is

$$\langle\sigma_i\rangle = \cos 2\phi \tag{1.83}$$

From the above equations one can get an alternative derivation of magnetization, of course it is identical to the previous results. From the above equations the correlation function can be expressed in the following way

$$g_{ij} = \langle\sigma_i\sigma_j\rangle - \langle\sigma_i\rangle\langle\sigma_j\rangle = \sin^2 2\phi(\frac{\lambda_2}{\lambda_1})^{j-i}, \quad j \geq i \tag{1.84}$$

g_{ij} does not tend to zero exponentially because $|\frac{\lambda_2}{\lambda_1}| < 1$. We denote the correlation length by ξ, in units of the lattice spacing it will have the form

$$\xi = [\ln(\lambda_1/\lambda_2)]^{-1} \tag{1.85}$$

1.2.3 Critical Behavior near $T = 0$

For all temperatures T and all real fields H $|\frac{\lambda_2}{\lambda_1}| < 1$ but if $H = 0$ then

$$\lim_{T\to 0^+}(\lambda_2/\lambda_1) = 1 \tag{1.86}$$

Therefore at $H = T = 0$ the correlation length is infinite. The definition of a critical point can be interpreted as $\xi = \infty$ therefore $H = T = 0$ can be regarded as a critical point. The scaling hypothesis can be articulated in terms of M, H and $t = (T - T_c)/T_c$. For further calculations it is more suitable to replace the variables M, $h = H/k_B T$ and

$$t = \exp(-2K) = \exp(-2J/k_B T) \tag{1.87}$$

this replacements are most suitable when $T_c = 0$.

In a sense the scaling hypothesis is equivalent to the statement that the relation between M, h and t is invariant when we substitute them with

$$\lambda^{\beta} M, \quad \lambda^{\beta\delta} h, \quad \lambda t \qquad \text{for } \lambda > 0 \tag{1.88}$$

Therefore

$$M = h|h|^{\delta^{-1}-1}\phi(t|h|^{-1/\beta\delta}) \tag{1.89}$$

here $\phi(x)$ represents a scaling function which is related to the function $h(x)$.

If $|h| \ll 1$ for the one-dimensional Ising model the magnetization can be expressed as follows

$$M = h/(t^2 + h^2)^{1/2} \tag{1.90}$$

Its obvious that the magnetization is a function depending only on t/h therefore the scaling hypothesis is satisfied so

$$\beta\delta = 1, \quad \delta = \infty \tag{1.91}$$

also

$$\phi(x) = (x^2+1)^{-1/2} \tag{1.92}$$

The above relations follow from the scaling hypothesis therefore they must always hold. From them follows

$$\alpha = 1, \quad \beta = 0, \quad \gamma = 1 \tag{1.93}$$

The eigenvalues of transfer matrix can be written in the following form when $h = 0$

$$\lambda_1 = 2\cosh K, \quad \lambda_2 = 2\sinh K \tag{1.94}$$

so

$$\lambda_1/\lambda_2 = (1+t)/(1-t) \tag{1.95}$$

If $t \ll 1$ the correlation length becomes

$$\xi \sim (2t)^{-1} \tag{1.96}$$

with

$$\nu = 1 \tag{1.97}$$

The eigenvalues of the transfer matrix are equal at the critical point, therefore the corelation function becomes constant.

$$\eta = 1 \tag{1.98}$$

1.3 Ising model on Bethe latices

1.3.1 The Bethe lattice

The Ising model on Bethe latices [66–75] has a central role in exactly solvable models. We construct the Bethe lattice with the following procedure: choose a starting point which we name central point 0 and add to it q points, these points are connected to the central point 0. The set of new created q points are called the the first shell. We repeat the previous step for the new created points by connecting each one with new points, but in contrast to the central point we add only $q-1$ new points for each point neighboring the central point. the second generation of points connected to the first shell are called two. One cane repeat this processes to obtain the number shells needed.

Generate the shells $2,\ldots,n$. The result will be a graph identical to the one in Fig. 1. If we calculate all point belonging to shell r we will have $q(q-1)^{r-1}$ points, so the total number of points in all the shells will be

$$q\left[(q-1)^n-1\right]/(q-2) \tag{1.99}$$

The points belonging to the outermost shell n are called boundary points as for any other point they are called interior points. The boundary points differ from interior points by the fact that they have only one direct neighbor in contrast to q neighbors of interior points.

Note that the above described graph has no circuits, also its called sometimes a Cayley tree. Assumed the boundary pints can be ignored it is sufficient for our purposes to consider it as a regular graph with coordination number q.

If we ignore the boundary points it is natural to expect that the number of boundary points is fare less then the interior points in a thermodynamic limit of a large system. Both sets have grow exponentially like $(q-1)^n$. To avoid complications connected with this we regard only points which are fare away from the boundary in the limit $n\to\infty$. Each such pints has a coordination number of q and are in some sense equivalent, these sites form the Bethe lattice.

If we constructed the Ising model on Cayley tree we are obliged to take into account both interior and boundary sites while calculating the partition function Z. Of course even in a thermodynamic limit the contribution of boundary points in comparison to interior point is is not small. In this section we will discuss only the Ising model on Bethe lattice i.e. the lattice created of Cayley trees sites that are deep within the lattice.

The dimensionality of any regular two or tree dimensional lattice is given by the following equation

$$\lim_{n\to\infty}(\ln c_n)/\ln n = d \tag{1.100}$$

where d is the dimensionality and $c_n = 1 + m_1 + \cdots + m_n$, here m_i is the number of neighbors with distance i. If we try to calculate the dimensionality of the Bethe lattice we will get a positive divergent value. So in a sense the Bethe lattice has infinite dimensionality.

1.3.2 Recurrence Relations for the Central Magnetization

By first considering Cayley tree and subsequently disregarding boundary condition on can effectively get the results for a Bethe lattice. The partition function of Cayley tree is

$$Z = \sum_{\sigma} P(\sigma) \tag{1.101}$$

where

$$P(\sigma) = \exp\left[K\sum_{(i,j)}\sigma_i\sigma_j + h\sum_i \sigma_i\right] \tag{1.102}$$

This expression consists of a sum over all edges and sites. The above expression can be regarded as a probability function which has not been normalized. The local magnetization can be expressed as follows

$$M = \langle\sigma_0\rangle = \sum_{\sigma}\sigma_0 P(\sigma)/Z \tag{1.103}$$

where σ_0 is the central site of the Bethe lattice. If we cut the Bethe lattice at the central site we will obtain q identical tree graphs. The tree graphs root is the site 0, such graphs are called rooted trees. By considering the above mentioned fact one can express $P(\sigma)$ as follows

$$P(\sigma) = \exp(h\sigma_0) \prod_{j=1}^{q} Q(\sigma_0|s^{(j)}) \tag{1.104}$$

the spins of the j-th sub tree except the 0 site are denoted by $s^{(j)}$. And

$$Q(\sigma_0|s) = \exp\left[K \sum_{(i,j)} s_i s_j + K s_1 \sigma_0 + h \sum_i s_i\right] \tag{1.105}$$

the spin of the i-th site of the selected sub-tree is denoted by s_i, except for the central site which has spin σ_0. The central site has q adjacent sites, one of them is site 1. In the above equation $\sum_{(i,j)} s_i s_j$ is over all edges of the sub tree, except for edge $(0,1)$. And $\sum_i s_i$ is over all sites likewise except for site 0. The first site and a boundary site have n steps distance, in other words the sub-tree has n shells. Lets cut the sub tree at the site 1 which is neighboring the central site 1. The result will be on one hand the the trunk consisting of $(0,1)$ edge and sites and on the other hand $q-1$ sub trees which are identical to the original except they have $n-1$ shells. Therefore

$$Q_n(\sigma_0|s) = \exp\left[K\sigma_0 s_1 + h s_1\right] \prod_{j=1}^{q-1} Q_{n-1}(s_1|t^{(j)}) \tag{1.106}$$

here the spins of the j-th branch are named $t^{(j)}$ except for s_1. Lets denote

$$g_n(\sigma_0) = \sum_s Q_n(\sigma_0|s) \tag{1.107}$$

using this equation the partition function can be expressed as follows

$$Z = \sum_{\sigma_0} \exp(h\sigma_0) \left[g_n(\sigma_0)\right]^q \tag{1.108}$$

Likewise the magnetization can be expressed as

$$M = Z^{-1} \sum_{\sigma_0} \sigma_0 \exp(h\sigma_0) \left[g_n(\sigma_0) \right]^q \tag{1.109}$$

Let

$$x_n = \frac{g_n(-)}{g_n(+)} \tag{1.110}$$

By taking in consideration the above expressions the magnetization will be

$$M = \frac{e^h - e^{-h} x_n^q}{e^h + e^{-h} x_n^q} \tag{1.111}$$

The calculation of M is dependent of x_n. By using the above equations $g_n(\sigma_0)$ can be written as

$$g_n(\sigma_0) = \sum_{s_1} \exp(K\sigma_0 s_1 + h s_1) \left[g_{n-1}(s_1) \right]^{q-1} \tag{1.112}$$

Taking into consideration that σ_0 and s_1 take the values $+1$ or -1 x_n can be written as

$$x_n = y(x_{n-1}) \tag{1.113}$$

where

$$y(x) = \frac{e^{-K+h} + e^{K-h} x^{q-1}}{e^{K+h} + e^{-K-h} x^{q-1}} \tag{1.114}$$

By employ the above recursion relation it's easy to se that

$$x_0 = g_0(\sigma_0) = 1 \tag{1.115}$$

After defining x_n the calculation of magnetization is straightforward.

1.3.3 Magnetization as a function of H

Lets study the variations of x and M when T is fixed (i.e. K is fixed) and with $h = H/k_BT$.

The magnetization of our system when $n \leftarrow \infty$ has the following form

$$M = \frac{e^{2h} - x^q}{e^{2h} + x^q} \tag{1.116}$$

here x is a solution for the following expression

$$x = y(x) \tag{1.117}$$

this equation can be expressed as follows

$$e^{2h} = x^{q-1}\frac{e^{2K} - x}{e^{2K}x - 1} \tag{1.118}$$

Considering the fact that all x_n are positive its obvious that their limit x must also be positive. From this follows that x must lie in the following region

$$e^{-2K} < x < e^{2K} \tag{1.119}$$

So we have an expression which for a fixed K gives h as a function depending on x. By differentiating this expression logarithmically we get

$$2x\frac{dh}{dx} = q - 1 - \frac{2\sinh 2K}{2\cosh 2K - x - x^{-1}} \tag{1.120}$$

Like before x lies in the above region. The right hand side of this expression assumes its maximum value at $x = 1$. When $K < K_c$ where

$$K_c = \frac{1}{2}\ln\left[q/(q-2)\right] \tag{1.121}$$

In this case when x becomes from e^{-2K} to e^{2K} the function h becomes a monotonic decreasing function with the minimum 0 and maximum ∞. Therefore if h has a real value our expression has only one solution x which is real and positive. This solution x is a analytic function depending on h which lies in the region $-\infty < h < \infty$. Now lets discus the case when $K > K_c$, here when x is sufficiently close to one $dh/dx > 0$. The function h has a form similar to the graphic depicted in Fig 1 also note that when $x = 1$ then $h = 0$. From the graphic it's also obvious that for small h there are three solutions.
In all solutions x is a decresing function depending on h.

$$x(-h) = \frac{1}{x(h)} \tag{1.122}$$

Also note tha the magnetization is an odd function depending on h. It is a monotonic increasing function with -1 as minimum and 1 as maximum. The magnetization goes from minimum to maximum as h goes from negative infinity to positive infinity also its analytic if $K < K_c$. When $K > K_c$ its also analytic everywhere except when h is becoming zero.
Such behavior coincides with the behavior of ferromagnet. Therefore the Ising model Bethe lattice is a good approximation of a ferromagnet which exhibits critical point at $H = 0$ and $T = T_c$, where.

$$\frac{J}{k_B T_c} = \frac{1}{2} \ln \left[\frac{q}{q-2} \right] \tag{1.123}$$

1.3.4 Free Energy

The free energy of the whole Cayley tree is given by the equation

$$F = -k_B T \ln Z \tag{1.124}$$

here Z is the total partition function of the tree. By differentiating the free energy with H

$$-\frac{\partial F}{\partial H} = \sum_i M_i \tag{1.125}$$

where $H = hk_BT$ and the sum goes over all states. And M_i is the magnetization of site i.

$$M_i = \langle \sigma_i \rangle \tag{1.126}$$

Note that M_i depends only on H (i.e. h) for a given temperature. To emphasis this more we denote it by $M_i(h)$. For a sufficiently large H with positive values the most dominant state in the partition function is the one with all up spins. Therefore

$$\frac{F}{k_BT} = -KN_e - hN \tag{1.127}$$

here N denotes the number of sites and N_e the number of edges. Note that in this limit the average value of all spins is one.

By integrating the sum of all local magnetizations with respect to H and using the above equation for the integration constant we get

$$\frac{F}{k_BT} = -KN_e - hN + \sum_i \int_h^\infty \left[M_i(h') - 1\right] dh' \tag{1.128}$$

By taking into consideration that $\sum_i q_i = 2N_e$ where q_i is the number of sites neighborer to site i.

$$F = \sum_i f_i \tag{1.129}$$

where

$$\frac{f_i}{k_BT} = -\frac{1}{2}Kq_i - h\int_h^\infty \left[M_i(h' - 1)\right] dh' \tag{1.130}$$

1.4 Abelian Sandpile model

1.4.1 Cellular automata

Cellular automata belong to the class of self-regulatory systems. Such systems are characterized by the ability to regulate over time, even with a random initial state. The cellular automata is a set of "cells" or vertices $V = (v_1, v_2, ...v_n)$ which have the following properties:

- The vertices are placed in the finite dimensional network Z^n
- Every vertex has a state, usually the set of these states is finite, we denote this set $S = 1, 2, ..., k$
- Every vertex has a set of neighboring vertices, which can be anywhere in the general case.
- 3×3 Von Neumann , 5×5 Von Neumann , and Moore are the most common neighbore selection. methods. For the future, we will accept if the opposite does not claim that neighbors are choosen via the 3×3 Von Neumann methode. The set of all neightbors of vertex v_j is denoted as $N(v_j)$.
- There are transitional laws for each vertex, in the general case these laws depend from the vertex, its neighbors, time and it's state. $F_{v_j}(s_{v_j}, N(v_j), t) = s_i$ where $j \in 1, 2, ..., n, ..., S_i, S_j \in S$. Usually these laws are independent of time and the vertex otherwise such cellular automata are called non homogenious

The cellular automata is called asynchronous if its vertices make state transitions independent of each other and abelian if the set of final states is independent from the order of the single vertex state transitions.

The classic algorithm for the implementation of the synchronous homogeneous cellular automata has two steps. If $A(t)$ is the set of all the vertices states at time t then the set $A(t+1)$ is obtained by the following equation.

$$A(t+1) = \{F(s_{v_1}, N(v_1)), F(s_{v_2}, N(v_2)), \ldots, F(s_{v_n}, N(v_n)), \} \tag{1.131}$$

1.4.2 Sandpile Model

Before we start discussing the Abelian sandpile model lets look at a specific group of cellular automata called frontal cellular automata. Frontal cellular automata belong to the class of homogenous asynchronous abelian cellular automata. Frontal cellular automata, as opposed to ordinary cellular automata, make it possible to dramatically decrease the runtime and save RAM. Unlike conventional cellular automata which use two sets $A(t)$ and $A(t+1)$ while modeling frontal cellular automata use only one. In frontal cellular automata the flow of information is reversed which allows to take into account only a subset of all vertices. This fact gives us the opportunity to abandon the approach of ordinary cellular automata where we apply the transitional law for all the vertices. If a vertex is in a stable state and there is no change in its neighbors, it remains in the same state. If the vertex becomes active, it checks its transition law and sends information to its neighbors as a result of which its neighbors check their transition laws. The Abelian sandpile model is a frontal cellular automata. The following is the definition of the Abelian sandpile model.

Consider the $G(V,E)$ directed graph. Lets denote the vertices of G by $v_1, v_2, \ldots, v_n$. the directed edge e can be considered as a ordered pair (v_i, v_j), where e is directed from vertex v_i to v_j. The model allows $e = (v_i, v_i)$, $e_m = (v_i, v_j)$ and $e_k = (v_j, v_i)$ types of edges where $e, e_m, e_k \in E$and $v_i, v_j \in V$. The number of edjes orginating from vertex v_i is denoted by d_{v_i} or just d_i. If the number of edges that originate from a vertex is equal to zero, then we call this vertex sink. We call the sink global if there is a guided path from any vertex. Note that if there is a global sink, it is the only one. Proof immediately follows from the fact that it does not have any outgoing edges. The neighborhood matrix A of graph G is a $n \times n$ square matrix withe elements a_{ij} being equal to the number of edges connecting vertex i to vertex j. The Laplacian of graph G has the following form.

$$\Delta = D - A \tag{1.132}$$

where D is a diagonal matrix which i,i-th element is equal to d_i. The elements of Laplacian are

$$\Delta_{ij} = \begin{cases} -a_{ij} & \text{for } i \neq j \\ d_i - a_{ii} & \text{for } i = j \end{cases} \qquad i,j \in 1,2,...,n, \tag{1.133}$$

The sum of the elements in each row of this matrix is equal to zero. All elements corresponding to a sinks row are equal to zero. The state(configuration) of graph G is a ordered set $H = h_1, H2, \ldots, h_n$ which elements are non negative and are in a one to one corespondent to the none sink vertices of the graph, they are also sorted correspondingly. We denote the number of sand grains on vertex i by h_i. In the H configuration vertex i is called active if the non-negative natural number corresponding to it is greater than or equal to the number of edges originating at the vertex i. The active vertex is possible to collapse, resulting in the configuration H transiting to a new configuration H'. H' is called a descendant of H.

$$H' = H - \Delta'_i \tag{1.134}$$

where Δ' is the reduced Laplacian, we get it from the Laplasia by removing the rows and columns corresponding too the sink. And Δ'_i is the i-th row of the reduced Laplacian. If we obtain the σ configuration by collapsing a vertex in σ' we call σ the predecessor of σ'. The following lemmas enable us to understand the model more deeply.

Lemma 1: Consider any directed Graph G. Lets examine a sequence of states $\sigma_0, \sigma_1, \ldots, \sigma_n$ where each state is a descendant of the state written previous to it, also consider a second sequence of states $\sigma'_0, \sigma'_1, \ldots, \sigma'_m$ with the same property. Construct these two sequences so that their first members are equal $\sigma'_0 = \sigma_0$.

1. If σ_n is stable then $m \leq n$, also there is no vertex on the graph which will be collapsed more times in the first sequence then in the second sequence.

2. If σ_n and σ'_m are stable simultaneously then $m = n$ also the number of collapses of each vertex is equal in bot sequences.

Lemma 2: If the graph has a global sink, it can always be brought to a stable state.

Lets define the sand-grain addition operator E_{v_i}. The operators adds a grain on top of vertex i and collapses all the active vertices until the configuration reaches a stable state.

$$E_{v_i}\sigma = (\sigma + 1_{v_i})^{\circ} = (h1, h2, \ldots, h_i + 1, \ldots, h_n)^{\circ} \tag{1.135}$$

Lemma 3: In the arbitrary oriented graph if there is a global sink operator E is commutative.

If the operator E is commutative, then we call the sandpile model abelian. It should be noted that the existence of a global sink is a sufficient and necessary condition for the operator E to be commutative. Affecting the configuration σ with a sequence of E operators, brings to the same stable state when we add the sand-grains simultaneously and bring to a stable configuration.

As it is desirable to view the configurations before and after collapses, we consider the group Z^{n-1}/H where $H = Z^{n-1}\Delta'$. Consider the directed graph G which has n vertices and a global sink s. The graph G sandpile group is the following adjacent group:

$$S(G) = \frac{Z^{n-1}}{Z^{n-1}\Delta'} \tag{1.136}$$

Lemma 4: $S(G)$ groups order is equal to the Δ' reduced Laplasian's determinant.

Lemma 5: Consider the oriented graph G that has a global root. Each class of equivalence Z^{n-1} mod Δ' contains at least one stable configuration.

Configuration σ is called accessible if it can be attained from any other configuration using a particular sequence of E operators. If a configuration is stable and accessible, we call it a recurrent.

Lemma 6: Consider the oriented graph G that has a global root. Each class of equivalence Z^{n-1} mod Δ' contains at least one recurrent configuration.

Lemma 7: Consider $\varepsilon = (2\delta) - (2\delta)^{\circ}$ where $\delta = (d_{v_1}, d_{v_2}, \ldots, d_{v_n - 1})$ if σ is recurrent then $(\sigma + \varepsilon)^{\circ} = \sigma$.

Lemma 8: Each class of equivalence Z^{n-1} mod Δ' contains maximum one recurrent configuration.

Lemma 8: The following four statements are equivalent

1. σ is recurrent

2. if ξ is accessible from σ then σ is accessible from ξ

3. from any $E_v\sigma$ (where v is any none sink vertex) type of configuration σ is accessible

4. for any strong connected G/s there is a vertex v such that σ is accessible from $E_v\sigma$.

1.5 Random number generation

1.5.1 Monte Carlo method

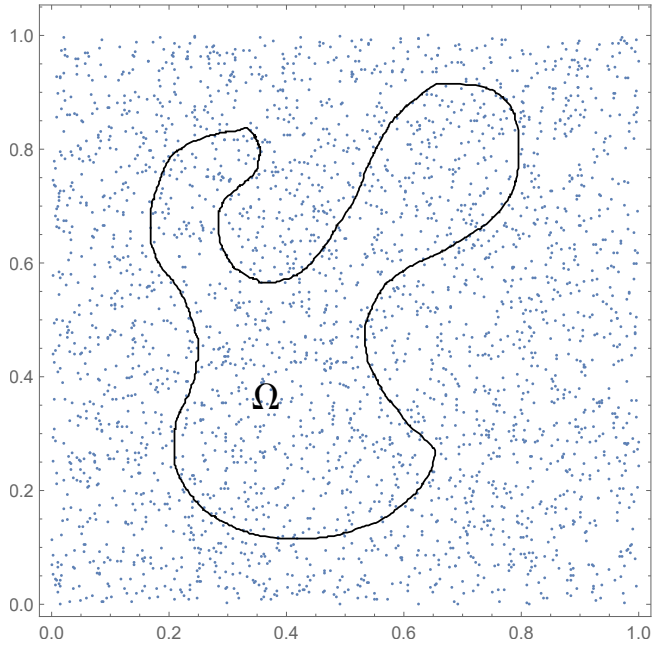

Figure 1.1: Finding Areas Using the Monte Carlo Method

Let us consider a unit square $\Pi \times \Pi$ (Π is the closed interval $[0,1]$). Inside the square we insert points ξ with unit probability distribution $\rho(\xi) = 1$ after this some region $\Omega \in \Pi^2$ is taken. The following expression which determines the area of Ω can be easily derived,

$$area\,\Omega = \frac{number\,of\,points\,inside\,\Omega}{N} \tag{1.137}$$

where N is the number of points ξ inside the square. Thus we are able to determine the area of regions. This method is widely known as the Monte Carlo method. The main challenge here is to generate

evenly distributed random numbers (two random numbers corresponds to every point in figure:1.1). Historically the first registered generator of pseudo-random numbers was the so called middle-square method. Let as discus the essence of the method with few words. The algorithm of generating pseudo-random numbers with the middle-square method has the following essential steps.

1. take a 2 digit number
2. square it
3. if it is shorter then 4 digits add zeros to the left side of the number
4. take the middle two digits of the number
5. repeat

For example $0(23)0 \to 0(52)9 \to 2(70)4 \to 4(90)0 \to 8(10)0 \to 0(10)0 \to 0(10)0$, our seed is 23 and the generated random numbers are $52, 70, 90, 10, 10, \ldots$. In practice it is not a good method, since its period is usually very short (as is in our example) and it has some other severe weaknesses, such as the output sequence converges to zero almost always.

1.5.2 Metropolis algorithm

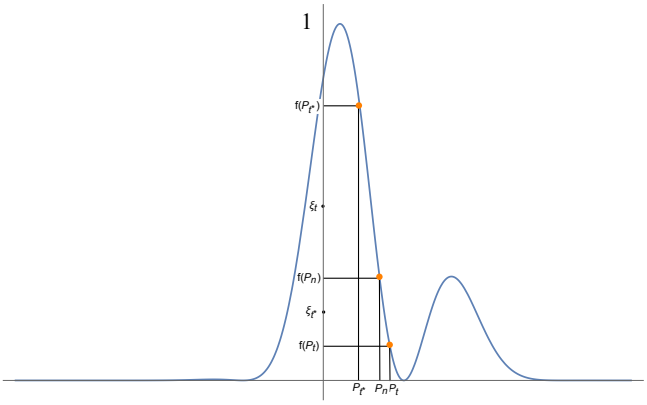

Figure 1.2: This picture presents the Metropolis algorithm, $\frac{f(P_t)}{f(P_n)} < \xi_t$ so we stayed at P_n, then we went on this time $\frac{f(P_{t*})}{f(P_n)} > \xi_{t*}$ so we jumped to P_{t*}

We introduce the so called Metropolis algorithm, and illustrate its application for the Ising model [76, 77]. The Metropolis Monte Carlo method is a computational approach (i.e., an algorithm)

for generating a set of N configurations of the system $P_0, P_1, \ldots, P_{N-1}$ such that

$$\frac{1}{N}\frac{dN(P)}{dP} = f(P)dP \tag{1.138}$$

where $N(P)dP$ is the multiplicity of configurations lying in the interval $[P, P+dP]$ and $f(P)$ is a given probability distribution.

The Metropolis algorithm can be understood as follows:

1. Pick a configuration P_n (the initial configuration can be any configuration of the system, a random point in the horizontal line of figure: 1.2).
2. Pick a trial configuration P_t and compute the ratio $R = \frac{f(P_t)}{f(P_n)}$.
3. Choose a random number ξ with value between 0 and 1 (any point on the vertical line of figure: 1.2).
4. if $\xi \leq R$ put $P_{n+1} = P_t$ else put $P_{n+1} = P_n$.
5. Go to the second step and replace P_n by P_{n+1}.

Repeat the same process N times.

Thus we'll obtain a one dimensional distribution which is given by the function $f(P)$. The prove that such an algorithm indeed produces an ensemble with distribution function $f(P)$ (see Eq.1.138) straightforward. Using the Metropolis algorithm one can easily compute the average of functions [78].

Figure 1.3: The picture shows the distribution of points after replaying the Metropolis algorithm

$$\int_{\Pi} f(P)dP = \frac{1}{N}\sum_{i=0}^{N-1} f(P_i), \tag{1.139}$$

$$\int_{\Pi} g(P)\ \frac{f(P)}{\int_{\Pi} f(P)dP}\ dP = \frac{1}{N}\sum_{i=0}^{N-1} g(\xi_i) \tag{1.140}$$

$$\int_{\Pi} g(P)\ f(P)dP = \frac{1}{N}\sum_{i=0}^{N-1} g(\xi_i)\ \int_{\Pi} f(P)dP \tag{1.141}$$

Note that Eq.1.141 reduces to Eq.1.139 by choosing $f(P) = 1$. In particular this algorithm can be used for the D dimensional Ising model by taking $f(x) = \exp^{-\beta V(x_1,\ldots,x_N)}$, as for the partition function it can be expressed as

$$Z(\beta) = \int \exp^{-\beta V(x_1,\ldots,x_N)}\ d^D x_1 \ldots d^D x_N \tag{1.142}$$

1.5.3 K-system pseudo-random numbers generators

Let us denote by $\Pi^{\mathfrak{D}}$ hypercube in $\mathfrak{D}$-dimensional space that is $\Pi^{\mathfrak{D}}$ consists of all points P with Cartesian coordinates $0 \leq x_i \leq 1\,(i = 1,\ldots,\mathfrak{D})$. The discrepancy is defined as

$$D_N(P_0,\ldots,P_{N-1}) = sup_{P\in\Pi^{\mathfrak{D}}} |N x_1 x_2 \ldots x_{\mathfrak{D}} - A_N| \tag{1.143}$$

where A_N is the number of points with coordinates P_i

$$0 \leq x_1^{(i)} \leq x_1, \ldots, 0 \leq x_{\mathfrak{D}}^{(i)} \leq x_{\mathfrak{D}}, \quad i = 0,\ldots,A_N - 1 \tag{1.144}$$

if the distribution is uniform $N x_1 \ldots x_{\mathfrak{D}}$ is the number of points in the region 1.144 see fig. 1.4. Therefore the maximal deviation of the real distribution of the points from the ideal one is estimated by D_N. One can get a maximal value for D_N by putting all points at $(1,1)$, thus $D_N = N$ so in general $D_N \leq N$. If $f(P)$ is continuous together with its first partial derivatives, it can be shown that

$$\left| \frac{1}{N}\sum_{k=0}^{\infty} f(P_k) - \int_{\Pi^{\mathfrak{D}}} f(P)\,dP \right| \leq C\frac{D_N}{N} \tag{1.145}$$

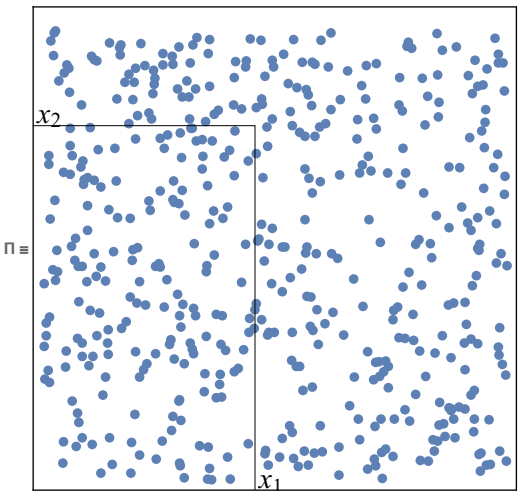

Figure 1.4: In this case $A_N = 5$

where $C > 0$ is a constant.

If one is not interested in the dynamical origin of the pseudo-random sequence P_i, but thinks of it as a sequence of a uniformly distributed random quantity ζ in a cube $\Pi^{\mathfrak{D}}$ with a probability density $\rho(\zeta) = 1$, therefore in agreement with the central limit theorem the rate of convergence in Eq. (1.145) with high probability will be $\frac{1}{\sqrt{N}}$. Thus for, ζ, $D_N \sim \sqrt{N}$.

To understand the behavior of D_N depending on the dynamical origin of P_i, let us consider the P_i sequence as a trajectory of some dynamical system. Let as assume that the cube $\Pi^{\mathfrak{D}}$ is the phase space of the dynamical system T, therefore

$$P_i = T \cdot T \cdot \cdots \cdot T \cdot P_0 \equiv T^i P_0 \tag{1.146}$$

where P_0 is the initial point of the trajectory. In this context the sequence of points P_i represents one of the trajectories of the dynamical system T. We assume that the Liouville theorem holds, i.e. the phase volume of this dynamical system is conserved. We can reformulate the statement in (1.145) by considering the pseudo-random number generator as a dynamical system. Then the rate of convergence is governed by the dynamical properties of a system T:

$$\left| \frac{1}{N} \sum_{i=0}^{N-1} f(T^i P_0) - \int_{\Pi^{\mathfrak{D}}} f(P)\, dP \right| \leq C \frac{D_N(T)}{N} \tag{1.147}$$

A natural question arises. How to get the best rate of convergence $D_N(T)$? Possible maps are classified as follows.

1. ergodic maps

$$\lim_{t\to\infty}\frac{1}{t}\int dt\,\mu(T^tA\cap B)=\mu(A)\mu(B)$$

2. mixing maps

$$\lim_{t\to\infty}\mu(T^tA\cap B)=\mu(A)\mu(B)$$

3. n-fold mixing maps

$$\lim_{t_1,t_2,\ldots,t_n\to\infty}\mu(A_0\cap T^{t_1}A_1\cap T^{t_2+t_1}A_2\cap\ldots T^{t_1+\cdots+t_n}A_n)=\mu(A_1)\mu(A_2)\ldots\mu(A_n)$$

One easily observes that if a map is n-fold mixing so it is mixing and if a map is mixing then it is also ergodic. In general the reverse statement is not true.

Kolmogorov entropy $(0\leq h(T)\leq\infty)$is one of the best ways to describe the statistical properties of a dynamical system [79–82]. One can define it by starting with the usual entropy $H(\xi)$ with ξ a collection of region C, $\xi=\{C\}$, so

$$H=\sum_{C\in\xi}\mu(C)\ln\mu(C) \tag{1.148}$$

To clarify this lets discus a simple example. Namely we will calculate the entropy of some ξ's depicted in figure: 1.5. Here a unit total area of regions is assumed.

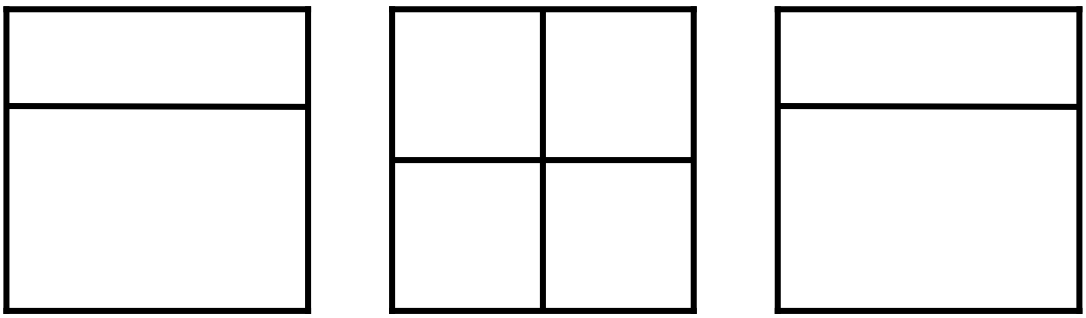

(a) (b) (c)

Figure 1.5: This picture shows haw ρ looks like

- region $\xi = \{C_1, C_2\}$ correspond to 1.5a

$$H = -\frac{1}{2}\ln\frac{1}{2} - \frac{1}{2}\ln\frac{1}{2} = \ln 2, \tag{1.149}$$

- region $\xi = \{C_1, C_2, C_3, C_4\}$ correspond to 1.5b

$$H = -\frac{1}{4}\ln\frac{1}{4} - \frac{1}{4}\ln\frac{1}{4} - \frac{1}{4}\ln\frac{1}{4} - \frac{1}{4}\ln\frac{1}{4} = -\ln\frac{1}{4} = 2\ln 2, \tag{1.150}$$

- region $\xi = \{C_1, C_2\}$ correspond to 1.5c

$$H = -\frac{1}{2}\ln\frac{1}{2} - \frac{2}{3}\ln\frac{2}{3} = \ln 3 - \frac{2}{3}\ln 2 \tag{1.151}$$

One observes from this examples that when the space is split into more and more pieces the entropy groves. If multiple splits $\xi_1, \xi_2, \ldots, \xi_\alpha, \ldots$ the entropy is

$$H(\bigvee_\alpha \xi_\alpha) = -\sum \mu\left[\bigcap_\alpha C_\alpha\right] \log \mu\left[\bigcap_\alpha C_\alpha\right] \tag{1.152}$$

This splits can be generated with the help of a dynamical system T, $T^{t=1} = T$ in such a way that the expression of the entropy becomes $(\xi, T\xi, T^2\xi, \ldots)$

$$H_n(\xi, T) = H\left(\xi \vee T\xi \vee T^2\xi, \ldots\right) \tag{1.153}$$

In this case the Kolmogorov entropy can be defined as [83–86]

$$h(T) = \sup_{\xi} \lim_{n\to\infty} \frac{1}{n} H_n(\xi, T) \tag{1.154}$$

The relaxation time is the time during which the system reaches a uniform distribution is called. K-systems are systems with nonzero Kolmogorov entropy. Because of the K-system have exponential instability their relaxation time is maximally rapid. The quick relaxation of a dynamical system T is equivalent to the slow grows of the discrepancy $D_N(T)$.

Let as consider a special case of Eq.(1.146) as an example:

$$P_i = \{KP_{i-1}\} \tag{1.155}$$

where the fractional part of a number is denoted by $\{\}$. We assume that $K \gg 1$ is a fixed integer number, under such condition the Liouville theorem holds. The correlation function for this system behaves like

$$R_N = \frac{1}{12} \exp^{-N \ln K} \tag{1.156}$$

The correlation splitting time is determined by the characteristic K.

$$\tau_0 = \frac{1}{\ln K} \tag{1.157}$$

Consider the set of points in a very small interval $\delta P^0 \ll \frac{1}{K}$. The trajectories, coming from these points, almost uniformly fill the interval $[0,1]$ in time τ:

$$\tau = \tau_0 \ln \frac{1}{\delta P^0} \tag{1.158}$$

In this system the characteristic are coupled by this relation

$$\tau_0 < \tau \tag{1.159}$$

We see that the pseudo-random number generators growth of the deviation $D_N(T)$, depends on the statistical properties of T and how this generator is characterized by the relaxation time τ. Certainly it is better to use more unstable systems T. We define the Anosov K-systems T to be a matrix $T = ||a_{kl}||$ satisfying two constrains

1. the unit determinant, $det||a_{kl}|| = 1$.

2. T can't have an eigenvalue with unit modulus , $|\lambda_k| \neq 1$.

The first condition ensures that the map defines a volume preserving automorphism. The second condition ensures that nearby trajectories diverge exponentially when the automorphism is viewed as a tool defining a dynamical system with discrete time $t \in \mathbb{Z}$, . The Kolmogorov entropy of this systems is

$$h(T) = \sum_{|\lambda_k|>0} \ln|\lambda_k| \tag{1.160}$$

and the correlation splitting time is

$$\tau_0 = \frac{1}{h(T)} = \frac{1}{\sum_{|\lambda_k|>0} \ln|\lambda_k|} \tag{1.161}$$

1.5.4 Results

Lets consider $T(N,s)$ which is a family of matrix operators which produces a K-system [87, 88],

$$T(N,s) = \begin{pmatrix} 1 & 1 & 1 & 1 & \cdots & 1 & 1 \\ 1 & 2 & 1 & 1 & \cdots & 1 & 1 \\ 1 & 3+s & 2 & 1 & \cdots & 1 & 1 \\ 1 & 4 & 3 & 2 & \cdots & 1 & 1 \\ \vdots & \vdots & \vdots & \vdots & \ddots & \vdots & \vdots \\ 1 & N & N-1 & N-2 & \cdots & 3 & 2 \end{pmatrix} \tag{1.162}$$

this matrix has dimensions of $N \times N$, where each element is a integer $A_{ij} \in \mathbb{Z}$ also s labels the members of the family. Notice that the determinant of this matrix is one and its eigenvalues don't lie on a unit circle.

The Kolmagorov entropy is one of the most important quantities that characterizes the ergodic properties of the K-system generators, see Eq. 1.160 .

Size	Magic	Entropy
N	s	h
256	-1	164.473
256	487013230256099064	193.583
240	487013230256099348	183.417
423	0	272.423
523	0	337.037
723	0	466.262

The entropy $h(T)$ defines the number $\pi(\tau)$ of periodic trajectories with period less or equal to τ

$$\pi(\tau) \to \frac{e^{h\tau}}{h\tau} \tag{1.163}$$

It is not possible to simulate on a computer trajectories that are not periodic. The following matrix operator also represents a K-system $A(N,m,s)$

$$A(N,m,s) = \begin{pmatrix} 1 & 1 & 1 & 1 & \cdots & 1 & 1 \\ 1 & 2 & 1 & 1 & \cdots & 1 & 1 \\ 1 & 2+m+s & 2 & 1 & \cdots & 1 & 1 \\ 1 & 2+2m & 2+m & 2 & \cdots & 1 & 1 \\ \vdots & \vdots & \vdots & \vdots & \ddots & \vdots & \vdots \\ 1 & 2+(N-2)m & 2+(N-3)m & 2+(N-4)m & \cdots & m+2 & 2 \end{pmatrix} \tag{1.164}$$

the family members of this operators are labeled by two parameters m and s. It's obvious that when we put $m = 1$ then $A = T$

Size N	Magic s	Magic m	Entropy h
8	0	$2^{53}+1$	220.421
17	0	$2^{36}+1$	374.299
40	0	$2^{42}+1$	1106.26
60	0	$2^{52}+1$	2090.53
96	0	$2^{55}+1$	3583.57
120	1	$2^{51}+1$	4171.36
240	487013230256099140	$2^{51}+1$	8418.8

Chapter 2

Superstable cycles and magnetization plateau for antiferromagnetic spin-1 Ising and Ising-Heisenberg models on diamond chains

2.1 Introduction

The theory of dynamical systems, besides its intrinsic theoretical relevance, recently had a significant impact on a wide range of disciplines from physics to ecology and economics, providing methodological tools which are currently employed in financial and economic forecasting, environmental modelling, medical diagnosis, industrial equipment diagnosis and so on [89, 90]. An important physical setting in which such dynamical techniques are profitably applied is equilibrium statistical mechanics of lattice models, more specifically in the investigation of physical properties of low-dimensional classic and quantum spin systems in an external magnetic field.

In this paper we apply dynamical techniques in the analysis of Ising and Ising-Heisenberg spin models on a diamond chain, which are of current interest for a number of reasons. As a matter of fact, these models can be solved exactly by using different mathematical methods, and they exhibit a wide range of interesting properties such as the appearance of intermediate plateaus in the magnetization curves, geometric spin frustration, multiple peak structure of the magnetic susceptibility and specific

heat [91–101].

The dynamical systems approach [102,103] has been used in many different physical situations, deepening our understanding of the phase structure and critical properties of spin and gauge models: it is particularly powerful in the analysis of exact solution of spin models on hierarchical lattices, which in many cases accurately approximate real ones (the so called Bethe-Peierls approximation). The specific dynamical method we will employ is the recursion relations method, where the lattice is cut into branches, and the full partition function is expressed in terms of the reduced partition functions of all branches. This procedure allows to derive one- or multi-dimensional mappings for branches of the partition function, providing as well recursion relations for the relevant thermodynamic quantities, such as magnetization, magnetic susceptibility and specific heat.

In order to motivate our analysis, we remark that spin-1 Ising and Ising-Heisenberg models on diamond chains are a very good approximation for atoms of homometallic magnetic complex $[Ni_3(C_4H_2O_4)_2(\mu_3-OH)_2\ (H_2O)_4]_n\cdot(2H_2O)_n$ [104] [105], and the molecular compound $[Ni_8(\mu_3-OH)_4(OMe)_2(O_3PR_1)_2\ (O_2C^tBu)_6\ (HO_2C^tBu)_8]$ [106]. Magnetic-property measurements on such compounds indicate the coexistence of both antiferromagnetic and ferromagnetic interactions between the magnetic centers, Ni ions with spin 1, which indeed suggests to investigate theoretically the magnetic properties of such compounds. Another related interesting material is $Cu_3(CO_3)_2(OH)_2$ -known as natural azurite (Copper Carbonate Hydroxide)- which can be well described by using the quantum antiferromagnetic Heisenberg model on a generalized diamond chain [7, 8, 107]. A remarkable feature of these systems is their exact solvability through recurrence relations techniques; within this method, as we already mentioned, statistical properties of a system are associated to one or multidimensional rational mappings. In the antiferromagnetic case both models exhibit a complex behavior, featuring superstable points and cycles, and magnetic plateaus.

The aim of this paper is to study the dynamical approach, and notably superstability in the above mentioned models [108–112]. We propose a non-trivial connection of superstable points and Lyapunov exponents to magnetic plateaus.

The paper is organized as follows: in the next section we give a brief description of the spin-1 Ising and Ising-Heisenberg models on diamond chains and we describe how the dynamical approach

allows a detailed analysis of physical properties. In Section 3 we address stability features of the dynamical mappings we derived for such models, and their connections with magnetization; in addition we compare our results with the experimental data in [104]. Finally, in Section 4, we present our concluding remarks.

2.2 Models and their dynamic solutions

In this section we describe the quantum spin-1 Ising-Heisenberg model and the classical spin-1 Ising model, both on diamond chain. Since the equations for both models are rather similar we will explicitly consider one case, providing further details in the Appendix. The spin-1 Ising-Heisenberg model on a diamond chain (see Fig 2.1) and its classic analogue (spin-1 Ising model on a diamond chain) are defined by the following Hamiltonians, written in terms of block contributions:

$$\begin{aligned} H_{IH} = \sum_{i}^{N} H_{IH,i} = \sum_{i}^{N} (J(S^x_{a,i}S^x_{b,i} + S^y_{a,i}S^y_{b,i} + S^z_{a,i}S^z_{b,i}) + K(S^x_{a,i}S^x_{b,i} \\ + S^y_{a,i}S^y_{b,i} + S^z_{a,i}S^z_{b,i})^2 + J_1(\mu^z_i + \mu^z_{i+1})(S^z_{a,i} + S^z_{b,i}) + K_1((\mu^z_i)^2 \\ + (\mu^z_{i+1})^2)((S^z_{a,i})^2 + (S^z_{b,i})^2) + \Delta((S^z_{a,i})^2 + (S^z_{b,i})^2) + \Delta_1 \frac{(\mu^z_i)^2 + (\mu^z_{i+1})^2}{2} \\ - h_H(S^z_{a,i} + S^z_{b,i}) - h_I \frac{\mu^z_i + \mu^z_{i+1}}{2}) \end{aligned} \tag{2.1}$$

and

$$\begin{aligned} H_I = \sum_{i}^{N} H_{I,i} = \sum_{i}^{N} (J(S_{a,i}S_{b,i}) + K(S_{a,i}S_{b,i})^2 + J_1(\mu_i + \mu_{i+1})(S_{a,i} + S_{b,i}) \\ + K_1((\mu_i)^2 + (\mu_{i+1})^2)((S_{a,i})^2 + (S_{b,i})^2) + \Delta((S_{a,i})^2 + (S_{b,i})^2) \\ + \Delta_1 \frac{(\mu_i)^2 + (\mu_{i+1})^2}{2} - h_H(S_{a,i} + S_{b,i}) - h_I \frac{\mu_i + \mu_{i+1}}{2}) \end{aligned} \tag{2.2}$$

In the Ising-Heisenberg Hamiltonian $S_{a,i}$, $S_{b,i}$ are quantum Heisenberg spins and μ_i, μ_{i+1} are classical Ising spins. The parameter J accounts for the interactions between the nearest-neighbouring Heisenberg spins ($S_{a,i}$-$S_{b,i}$) and J_1 is the interactions parameter for nearest-neighbouring Ising and Heisenberg spins ($S_{a/b,i}$-$\mu_{i/i+1}$). Analogously, K and K_1 govern quadratic interactions. Δ and Δ_1 are

the single-ion anisotropy parameters (crystal fields), h_I and h_H represent contributions of a longitudinal external magnetic field, interacting with the Heisenberg spins and Ising spins correspondingly. The parameters in Ising Hamiltonian are the same as in Ising-Heisenberg but in such a case $S_{a,i}$, $S_{b,i}$ are Ising spins. For the quantum Ising-Heisenberg case it can be shown that the block Hamiltonian commutes with Ising and Heisenberg spins, i.e. $[H_{IH,i},\mu_j^z] = [H_{IH,i},S_{a,j}^z + S_{b,j}^z] = 0$ for any values of the model parameters. On the other side, block Hamiltonian and quadrupole moment commute, ($[H_{IH,i},(S_{a,j}^z)^2 + (S_{b,j}^z)^2] = 0$), only when $J = K$. In further calculations we assume that $K = J$, $K_1 = J_1$, $\Delta = \Delta_1$, $h_H = h_I = h$.

The partition functions, single site magnetic and quadrupole moments for the quantum case are given by the following expressions:

$$Z_{IH} = \sum_{\mu_i,S_{a,i},S_{b,i}} e^{-\beta\mathcal{H}_{IH}} = \sum_{\mu_0} e^{-\frac{-h_I\mu_0^z+\Delta_1(\mu_0^z)^2}{T}} g_n(\mu_0^z)^2 \tag{2.3}$$

$$m_\mu = <\mu_i^z> = \frac{\sum_{\mu_i,S_{a,i},S_{b,i}}(\mu_i^z)e^{-\beta\mathcal{H}_{IH}}}{Z_{IH}} \tag{2.4}$$

$$m_S = \frac{<S_{a,i}^z + S_{b,i}^z>}{2} = \frac{\sum_{\mu_i,S_{a,i},S_{b,i}}(S_{a,i}^z + S_{b,i}^z)e^{-\beta\mathcal{H}_{IH}}}{Z_{IH}} \tag{2.5}$$

$$p_\mu = <(\mu_i^z)^2> = \frac{\sum_{\mu_i,S_{a,i},S_{b,i}}(\mu_i^z)^2 e^{-\beta\mathcal{H}_{IH}}}{Z_{IH}} \tag{2.6}$$

$$p_S = \frac{<(S_{a,i}^z)^2 + (S_{b,i}^z)^2>}{2} = \frac{\sum_{\mu_i,S_{a,i},S_{b,i}}(S_{a,i}^z)^2 + (S_{b,i}^z)^2 e^{-\beta\mathcal{H}_{IH}}}{Z_{IH}} \tag{2.7}$$

where we have set $k_B = 1$ (see the Appendix for the classical case). The total magnetization and quadrupole moment per site are given by the following expressions:

$$m = \frac{m_\mu + 2m_S}{3}, \quad p = \frac{p_\mu + 2p_S}{3} \tag{2.8}$$

By cutting the diamond chain at μ_0 into two branches -$g_n(\mu_0)$- (see Fig 2.1) an exact recursion relation for the partition function can be derived:

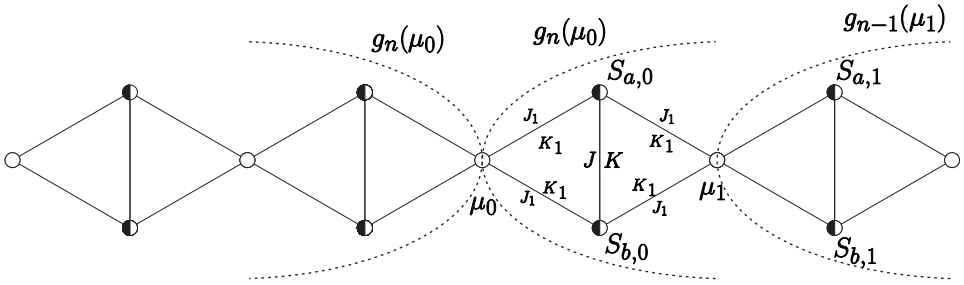

Figure 2.1: The structure for the Ising (S_a and S_b are white) and Ising-Heisenberg (S_a and S_b are black) diamond chain. White circles are Ising spins and black ones are Heisenberg spins.

$$x_n = \frac{g_n(1)}{g_n(0)} = f_1(x_{n-1}, y_{n-1}), \qquad y_n = \frac{g_n(-1)}{g_n(0)} = f_2(x_{n-1}, y_{n-1}), \tag{2.9}$$

For both models the recursion functions have the following form:

$$f_1(x,y) = \frac{a_0 + a_1 x + a_2 y}{c_0 + c_1 x + c_2 y} \tag{2.10}$$

$$f_2(x,y) = \frac{b_0 + b_1 x + b_2 y}{c_0 + c_1 x + c_2 y}, \tag{2.11}$$

where the parameters $a_0 - c_2$ can be found in the Appendix. By using the recursion relations, the calculations of magnetic and quadrupole moments are straightforward. The magnetic and quadrupole moments are shown in Fig 2.2 and 2.3 for the Ising case, and, for the Ising-Heisenberg case, in Fig 2.4 and 2.5.

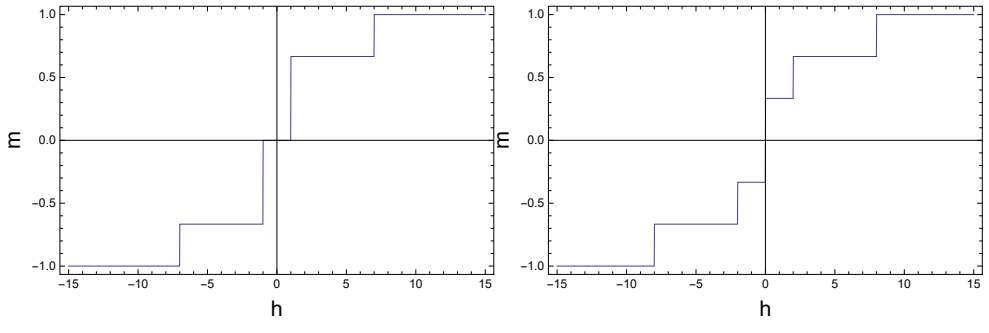

(a) $\Delta = -1$ (b) $\Delta = 0$

(c) $\Delta = 1$ (d) $\Delta = 2$

Figure 2.2: Magnetization dependence on the external field for the classical case ($J = 1$, $J_1 = 1$, $T = 10^{-7}$).

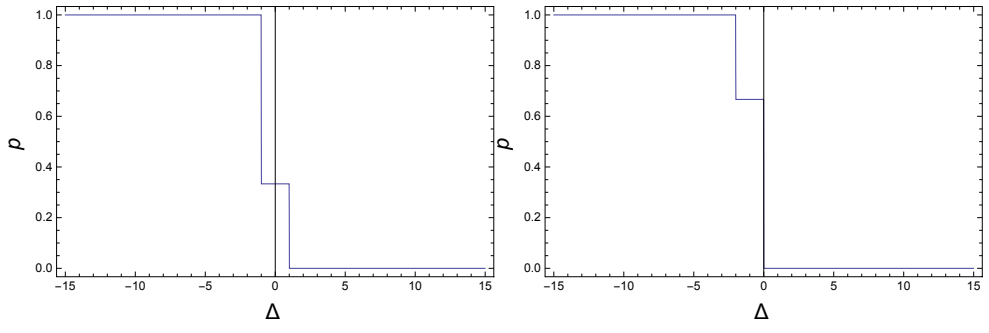

(a) $h = -1$ (b) $h = 0$

(c) $h = 1$ (d) $h = 2$

Figure 2.3: Quadrupole moment dependence on the single-ion anisotropy parameter for the classical case ($J = 1$, $J_1 = 1$, $T = 10^{-6}$).

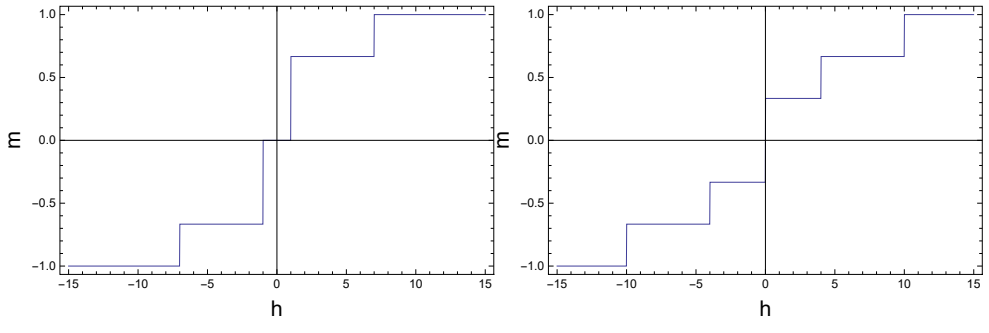

(a) $\Delta = -1$ (b) $\Delta = 2$

(c) $\Delta = 3$ (d) $\Delta = 5$

Figure 2.4: Magnetization dependence on the external field for the quantum case ($J = 1$, $J_1 = 1$, $T = 10^{-7}$).

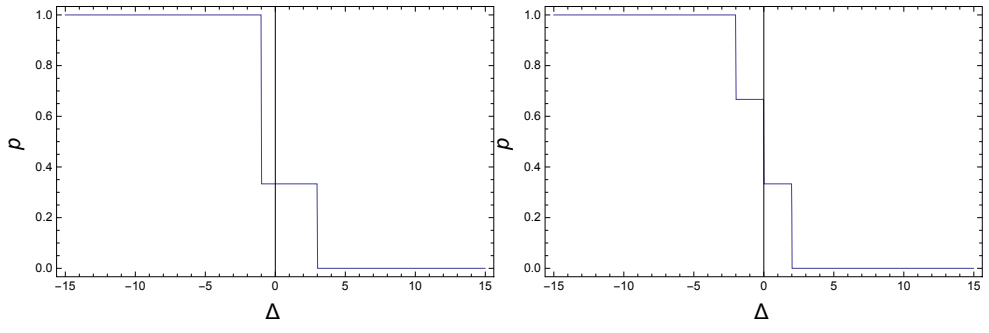

(a) $h = -1$ (b) $h = 0$

(c) $h = 1$ (d) $h = 2$

Figure 2.5: Quadrupole moment dependence on the single-ion anisotropy parameter for the quantum case ($J = 1$, $J_1 = 1$, $T = 10^{-6}$).

2.3 Lyapunov exponents and superstable points

Lyapunov exponents [113] quantify the growth rate of an infinitesimal perturbation on a reference trajectory, and they provide a measure of the degree of "instability" of the system: a positive maximum Lyapunov exponent corresponds to chaotic, unstable states, while a negative maximum Lyapunov exponent signals stable states. Such exponents are computed from dynamical recursion equations: a zero maximum Lyapunov exponents is the dynamic counterpart of a second-order phase transition. We recall that if we have a N dimensional map then a spectrum of N exponents is present; the $i-th$ Lyapunov exponent is calculated by the following equation (see [113–115])

$$\lambda_i = \lim_{n\to\infty} \frac{\log H_i}{2n}, \;\; \mathbf{H} = J(x_0)J(x_1)...J(x_n) \tag{2.12}$$

where H_i is the $i-th$ eigenvalue of $\mathbf{H}^\dagger\mathbf{H}$ and $J(x_k)$ is the Jacobian matrix of our N dimensional map after k iterations from the initial point x_0. We used a standard (Gram-Schmidt) [113] numerical procedure to compute both Lyapunov exponents for our 2 dimensional recursion relations.

When examining dynamical properties of recursion relations, it is natural to start by an investigation of fixed points, such that $f_1(x,y) = x$ and $f_2(x,y) = y$. For both classical and quantum models the structure of fixed point equations greatly simplifies when $h = 0$, as in this case we get:

$$f_1(x,y) = \frac{a_0 + a_1 x + a_2 y}{c_0 + c_1 x + c_1 y} \tag{2.13}$$

$$f_2(x,y) = \frac{a_0 + a_2 x + a_1 y}{c_0 + c_1 x + c_1 y}; \tag{2.14}$$

for which a stable fixed point with $x = y$ can be found. This turns out to be the only physically significant fixed point, as the other goes to infinity when $T \to 0$. We notice a striking similarity between the structure of ground states ($T = 0$), and the parameters dependence of both the stable fixed point and quadrupole moment, see Fig. 2.6: this suggests a strong connection between magnetization, quadrupole moment and Lyapunov exponents. We also investigated numerically when stable fixed points become superstable, that is when stability is maximal, yielding a negatively diverging maximal

Lyapunov exponent (see Fig. 2.7). The computation of Lyapunov exponents for physically reasonable parameters leads to the observation of a remarkable symmetry between superstable points and magnetization plateaus. Our investigations show the existence of a zero magnetization plateau around $h = 0$ if there is a superstable point. We have performed a detailed search on the conditions for the existence of superstable orbits: in the classical case it is $\Delta > 0$ (see Fig 2.8): this coincides with the the non-magnetic (NM) phase in the ground states diagram as well as with a well defined region in the stable fixed points diagram and the quadrupole moment $p = 0$ plateau (see Fig 2.6a, 2.6b, 2.6c). In the quantum case the superstable points existence condition is $\Delta > 2J$ (see Fig 2.9); like in the classical case this condition also coincides with the non-magnetic phase in the ground states (for a detailed discussion on the ground states with transfer matrix technique see [12], the eigenvectors and eigenvalues of the phases can be found in the Appendix see Eq. 2.24,2.25,2.26,2.27,2.28), a region in stable fixed points diagram and the quadrupole moment $p = 0$ plateau (see Fig 2.6d, 2.6e, 2.6f). We observe a magnetization plateau correspondence with a non superstable maximum Lyapunov exponent plateau at or near $h = 0$ (see Fig. (2.2a,2.8a),(2.2b,2.8b) for the classical case and Fig (2.4a,2.9a) for the quantum caseand for $J = \Delta$ see Fig. (2.4b,2.9b). Another interesting observation is the one to one correspondence of the first plateau of the Lyapunov exponent and first non zero plateau of magnetization in the presence of a superstable point (for the classical case $\Delta > 0$ and for the quantum case $\Delta > 2J$). Unfortunately the next plateau for $T = 0.03$ does not fit in this picture, maybe due to T being not sufficiently close to zero.

We conclude with a comment on our results when compared with the experimental data from [104], where spin-1 antiferromagnetic nodal-interstitial (dimer-monomer) Ising coupling and ferromagnetic interstitial-interstitial Heisenberg coupling on a diamond chain was considered. To this end we assume that $K = K_1 = 0$ and the existence of different crystal fields [105]. The numerical calculations show that there are a number of configurations with superstable points, two of the more interesting configurations being $J = -2$, $\Delta_1 = 2$, $J_1 = 1$ and $J = -6$, $\Delta_1 = 4$, $J_1 = 1$ with ferromagnetic Heisenberg coupling constant and antiferromagnetic Ising couplings, see Fig. (2.10). In these cases the decreasing part close to superstable point as well as the first Lyapunov exponent plateau again correspond to magnetization plateaus.

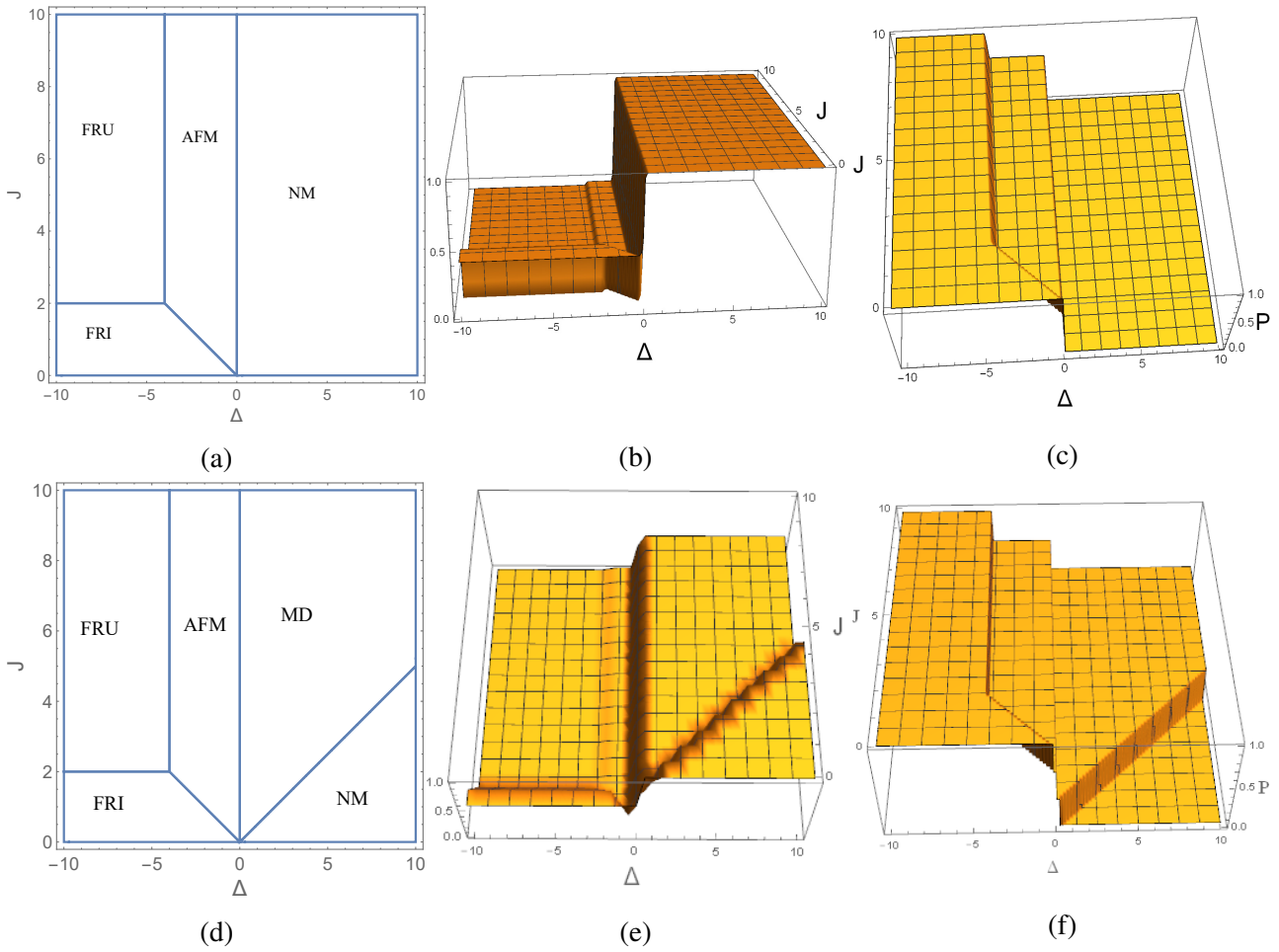

Figure 2.6: Figures a, b, c show the ground states, stable fixed point x diagrams and quadrupole moment for classical case, while figures d, e, f refer to the quantum case. In the above figures $J = 1$, $J_1 = 1$, $h = 0$ for the stable point x diagrams and quadrupole moments: the temperatures are $T = 0.025$ and $T = 0.001$ respectively.

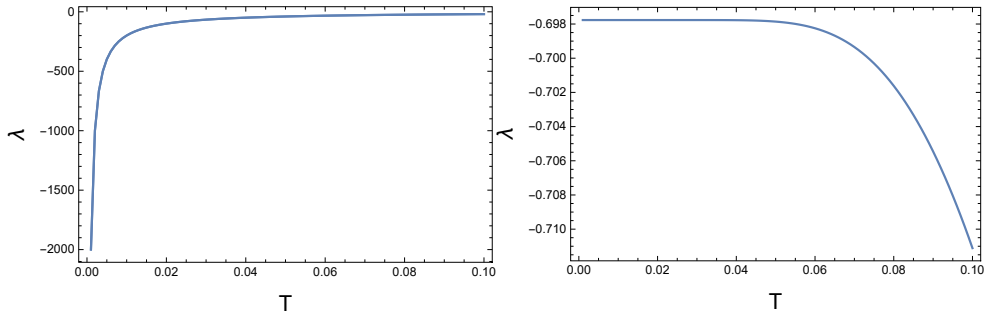

(a) $h = 0$ (b) $h = 1.5$

Figure 2.7: The maximum Lyapunov exponent as a function of $0.001 < T < 0.1$ for the classical case ($J = 1, J_1 = 1, \Delta = 1$).

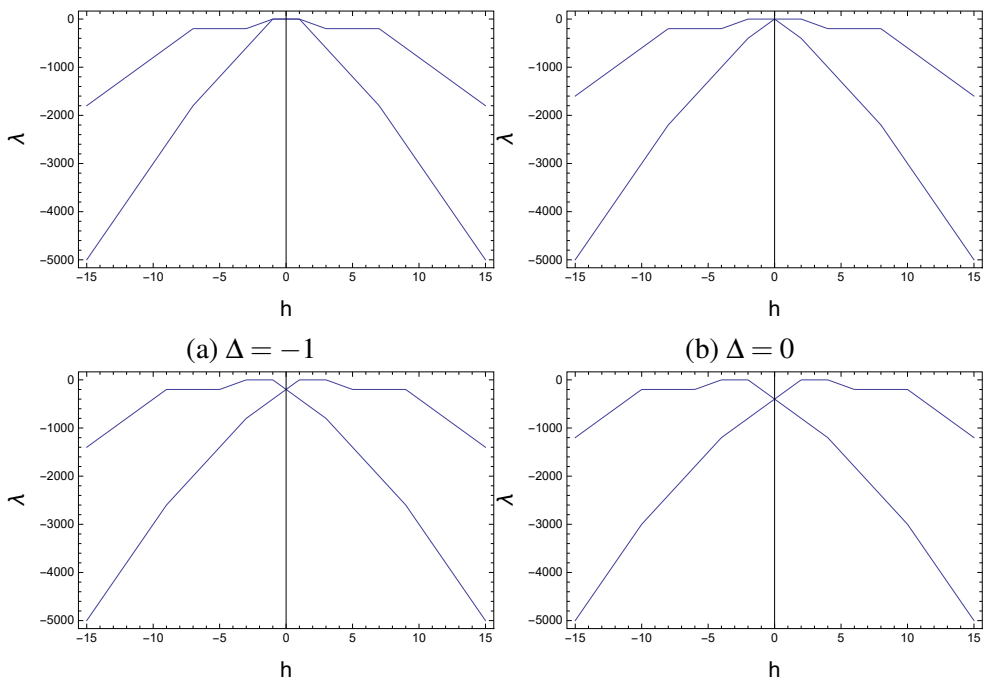

(a) $\Delta = -1$ (b) $\Delta = 0$

(c) $\Delta = 1$ (d) $\Delta = 2$

Figure 2.8: The Lyapunov exponent dependence on the external magnetic field for the classical case($J = 1, J_1 = 1, T = 0.01$) .

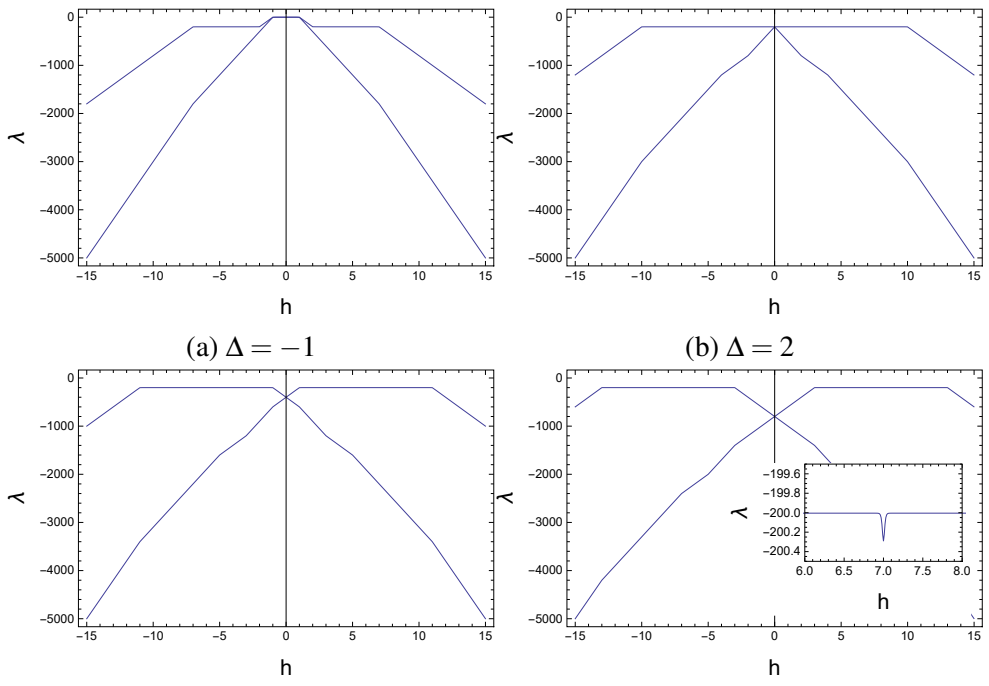

(a) $\Delta = -1$ (b) $\Delta = 2$

(c) $\Delta = 3$ (d) $\Delta = 5$

Figure 2.9: The Lyapunov exponent dependence on the external magnetic field for the quantum case ($J = 1, J_1 = 1, T = 0.01$).

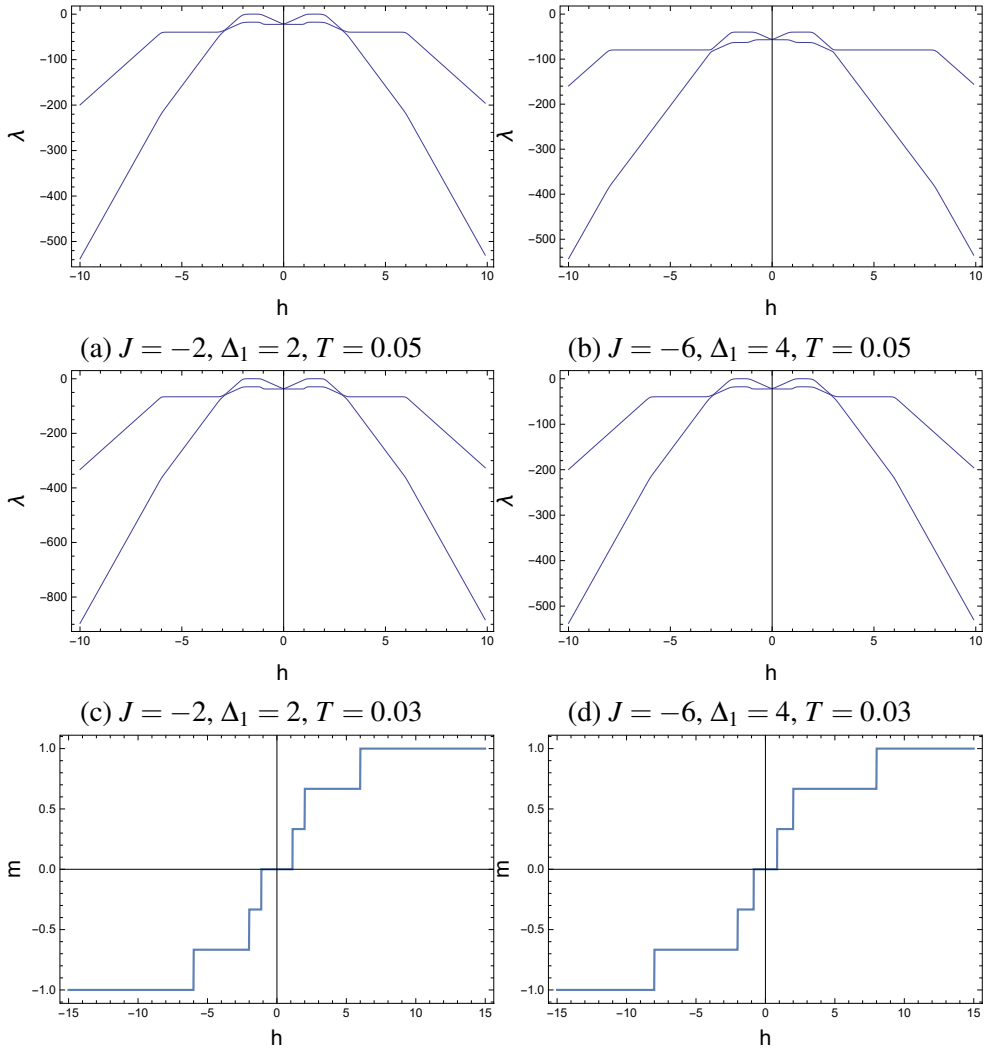

(a) $J = -2$, $\Delta_1 = 2$, $T = 0.05$ (b) $J = -6$, $\Delta_1 = 4$, $T = 0.05$

(c) $J = -2$, $\Delta_1 = 2$, $T = 0.03$ (d) $J = -6$, $\Delta_1 = 4$, $T = 0.03$

(e) $J = -2$, $\Delta_1 = 2$, $T = 10^{-6}$ (f) $J = -6$, $\Delta_1 = 4$, $T = 10^{-6}$

Figure 2.10: Figures *a*, *b*, *c* and *d* show the behavior of Lyapunov exponents for $K = K_1 = 0$, $J_1 = 1$ and $\Delta = 2$, while figures *e*, *f* display the magnetization for the same values of the parameters

2.4 Discussion and conclusions

In the present work, we studied the connections between stability and magnetic properties of the spin-1 Ising and Ising-Heisenberg models on the diamond chain. The dynamical solution of the model is obtained by using the recursion relations method. The Lyapunov exponents, magnetic and quadrupole moments, superstable points and cycles of the system at $T \to 0$ have been analyzed. For the first time in spin-1 models on a diamond chain we provide evidence of the existence of zero magnetization plateau around superstable points. Also the first maximum Lyapunov exponent plateau is rather similar to the second plateau of magnetization if there exists a superstable point. This is conjectured to be indicative of a more general connection between magnetization plateaus and maximum Lyapunov exponents for both classical and quantum models. Furthermore the remarkable connection between ground states and stable fixed points suggests a non-trivial relation between them. The superstable points and quadrupole moment $p = 0$ plateau relation at zero external magnetic field is also noteworthy. Finally we believe its worthwhile investigating connections of a similar nature for more complex systems such as a diamond-like decorated Bethe lattice for different temperatures.

2.5 Appendix

The partition function for the classical case has the following form:

$$Z_I = \sum_{\mu_i, S_{a,i}, S_{b,i}} e^{-\beta \mathcal{H}_I} = \sum_{\mu_0} e^{-\frac{-h_I \mu_0 + \Delta_1 \mu_0^2}{T}} g_n(\mu_0)^2 \tag{2.15}$$

Similarly single site magnetic and quadrupole moments for the classical case have the following expression:

$$m_\mu = <\mu_i> = \frac{\sum_{\mu_i, S_{a,i}, S_{b,i}} (\mu_i) e^{-\beta \mathcal{H}_I}}{Z_I} \tag{2.16}$$

$$m_S = \frac{< S_{a,i} + S_{b,i} >}{2} = \frac{\sum_{\mu_i, S_{a,i}, S_{b,i}} (S_{a,i} + S_{b,i}) e^{-\beta \mathcal{H}_I}}{Z_I} \tag{2.17}$$

$$p_\mu = < (\mu_i)^2 > = \frac{\sum_{\mu_i, S_{a,i}, S_{b,i}} (\mu_i)^2 e^{-\beta \mathcal{H}_I}}{Z_I} \tag{2.18}$$

$$p_S = \frac{< (S_{a,i})^2 + (S_{b,i})^2 >}{2} = \frac{\sum_{\mu_i, S_{a,i}, S_{b,i}} (S_{a,i})^2 + (S_{b,i})^2 e^{-\beta \mathcal{H}_I}}{Z_I} \tag{2.19}$$

Note that $g_n(\mu_0)$ in the quantum case has a different form than in classical case: $g_n(\mu_0)$ in the quantum case is given by the following equation:

$$\begin{aligned} g_n(\mu_0) = \sum_{S_{a,0}, S_{b,0}, \mu_1} \exp \Big(& J(S^x_{a,0} S^x_{b,0} + S^y_{a,0} S^y_{b,0} + S^z_{a,0} S^z_{b,0}) + K(S^x_{a,0} S^x_{b,0} + S^y_{a,0} S^y_{b,0} \\ & + S^z_{a,0} S^z_{b,0})^2 + J_1(\mu^z_0 + \mu^z_1)(S^z_{a,0} + S^z_{b,0}) + K_1((\mu^z_0)^2 + (\mu^z_1)^2)((S^z_{a,0})^2 \\ & + (S^z_{b,0})^2) + \Delta((S^z_{a,0})^2 + (S^z_{b,0})^2) + \Delta_1(\mu^z_1)^2 - h_H(S^z_{a,0} + S^z_{b,0}) \\ & - h_I \mu^z_1 \Big) g_{n-1}(\mu^z_1) \end{aligned} \tag{2.20}$$

while for the classical case $g_n(\mu_0)$ has the following form:

$$\begin{aligned} g_n(\mu_0) = \sum_{S_{a,0}, S_{b,0}, \mu_1} \exp \Big(& J(S_{a,0} S_{b,0}) + K(S_{a,0} S_{b,0})^2 + J_1(\mu_0 + \mu_1)(S_{a,0} + S_{b,0}) \\ & + K_1(\mu_0^2 + \mu_1^2)((S_{a,0})^2 + (S_{b,0})^2) + \Delta((S_{a,0})^2 + (S_{b,0})^2) + \Delta_1(\mu_1)^2 \\ & - h_H(S_{a,0} + S_{b,0}) - h_I \mu_1 \Big) g_{n-1}(\mu_1) \end{aligned} \tag{2.21}$$

$g_{n-1}(\mu_1)$ in both cases is analogous to $g_n(\mu_0)$. From $g_n(\mu_0)$ one can derive the recursion relations for the model. Finally we give the parameters of the recursion functions for the quantum and classical cases.

For the Ising-Heisenberg case, we get the corresponding expressions:

$$
\begin{aligned}
a_0 &= e^{-\frac{2J}{T}} + e^{-\frac{h+\Delta}{T}} + e^{-\frac{h+2J+\Delta}{T}} + e^{-\frac{-h+2J_1+\Delta}{T}} + e^{-\frac{-h+2J+2J_1+\Delta}{T}} + e^{-\frac{2h+2J+2\Delta}{T}} \\
&+ e^{-\frac{2J_1+2\Delta}{T}} + e^{-\frac{2(J+J_1)+2\Delta}{T}} + e^{-\frac{-2h+2(J+2J_1)+2\Delta}{T}} \\
a_1 &= e^{-\frac{2\Delta}{T}} + e^{-\frac{-h+2J+\Delta}{T}} + e^{-\frac{2(-h+2J_1+\Delta)}{T}} + e^{-\frac{2J+2\Delta}{T}} + e^{-\frac{-2h+2(J+2J_1)+2\Delta}{T}} \\
&+ e^{-\frac{h+2J+3\Delta}{T}} + e^{-\frac{-h+4J_1+3\Delta}{T}} + e^{-\frac{-h+2(J+2J_1)+3\Delta}{T}} + e^{-\frac{-3h+2(J+4J_1)+3\Delta}{T}} \\
a_2 &= e^{-\frac{h+2J+\Delta}{T}} + e^{-\frac{2J_1+2\Delta}{T}} + e^{-\frac{2h+2J_1+2\Delta}{T}} + e^{-\frac{2h+2J+2J_1+2\Delta}{T}} + e^{-\frac{2(J+J_1)+2\Delta}{T}} \\
&+ e^{-\frac{h+4J_1+3\Delta}{T}} + e^{-\frac{-h+2(J+2J_1)+3\Delta}{T}} + e^{-\frac{h+2(J+2J_1)+3\Delta}{T}} + e^{-\frac{3h+2(J+2J_1)+3\Delta}{T}} \\
c_0 &= e^{-\frac{2J}{T}} + e^{-\frac{2\Delta}{T}} + e^{-\frac{-h+\Delta}{T}} + e^{-\frac{h+\Delta}{T}} + e^{-\frac{-h+2J+\Delta}{T}} + e^{-\frac{h+2J+\Delta}{T}} + e^{-\frac{2J+2\Delta}{T}} \\
&+ e^{-\frac{-2h+2J+2\Delta}{T}} + e^{-\frac{2h+2J+2\Delta}{T}} \\
c_1 &= e^{-\frac{2\Delta}{T}} + e^{-\frac{-h+2J+\Delta}{T}} + e^{-\frac{2J+2\Delta}{T}} + e^{-\frac{-2h+2J_1+2\Delta}{T}} + e^{-\frac{-2h+2J+2J_1+2\Delta}{T}} \\
&+ e^{-\frac{h+2J+3\Delta}{T}} + e^{-\frac{-h+2J_1+3\Delta}{T}} + e^{-\frac{-h+2(J+J_1)+3\Delta}{T}} + e^{-\frac{-3h+2(J+2J_1)+3\Delta}{T}} \\
c_2 &= e^{-\frac{2\Delta}{T}} + e^{-\frac{h+2J+\Delta}{T}} + e^{-\frac{2J+2\Delta}{T}} + e^{-\frac{2h+2J_1+2\Delta}{T}} + e^{-\frac{2h+2J+2J_1+2\Delta}{T}} + e^{-\frac{-h+2J+3\Delta}{T}} \\
&+ e^{-\frac{h+2J_1+3\Delta}{T}} + e^{-\frac{h+2(J+J_1)+3\Delta}{T}} + e^{-\frac{3h+2(J+2J_1)+3\Delta}{T}} \\
b_0 &= e^{-\frac{2J}{T}} + e^{-\frac{-h+\Delta}{T}} + e^{-\frac{-h+2J+\Delta}{T}} + e^{-\frac{h+2J_1+\Delta}{T}} + e^{-\frac{h+2J+2J_1+\Delta}{T}} + e^{-\frac{-2h+2J+2\Delta}{T}} \\
&+ e^{-\frac{2J_1+2\Delta}{T}} + e^{-\frac{2(J+J_1)+2\Delta}{T}} + e^{-\frac{2h+2(J+2J_1)+2\Delta}{T}} \\
b_1 &= e^{-\frac{-h+2J+\Delta}{T}} + e^{-\frac{2J_1+2\Delta}{T}} + e^{-\frac{-2h+2J_1+2\Delta}{T}} + e^{-\frac{-2h+2J+2J_1+2\Delta}{T}} + e^{-\frac{2(J+J_1)+2\Delta}{T}} \\
&+ e^{-\frac{-h+4J_1+3\Delta}{T}} + e^{-\frac{-3h+2(J+2J_1)+3\Delta}{T}} + e^{-\frac{-h+2(J+2J_1)+3\Delta}{T}} + e^{-\frac{h+2(J+2J_1)+3\Delta}{T}} \\
b_2 &= e^{-\frac{2\Delta}{T}} + e^{-\frac{h+2J+\Delta}{T}} + e^{-\frac{2(h+2J_1+\Delta)}{T}} + e^{-\frac{2J+2\Delta}{T}} + e^{-\frac{2h+2(J+2J_1)+2\Delta}{T}} + e^{-\frac{-h+2J+3\Delta}{T}} \\
&+ e^{-\frac{h+4J_1+3\Delta}{T}} + e^{-\frac{h+2(J+2J_1)+3\Delta}{T}} + e^{-\frac{3h+2(J+4J_1)+3\Delta}{T}}.
\end{aligned}
\tag{2.22}
$$

For the Ising case the parameters have the following form:

$$
\begin{aligned}
a_0 &= e^{D-\frac{4J_1}{T}}(e^{\frac{5h}{T}+\frac{4J_1}{T}+\frac{\Delta}{T}}+2e^{\frac{3h}{T}+\frac{2J}{T}+\frac{6J_1}{T}+\frac{\Delta}{T}}+e^{\frac{h}{T}+\frac{8J_1}{T}+\frac{\Delta}{T}}+2e^{\frac{4h}{T}+\frac{2J}{T}+\frac{6J_1}{T}+\frac{2\Delta}{T}} \\
&+2e^{\frac{2h}{T}+\frac{2J}{T}+\frac{8J_1}{T}+\frac{2\Delta}{T}}+e^{\frac{3h}{T}+\frac{2J}{T}+\frac{8J_1}{T}+\frac{3\Delta}{T}}) \\
a_1 &= e^{-\frac{4J_1}{T}}(2e^{\frac{4h}{T}+\frac{2J}{T}+\frac{4J_1}{T}}+e^{\frac{2h}{T}+\frac{8J_1}{T}}+e^{\frac{6h}{T}}+2e^{\frac{5h}{T}+\frac{2J}{T}+\frac{4J_1}{T}+\frac{\Delta}{T}}+2e^{\frac{3h}{T}+\frac{2J}{T}+\frac{8J_1}{T}+\frac{\Delta}{T}} \\
&+e^{\frac{4h}{T}+\frac{2J}{T}+\frac{8J_1}{T}+\frac{2\Delta}{T}}) \\
a_2 &= e^{-\frac{4J_1}{T}}(e^{\frac{4h}{T}+\frac{4J_1}{T}}+2e^{\frac{2h}{T}+\frac{2J}{T}+\frac{4J_1}{T}}+e^{\frac{4J_1}{T}}+2e^{\frac{h}{T}+\frac{2J}{T}+\frac{6J_1}{T}+\frac{\Delta}{T}}+2e^{\frac{3h}{T}+\frac{2J}{T}+\frac{6J_1}{T}+\frac{\Delta}{T}} \\
&+e^{\frac{2h}{T}+\frac{2J}{T}+\frac{8J_1}{T}+\frac{2\Delta}{T}}) \\
c_0 &= e^{\frac{h}{T}+\frac{4J_1}{T}+\frac{\Delta}{T}}+e^{\frac{5h}{T}+\frac{4J_1}{T}+\frac{\Delta}{T}}+2e^{\frac{3h}{T}+\frac{2J}{T}+\frac{4J_1}{T}+\frac{\Delta}{T}}+2e^{\frac{2h}{T}+\frac{2J}{T}+\frac{4J_1}{T}+\frac{2\Delta}{T}} \\
&+2e^{\frac{4h}{T}+\frac{2J}{T}+\frac{4J_1}{T}+\frac{2\Delta}{T}}+e^{\frac{3h}{T}+\frac{2J}{T}+\frac{4J_1}{T}+\frac{3\Delta}{T}} \\
c_1 &= 2e^{\frac{4h}{T}+\frac{2J}{T}+\frac{2J_1}{T}}+e^{\frac{2h}{T}+\frac{4J_1}{T}}+e^{\frac{6h}{T}}+2e^{\frac{5h}{T}+\frac{2J}{T}+\frac{2J_1}{T}+\frac{\Delta}{T}}+2e^{\frac{3h}{T}+\frac{2J}{T}+\frac{4J_1}{T}+\frac{\Delta}{T}} \\
&+e^{\frac{4h}{T}+\frac{2J}{T}+\frac{4J_1}{T}+\frac{2\Delta}{T}} \\
c_2 &= 1+2e^{\frac{2h}{T}+\frac{2J}{T}+\frac{2J_1}{T}}+e^{\frac{4h}{T}+\frac{4J_1}{T}}+2e^{\frac{h}{T}+\frac{2J}{T}+\frac{2J_1}{T}+\frac{\Delta}{T}}+2e^{\frac{3h}{T}+\frac{2J}{T}+\frac{4J_1}{T}+\frac{\Delta}{T}} \\
&+e^{\frac{2h}{T}+\frac{2J}{T}+\frac{4J_1}{T}+\frac{2\Delta}{T}} \\
b_0 &= e^{-\frac{4J_1}{T}}(e^{\frac{h}{T}+\frac{4J_1}{T}+\frac{\Delta}{T}}+2e^{\frac{3h}{T}+\frac{2J}{T}+\frac{6J_1}{T}+\frac{\Delta}{T}}+e^{\frac{5h}{T}+\frac{8J_1}{T}+\frac{\Delta}{T}}+2e^{\frac{2h}{T}+\frac{2J}{T}+\frac{6J_1}{T}+\frac{2\Delta}{T}} \\
&+2e^{\frac{4h}{T}+\frac{2J}{T}+\frac{8J_1}{T}+\frac{2\Delta}{T}}+e^{\frac{3h}{T}+\frac{2J}{T}+\frac{8J_1}{T}+\frac{3\Delta}{T}}) \\
b_1 &= e^{-\frac{4J_1}{T}}(e^{\frac{2h}{T}+\frac{4J_1}{T}}+e^{\frac{6h}{T}+\frac{4J_1}{T}}+2e^{\frac{4h}{T}+\frac{2J}{T}+\frac{4J_1}{T}}+2e^{\frac{3h}{T}+\frac{2J}{T}+\frac{6J_1}{T}+\frac{\Delta}{T}} \\
&+2e^{\frac{5h}{T}+\frac{2J}{T}+\frac{6J_1}{T}+\frac{\Delta}{T}}+e^{\frac{4h}{T}+\frac{2J}{T}+\frac{8J_1}{T}+\frac{2\Delta}{T}}) \\
b_2 &= e^{-\frac{4J_1}{T}}(1+2e^{\frac{2h}{T}+\frac{2J}{T}+\frac{4J_1}{T}}+e^{\frac{4h}{T}+\frac{8J_1}{T}}+2e^{\frac{h}{T}+\frac{2J}{T}+\frac{4J_1}{T}+\frac{\Delta}{T}}+2e^{\frac{3h}{T}+\frac{2J}{T}+\frac{8J_1}{T}+\frac{\Delta}{T}} \\
&+e^{\frac{2h}{T}+\frac{2J}{T}+\frac{8J_1}{T}+\frac{2\Delta}{T}}),
\end{aligned}
\tag{2.23}
$$

The phases in Fig. 2.6d are characterized by the following spin configurations, values of the single-site magnetization and quadrupole moment at zero magnetic field.

• The antiferromagnetic phase:

$$\left|AFM\right\rangle = \begin{cases} \prod_{i=1}^{N} \frac{1}{\sqrt{2}}(|-1\rangle_i \otimes (|1,0\rangle - |0,1\rangle))_{a_i,b_i} \\ \prod_{i=1}^{N} \frac{1}{\sqrt{2}}(|1\rangle_i \otimes (|0,-1\rangle - |-1,0\rangle))_{a_i,b_i} \end{cases}, \quad E = 2(-J_1 + K_1 + \Delta) \tag{2.24}$$

$$m_\mu = \mp 1, m_S = \pm\frac{1}{2}, m = 0, p_\mu = 1, p_S = \frac{1}{2}, p = \frac{2}{3}$$

• The ferrimagnetic phase:

$$\left|FRI\right\rangle = \prod_{i=1}^{N}(|-1\rangle_i \otimes (|1,1\rangle)_{a_i,b_i}, \quad E = 2J - 4J1 + 4K_1 + 3\Delta \tag{2.25}$$

$$m_\mu = -1, m_S = 1, m = \frac{1}{3}, p_\mu = 1, p_S = 1, p = 1$$

• The monomer-dimer phase:

$$\left|MD\right\rangle = \prod_{i=1}^{N} \frac{1}{\sqrt{2}}(|0\rangle_i \otimes (|1,0\rangle - |0,1\rangle))_{a_i,b_i}, \quad E = \Delta \tag{2.26}$$

$$m_\mu = 0, m_S = \frac{1}{2}, m = \frac{1}{3}, p_\mu = 0, p_S = \frac{1}{2}, p = \frac{1}{3}$$

• The frustrated phase:

$$\left|FRU\right\rangle = \prod_{i=1}^{N} \frac{1}{\sqrt{2}}(|\pm 1\rangle_i \otimes (|1,-1\rangle - |-1,1\rangle))_{a_i,b_i}, \quad E = 4K1 + 3\Delta \tag{2.27}$$

$$m_\mu = 0, m_S = 0, m = 0, p_\mu = 1, p_S = 1, p = 1$$

• The non-magnetic phase:

$$\left|NM\right\rangle = \prod_{i=1}^{N}(|0\rangle_i \otimes (|0,0\rangle)_{a_i,b_i}, \quad E = 2J \tag{2.28}$$

$$m_\mu = 0, m_S = 0, m = 0, p_\mu = 0, p_S = 0, p = 0$$

Chapter 3

Magnetization Plateaus and Thermal Entanglement of Spin Systems

3.1 Introducion

The magnetic plateau and entanglement properties exhibit common features observable via antferromagnetic coupling constant, external magnetic, crystal (single-ion anisotropy) fields and chemical potential. The family of known non-trivial quantum effects in the condensed matter physics is enriched with the novel phenomenonintermediate plateaus in the magnetization processes [6, 15]. The observation of a 1/3 magnetization plateau in natural azurite $Cu_3(CO_3)_2(OH)_2$ has been proposed as a realization of the exotic diamond chain of antiferromagnetically coupled of spin-1/2 Cu^{+2}-monomers [7, 8]. The theoretical study of magnetization plateaus in azurite were obtained by using the density functional theory [10, 107], mean-field-like treatment based on the Gibbs-Bogoliubov inequality [13] , the density-matrix renormalization-group (DMRG) technique [116, 117] and the decoration-iteration transformation [95]. On a diamond chain there were observed the plateaus of electron density as a function of chemical potential on spinless fermion, extended Hubbard and magnetization as a function of external magnetic field on distorted Ising-Hubbard models [118–120]. The magnetic behavior and magnetic susceptibility of the metal-containing complex $[Ni_3(fum)_2-(\mu_3-OH)_2(H_2O)_4]_n\cdot(2H_2O)_n$ was measured [104]. The spin-1 diamond-chain of the compound is charac-

terized by both ferromagnetic and antiferromagnetic exchanges. In this article we would get magnetization and quadrupole moment plateaus at low temperatures as a function of external magnetic field and single-ion anisotropy. Quantum entanglement is considered to play a key role for understanding of strongly correlated quantum systems, quantum phase transitions and collective quantum phenomena in particular many-body spin and fermionic lattice systems [16–18] especially in antferromagnetic models. Another important observation is the strong relationship between magnetic and entanglement properties of the antiferromagnetic system on diamond chain models [105, 119, 121–126]. One also regard magnetic behavior of spin lattice models applying the dynamic system method [127–129]. The dynamical approach represents an essential tool in the theory of phase transitions and criticality and it enhanced our understanding of the phase structure and critical properties of spin models. In the case of antiferromagnetic coupling between lattice nodes of the three site interaction Ising and the Q-state Potts models $(Q < 2)$ on Husimi and Bethe lattices exhibit a complex behavior, featuring doubling bifurcations, chaotic regimes, intermittency, and superstable points [100, 112]. The plateaus of the maximal Lyapunov exponent coincide with magnetization plateaus on a kagome chain for multidimensional mapping [130]. The existence of the magnetization plateau has been observed at one third of the saturation magnetization in the antiferromagnetic spin-1/2 IsingHeisenberg model on a diamond chain using the multidimensional mapping [110]. It has been detected that the maximal Lyapunov exponent exhibits plateau like magnetization one and found the existence of the supercritical point at $T \to 0$ in the absence of the external magnetic field corresponding to the phase transition point.

In the present paper we shall mainly deal with the quantum entanglement and magnetic curve behavior of symmetric Hubbard dimers with delocalized interstitial electrons and spin-1 Ising - Heisenberg model using transfer matrix technique on a diamond chain. Applying the recurrence relation of the two-dimensional mapping we shall study magnetic plateau and their relation to maximal Lyapunov exponents, superstable point of spin-1 classical and Ising - Heisenberg models on a diamond chain. The paper is organized as follows. In Section 2 the phase behaviour of the diamond chain is presented of a symmetric Hubbard-Ising model and studied the magnetic and thermal properties. We research the quantum entanglement of electrons in Hubbard dimers and dependence of Hamiltonian parame-

ters as well as on temperature. We give an exact solution of spin-1 Ising - Heisenberg model by means of the transfer-matrix method and study the magnetization plateaus and negativity in Section 3. In Section 4 we apply the dynamical system approach in researching magnetic plateaus and maximal Lyapunov exponent plateaus. It is observed that the superstable coincide with phase transition point at $T \to 0$ in the spin-1 classical and Ising-Heisenberg models on the diamond chain. Some concluding remarks are given in section 5.

3.2 Symmetric diamond chain with delocalized Hubbard interstitial spins

The Hamiltonian of symmetric Ising- Hubbard model [131] describing the diamond chain (Fig. 1)is $\mathcal{H} = \sum_{i=1}^{N} \mathcal{H}_{i,i+1}$, where

$$\mathcal{H}_{i,i+1} = -\tilde{t}\left(a_{i\uparrow}^{+}b_{i\uparrow} + a_{i\uparrow}b_{i\uparrow}^{+} + a_{i\downarrow}^{+}b_{i\downarrow} + a_{i\downarrow}b_{i\downarrow}^{+}\right) + \widetilde{V}n_{ai}n_{bi} + \widetilde{U}\left(n_{ai\uparrow}n_{ai\downarrow} + n_{bi\uparrow}n_{bi\downarrow}\right) \tag{3.1}$$
$$+\widetilde{J}_m s_{ci}s_{ci+1} + J\left(s_{ai}^{z} + s_{bi}^{z}\right)\left(s_{ci} + s_{ci+1}\right) - \widetilde{\mu}\left(n_{ai} + n_{bi}\right) - \widetilde{h}\left(s_{ai}^{z} + s_{bi}^{z} + \frac{s_{ci} + s_{ci+1}}{2}\right).$$

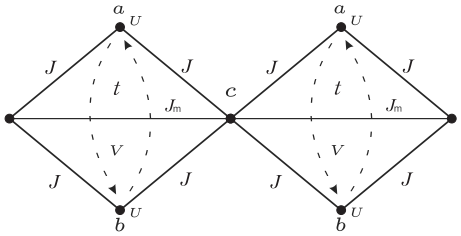

Figure 3.1: Two sites of the Hubbard dimer are denoted as a– and b–. There is an electron hopping between them with amplitude t. One–site (U) and two–site (V) Coulomb interactions are also present. The diamonds are connected to each other at nodal c–sites. There is an Ising–like direct interaction with J_m coupling constant between the nodal sites. The nodal sites are also connected to a– and b–sites by means of Ising–like interactions with coupling constant J.

Here $a_{i\sigma}^{+}$ ($a_{i\sigma}$) and $b_{i\sigma}^{+}$ ($b_{i\sigma}$) are the electron creation (annihilation) operators with the spin value σ=($\uparrow,\downarrow$), respectively on sites a_i and b_i. The $n_{ai\sigma} = a_{i\sigma}^{+}a_{i\sigma}$ and $n_{bi\sigma} = b_{i\sigma}^{+}b_{i\sigma}$ are the electron number operators, respectively on sites a_i and b_i and $\tilde{t}$ is the hopping amplitude. We denote $n_{\alpha i} = n_{\alpha i\uparrow} + n_{\alpha i\downarrow}$,

$s^z_{\alpha i} = \frac{1}{2}\left(n_{\alpha i\uparrow} - n_{\alpha i\downarrow}\right)$, $(\alpha = a,b)$ and $s_{ci} = \pm\frac{1}{2}$. Here $\tilde{\mu}$ and $\widetilde{h}$ are the values of the chemical potential and the external magnetic field ($\widetilde{h} = g\mu_B B_z$) respectively. The terms which contain $\widetilde{U}$ and $\widetilde{V}$ correspond respectively to one–site and two–site Coulomb repulsions in the Hubbard dimer(interstitial spins). The terms which contain the symmetric coupling J that describe Hubbard dimer interactions with nodal Ising-type spins. The term containing $\widetilde{J_m}$ describes two nodal Ising–like spins interaction.

From the identity

$$\widetilde{V}n_a n_b + \widetilde{U}\left(n_{a\uparrow}n_{a\downarrow} + n_{b\uparrow}n_{b\downarrow}\right) = \left(\widetilde{U} - \widetilde{V}\right)\left(n_{a\uparrow}n_{a\downarrow} + n_{b\uparrow}n_{b\downarrow}\right) + \frac{n(n-1)}{2}\widetilde{V}, \tag{3.2}$$

(where $n = n_{a\uparrow} + n_{a\downarrow} + n_{b\uparrow} + n_{b\downarrow}$ is the total number of electrons in the Hubbard dimer), it follows that the differences between energy levels depend on $\widetilde{U} - \widetilde{V} \equiv \widetilde{W}$ only, if n is fixed. In particular, for fixed $n \neq 2$, $\left(n_{a\uparrow}n_{a\downarrow} + n_{b\uparrow}n_{b\downarrow}\right)$ is constant and the behavior of the system does not depend on $\widetilde{W}$ at all, which is physically obvious.

As all $\mathcal{H}_{i,i+1}$ commute, therefore the partition function can be written as:

$$Z_N = Tr\left(e^{-\beta\mathcal{H}}\right) = \sum_{s_{ci}=\pm\frac{1}{2}} \prod_{i=1}^{N} Tr_{a,b}\left(e^{-\beta\mathcal{H}_{i,i+1}(s_{ci},s_{ci+1})}\right) = Tr\mathbf{V}^N, \tag{3.3}$$

where $\mathbf{V} = \begin{pmatrix} V(+,+) & V(+,-) \\ V(-,+) & V(-,-) \end{pmatrix}$ is the transfer matrix, with $V(\pm,\pm) = \sum_j e^{-\beta E_j(\pm,\pm)}$, where $E_j(\pm,\pm) \equiv E_j\left(\pm\frac{1}{2},\pm\frac{1}{2}\right)$ are the eigenvalues of the $\mathcal{H}_{i,i+1}(\pm,\pm) \equiv \mathcal{H}_{i,i+1}\left(\pm\frac{1}{2},\pm\frac{1}{2}\right)$ Hamiltonian.

In the thermodynamic limit the free energy per diamond is

$$F = \lim_{N\to\infty} \frac{-T}{N} \ln Z_N = -\ln\lambda_1, \tag{3.4}$$

where $\lambda_1 = \frac{1}{2}\left(Tr\mathbf{V} + \sqrt{(Tr\mathbf{V})^2 - 4\det\mathbf{V}}\right)$ is the largest eigenvalue of the transfer matrix.

On this basis it is easy to calculate magnetization and specific heat. Analogously we use the following expression for reduced density matrix of a Hubbard dimer to study entanglement properties:

$$\rho' = \frac{1}{\lambda_1}\left[\frac{e^{-\beta H(+,+)}+e^{-\beta H(-,-)}}{2}+e^{-\beta H(+,-)}\sin 2\theta + \right.$$
$$\left. + \frac{e^{-\beta H(+,+)}-e^{-\beta H(-,-)}}{2}\cos 2\theta\right], \tag{3.5}$$

with $\sin 2\theta = \frac{2V(+,-)}{\sqrt{(Tr\mathbf{V})^2-4\det\mathbf{V}}}$, $\cos 2\theta = \frac{V(+,+)-V(-,-)}{\sqrt{(Tr\mathbf{V})^2-4\det\mathbf{V}}}$.

In the sequel we rescale all quantities by the J absolute value, substituting $t=\tilde{t}/|J|$, $h=\tilde{h}/|J|$, $\mu=\tilde{\mu}/|J|$, $U=\widetilde{U}/|J|$, $V=\widetilde{V}/|J|$, $W=\widetilde{W}/|J|$ and $J_m=\tilde{J}_m/|J|$.

The magnetization curves at nonzero temperature are derived from $m=-\frac{\partial F}{\partial h}$. Here we take the number of electrons in a Hubbard dimer fixed and equals to 2. Fig. 3.2 shows possible forms of magnetization curves at zero and nonzero temperatures. The following types of plateaus exist here: at 0, 1/3 and 2/3 values and of classical (electrons in the Hubbard dimers are not entangled and their spin projections have definite value at each site) and nonclassical (electrons in the Hubbard dimers are entangled) types.

The entanglement of formation in the special case of two spin-1/2 particles has the analytical expression [132]: $E_F = H\left(\frac{1+\sqrt{1-C^2}}{2}\right)$, where $H(x)=-x\log_2(x)-(1-x)\log_2(1-x)$, and C is the quantity called *concurrence*.

For fixed values of t and J_m we have plotted the concurrence as a function of the temperature and the external magnetic field (Figs. 3.3). The thermal entanglement becomes significantly large when the energy level of the (non-entangled) ground state and the nearest energy level (corresponding to the entangled state) are close to each other.

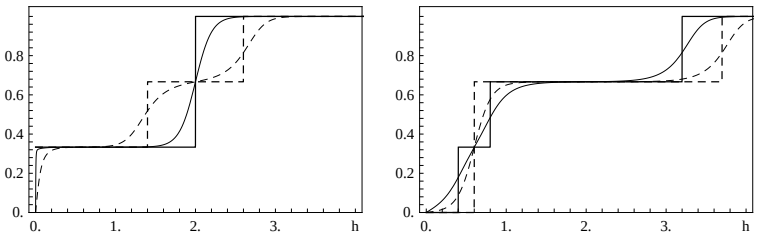

a) $J_m = 0$, $J_m = 0.6$ b) $J_m = 1.2$, $J_m = 1.7$

Figure 3.2: Dependence of the diamond chain magnetization (m) (per diamond in $g\mu_B$ units) on the external magnetic field (h) for different values of the internodal change interaction (J_m) at $T = 0$. The fixed chain parameters are $t = 0.3$, $W = 0$, $\mu = 0$. The case of $T = 0.1$ is also shown. In this case thermal fluctuations smoothen magnetization jumps.

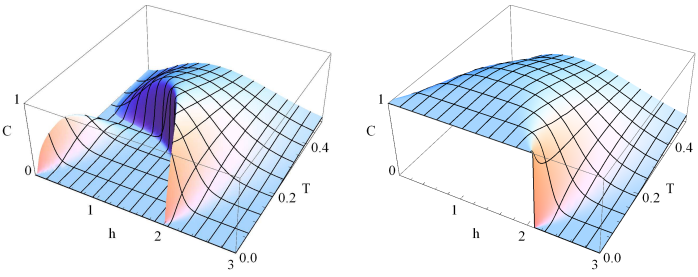

a) $t = 0.45, J_m = -2$ b) $t = 0.55, J_m = -2$

Figure 3.3: The dependence of the concurrence from temperature and external magnetic field for various values of hopping amplitude. Concurrence vanishes in high temperature limit.

3.3 Magnetization plateaus and negativity in spin-1 Ising - Heisenberg model

Let us consider spin-1 Ising-Heisenberg model on a diamond chain (see Fig. 3.6) without biquadratic coupling terms using the transfer matrix technique. The magnetic behavior of homometallic molecular ferrimagnet $[Ni_3(fum)_2 - (\mu_3 - OH)_2(H_2O)_4]_n \cdot (2H_2O)_n$ was measured by [104] without single-ion anisotropy parameters. We observe magnetisation plateau and thermal quantum negativity in the presence of an external magnetic fields and single-ion anisotropy terms. The Hamiltonian is equal to the sum over block Hamiltonians $\mathcal{H} = \sum_i \mathcal{H}_i$ with

$$\begin{aligned} \mathcal{H}_i &= J\vec{S}_{a,i}\vec{S}_{b,i} + J_1(S^z_{a,i} + S^z_{b,i})(\sigma^z_i + \sigma^z_{i+1}) + D_H((S^z_{a,i})^2 + (S^z_{b,i})^2) + \frac{D_I}{2}\left((\sigma^z_i)^2 + (\sigma^z_{i+1})^2\right) \\ &- h_H g\mu_B(S^z_{a,i} + S^z_{b,i}) - \frac{h_I g\mu_B}{2}\left(\sigma^z_i + \sigma^z_{i+1}\right), \end{aligned} \tag{3.6}$$

where $S^{\alpha}_{a/b,i}$ ($\alpha = x,y,z$) are spin-1 operators on the sites with coordinates $(a/b,i)$, while σ^z_i's are z projections of spin-1 operator resting on the sites i, J denotes the XXX interaction within the Heisenberg dimer and J_1 stands for the interaction between nodal and dimer spins. Coefficients D_I and D_H correspond to the longitudinal crystal(single-ion anisotropy) fields in the z direction. The gyromagnetic ratio is taken to be $g = 2.2$ in the plots drawn below, which is more or less typical for nickel containing compounds. We assume that cyclic boundary condition $\sigma_{N+1} = \sigma_1$ is applied. The block Hamiltonians($\mathcal{H}_i$) are commutative, therefore the partition function can be written like in equation (3).

After direct diagonalization of the block Hamiltonian $\mathcal{H}_i$ one gets the energy spectrum of a diamond block depending on Ising spins:

$$\begin{aligned}
E_1 &= -J - \frac{h_I g\mu_B}{2}(\sigma_i + \sigma_{i+1}) + \frac{D_I}{2}\left(\sigma_i^2 + \sigma_{i+1}^2\right) + 2D_H,\\
E_{2,3} &= \pm J - \left(J_1 + \frac{h_I g\mu_B}{2}\right)(\sigma_i + \sigma_{i+1}) + h_H g\mu_B + D_H + \frac{D_I}{2}\left(\sigma_i^2 + \sigma_{i+1}^2\right),\\
E_{4,5} &= \pm J + (J_1 - \frac{h_I g\mu_B}{2})(\sigma_i + \sigma_{i+1}) - h_H g\mu_B + D_H + \frac{D_I}{2}\left(\sigma_i^2 + \sigma_{i+1}^2\right),\\
E_{6,7} &= J + \left(\pm 2J_1 - \frac{h_I g\mu_B}{2}\right)(\sigma_i + \sigma_{i+1}) \mp 2h_H g\mu_B + \frac{D_I}{2}\left(\sigma_i^2 + \sigma_{i+1}^2\right) + 2D_H,\\
E_{8,9} &= \frac{-J \pm \Lambda}{2} - \frac{h_I g\mu_B}{2}(\sigma_i + \sigma_{i+1}) + \frac{D_I}{2}\left(\sigma_i^2 + \sigma_{i+1}^2\right) + D_H,
\end{aligned} \tag{3.7}$$

where $\Lambda = \sqrt{(2D_H - J)^2 + 8J^2}$. Knowledge of the spectrum allows us to perform partial trace-overs along Heisenberg degrees of freedom. Which makes representation $Z_N = \sum_{\sigma_i} \prod_{i=1}^{N} V_{\sigma_i,\sigma_{i+1}}$, with $V_{\sigma_i,\sigma_{i+1}} = Tr_i e^{-\beta\mathcal{H}_i} = \sum_{i=1}^{9} e^{-\beta E_i(\sigma_i,\sigma_{i+1})}$. $V_{\sigma_i,\sigma_{i+1}}$'s may be viewed as components of a 3×3 transfer matrix:

$$V_{\sigma_i,\sigma_{i+1}} = \begin{pmatrix} V_{-1,-1} & V_{-1,0} & V_{-1,1} \\ V_{0,-1} & V_{0,0} & V_{0,1} \\ V_{1,-1} & V_{1,0} & V_{1,1} \end{pmatrix}, \tag{3.8}$$

where matrix indexes are the three possible projections of Ising spins. Taking into account the cyclic boundary conditions one may write $Z_N = Tr(V^N)$ in transfer matrix notations. Hence the partition

function may be expressed in terms of the transfer matrix eigenvalues:

$$Z_N = \lambda_1^N + \lambda_2^N + \lambda_3^N. \tag{3.9}$$

As usual, in the thermodynamic limit $N \to \infty$ only the contribution of the largest eigenvalue must be considered. Denoting the maximal eigenvalue as λ, the free energy per block for infinitely long chain takes the form

$$f = -\frac{1}{\beta} \lim_{N\to\infty} \frac{1}{N} \ln Z_N = -\frac{1}{\beta} \ln \lambda. \tag{3.10}$$

The exact expression of the free energy will allow us to calculate thermodynamic quantities of the system. In the present paper we will consider the sublattice magnetization and quadrupole moment of Ising spins and the sublattice magnetization of Heisenberg spins. They are given by

$$m_I = -\frac{\partial f}{\partial h_I}, \quad m_H = -\frac{1}{2}\frac{\partial f}{\partial h_H}, \quad q_I = \frac{\partial f}{\partial D_I}. \tag{3.11}$$

The total magnetization is equal to the average of m_I and two m_H. To illustrate the magnetization process in a few interesting cases. We show the magnetization at sufficiently low temperature ($T = 0.01K$) as a function of the magnetic field with several plateaus (Fig. 3.4). Thermal quantum

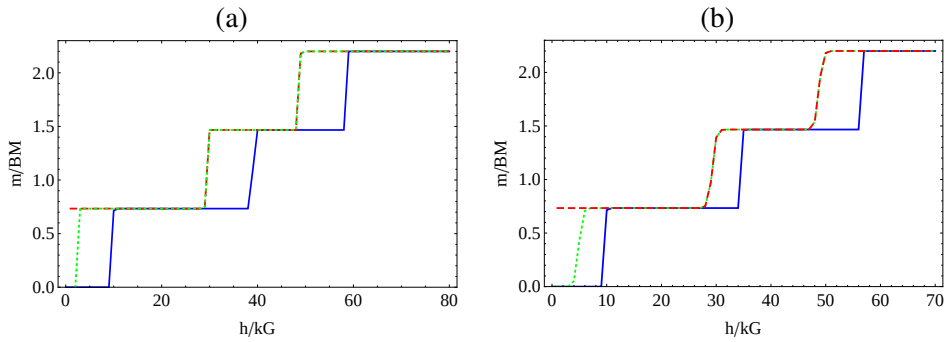

Figure 3.4: Low temperature ($T = 0.01K$) magnetization curves in Bohr magneton units when $J_1 = D_I = 1cm^{-1}$ and (a) $J = -6cm^{-1}$, $D_H = 1cm^{-1}$ (dashed), $D_H = 2.25cm^{-1}$ (dotted), $D_H = 4cm^{-1}$ (solid), (b) $J = 0.9cm^{-1}$, $D_H = -1cm^{-1}$ (dashed), $D_H = 0.7cm^{-1}$ (dotted), $D_H = 2cm^{-1}$ (solid).

entanglement (negativity) can be defined as [133]. We have plotted negativity vs. magnetic field Fig. 3.5(a) , demonstrating the change of negativity by varying D_H as well as the sharp step like be-

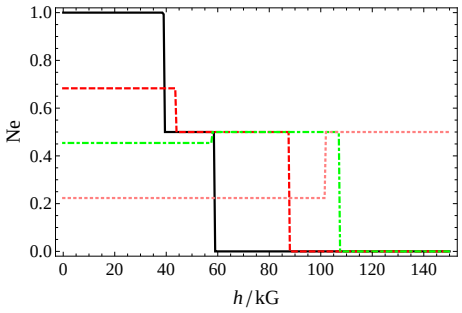

Figure 3.5: Negativity via magnetic field for different values of the single-ion anisotropy $D_H = 0,3,5,10cm^{-1}$ (solid, dashed, dotted-dashed and dotted curves, respectively) at low temperature $T = 10^{-4}K$ and for $J = 2cm^{-1}$. Here $J_1 = D_I = 1cm^{-1}$.

havior of the entanglement at transitions. The introduction of the single-ion anisotropy is essential for the observation of magnetic and entanglement properties for homometallic molecular ferrimagnet $[Ni_3(fum)_2 - (\mu_3 - OH)_2(H_2O)_4]_n \cdot (2H_2O)_n$.

3.4 Magnetic plateaus and quantum entanglement: Dynamical approach

In this section we utilise two models the spin-1 Ising and Ising-Heisenberg models. Let us first consider the spin-1 Ising model on diamond chain with free boundary conditions in the presence of an external magnetic field (see Fig. 3.6). The Hamiltonian operator of the model is equal to the summation of the block Hamiltonians and can be written as

$$\mathcal{H} = \sum_{i}^{N} \mathcal{H}_i = \sum_{i}^{N} (J(S_{a,i}S_{b,i}) + K(S_{a,i}S_{b,i})^2 + J_1(\mu_i + \mu_{i+1})(S_{a,i} + S_{b,i}) \tag{3.12}$$
$$+K_1((\mu_i)^2 + (\mu_{i+1})^2)((S_{a,i})^2 + (S_{b,i})^2) + \Delta((S_{a,i})^2 + (S_{b,i})^2) + \Delta_1 \frac{(\mu_i)^2 + (\mu_{i+1})^2}{2}$$
$$-h_H(S_{a,i} + S_{b,i}) - h_I \frac{\mu_i + \mu_{i+1}}{2})$$

Where $S_{a,i}$, $S_{b,i}$ and μ_i, μ_{i+1} are classic Ising spins and can take the valuse $1,0,-1$. The parameter J stands for the linear interactions between the nearest-neighbouring $S_{a,i} - S_{b,i}$ elements and J_1 is the

linear interactions parameter for nearest-neighbouring $S-\mu$ elements ($S_{a,i}-\mu_i$, $S_{a,i}-\mu_{i+1}$, $S_{b,i}-\mu_i$, $S_{b,i}-\mu_{i+1}$). Analogously K and K_1 stand for the quadratic interactions. Δ and Δ_1 are the single-ion anisotropy parameters, h_I and h_H are contributions of a longitudinal external magnetic field interacting with the Ising spins ($S_{a,i}, S_{b,i}-h_H$ and $\mu_i - h_I$).This notations are made to highlight the similarities between the spin-1 Ising and Ising-Heisenberg models. In our further calculations we will consider the case when $K=J$, $K_1=J_1$, $\Delta=\Delta_1$, $h_H=h_I=h$. The partition function of the system with

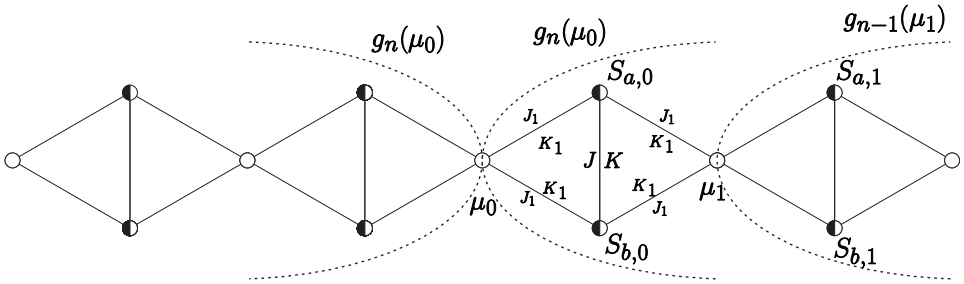

Figure 3.6: The procedure for derivation of the Ising (S_a and S_b are white) and Ising-Heisenberg (S_a and S_b are black) diamond chain. White circles are Ising spins and black are Heisenberg spins

Hamiltonian (3.12) is

$$Z=\sum_{\mu_i,S_{a,i},S_{b,i}} \exp -\beta\mathcal{H}=\sum_{\mu_0} e^{-\frac{-h_I\mu_0+\Delta_1\mu_0^2}{T}} g_n(\mu_0)^2 \tag{3.13}$$

where $\beta=(T)^{-1}$, T is the absolute temperature. By cutting diamond chain at μ_0 into two branches $g_n(\mu_0)$ (Fig. 1) the exact recursion relation for the partition function can be derived. The relation between $g_n(0)$ and $g_{n-1}(\mu_1)$ is given by the following equation.

$$\begin{aligned} g_n(\mu_0)=\sum_{\mu_1=-1}^{1}\sum_{S_{a,0}=-1}^{1}\sum_{S_{b,0}=-1}^{1} \exp[-\beta(J(S_{a,0}S_{b,0})+K(S_{a,0}S_{b,0})^2+J_1(\mu_1+\mu_0)(S_{a,0}+S_{b,0})+ \\ K_1((S_{a,0}\mu_1)^2+(S_{a,0}\mu_0)^2+(S_{b,0}\mu_1)^2+(S_{b,0}\mu_0)^2)+\Delta((S_{a,0})^2+(S_{b,0})^2)+\Delta_1\mu_1^2 \\ -h_H(S_{a,0}+S_{b,0})-h_I\mu_1)]*g_{n-1}(\mu_1) \end{aligned} \tag{3.14}$$

By introducing the following notation

$$x_n=\frac{g_n(1)}{g_n(0)},\ \ y_n=\frac{g_n(-1)}{g_n(0)} \tag{3.15}$$

we can get two-dimensional recursion relation for the partition function

$$x_n = f1(x_{n-1}, y_{n-1}), \;\; f_1(x,y) = \frac{a_1 + a_{11}x + a_{12}y}{b_0 + b_1 x + b_2 y} \tag{3.16}$$
$$y_n = f2(x_{n-1}, y_{n-1}), \;\; f_2(x,y) = \frac{a_2 + a_{21}x + a_{22}y}{b_0 + b_1 x + b_2 y}$$

where the coefficients are easily calculated from equations (3.14) and (3.15).

Recursion relation (3.16) plays a crucial role in our further investigation because the order parameters magnetic and quadrupole moments can be expressed through two-dimensional rational mapping. The equations for total magnetic and quadrupole moments are expressed similar as [134].

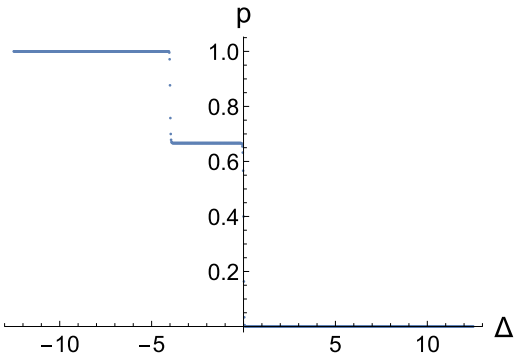

Figure 3.7: Classical Ising spin-1 quadrupole moment(p) for $J = 2, J_1 = 1, h = 0, T = 0.01$.

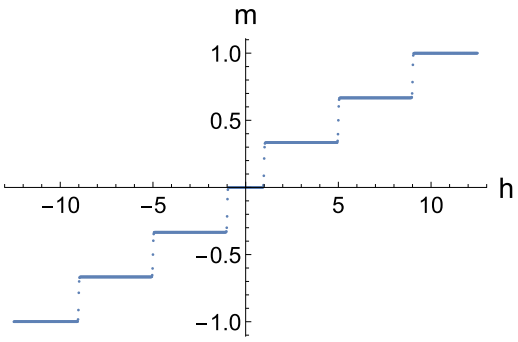

Figure 3.8: Classical Ising spin-1 magnetic moment(m) for $J = 2, J_1 = 1, \Delta = 1, T = 0.01$.

Now lets discus the spin-1 Ising-Heisenberg model on diamond chain with free boundary conditions in the presence of an external magnetic and crystal(single-ion anisotropy) fields (see Fig. 3.6). This two models are very similar therefore this time our narration will be more concise. The blocks of the diamond chain consist of two Heisenberg interstitial spins ($S^{\alpha}_{a,i}$ and $S^{\alpha}_{b,i}$). The z components of interstitial spins are coupled with nearest-neighboring nodal Ising spins (μ_i and μ_{i+1}). Like in the previous model the Hamiltonian of the system may be represented as a sum over block Hamiltonians

$$\mathcal{H} = \sum_i^N \mathcal{H}_i = \sum_i^N (J(S^x_{a,i}S^x_{b,i} + S^y_{a,i}S^y_{b,i} + DS^z_{a,i}S^z_{b,i}) + K(S^x_{a,i}S^x_{b,i} + S^y_{a,i}S^y_{b,i} + D_1 S^z_{a,i}S^z_{b,i})^2 \tag{3.17}$$
$$+J_1(\mu^z_i + \mu^z_{i+1})(S^z_{a,i} + S^z_{b,i}) + K_1((\mu^z_i)^2 + (\mu^z_{i+1})^2)((S^z_{a,i})^2 + (S^z_{b,i})^2) + \Delta((S^z_{a,i})^2 + (S^z_{b,i})^2)$$
$$+\Delta_1 \frac{(\mu^z_i)^2 + (\mu^z_{i+1})^2}{2} - h_H(S^z_{a,i} + S^z_{b,i}) - h_I \frac{\mu^z_i + \mu^z_{i+1}}{2})$$

In this equation, $S^{\alpha}_{a,i}$, $S^{\alpha}_{b,i}$ ($\alpha = x,y,z$) and μ^z_i represent relevant components of Heisenberg and Ising spin-1 operators. In equation (3.17) J is the linear Heisenberg interaction term, K is the quadratic interaction term parameter, D and D_1 are anisotropy parameters, J_1 is the interaction parameter between the nearest-neighboring Ising and Heisenberg spins, Δ (Δ_1) is the single-ion anisotropy parameter of Heisenberg (Ising) spins and the parameter K_1 is the analogue of a quadratic Ising interaction term. The last two terms in the Hamiltonian are contributions of a longitudinal external magnetic eld interacting with the Heisenberg and Ising spins. It is important to notice that the commutation relation between different block Hamiltonians is zero ($[H_i,H_j] = 0$). Furthermore it can be shown that the block Hamiltonian commutes with Ising and Heisenberg spins, i.e. $[H_i,\mu^z_i] = [H_i,S^z_{a,i}+S^z_{b,i}]$ for any values of the model parameters J , K , J_1, K_1, D, D_1, Δ, Δ_1 and magnetic field, but the block Hamiltonian and quadrupole moment commute,$[H_i,(S^z_{a,i})^2+(S^z_{b,i})^2] = 0$, only when $J = KD_1$. In the present work we consider only the case when $J = K$, $J_1 = K_1$, $D = D_1 = 1$, $\Delta = \Delta_1$, $h_H = h_I = h$. Equation (2) and (3) are conserved for this model if instead of μ_i we insert μ^z_i considering the fact that here we also cut the diamond chain at μ_0 (see Fig. 3.6). From them its easy to calculate the equivalent of equation (3.14)

$$g_n(\mu_0) = \sum_{\mu_1,S_{a,0},S_{b,0}} \exp[-\beta(J(S^x_{a,0}S^x_{b,0}+S^y_{a,0}S^y_{b,0}+DS^z_{a,0}S^z_{b,0})+K(S^x_{a,0}S^x_{b,0}+S^y_{a,0}S^y_{b,0}+D_1S^z_{a,0}S^z_{b,0})^2 \tag{3.18}$$

$$+J_1(\mu^z_1+\mu^z_0)(S^z_{a,0}+S^z_{b,0})+K_1((S^z_{a,0}\mu^z_1)^2+(S^z_{a,0}\mu^z_0)^2+(S^z_{b,0}\mu^z_1)^2+(S^z_{b,0}\mu^z_0)^2)+\Delta((S^z_{a,0})^2+(S^z_{b,0})^2)$$
$$+\Delta_1(\mu^z_1)^2-h_H(S^z_{a,0}+S^z_{b,0})-h_I\mu^z_1)]*g_{n-1}(\mu_1)$$

by inserting the eigenvalues of the operators and by using the equivalents of equations (3.15,3.16) the recursion relation has the following form

$$x_n = f1(x_{n-1},y_{n-1}),\ \ f_1(x,y) = \frac{a_1+a_{11}x+a_{12}y}{b_0+b_1x+b_2y} \tag{3.19}$$
$$y_n = f2(x_{n-1},y_{n-1}),\ \ f_2(x,y) = \frac{a_2+a_{21}x+a_{22}y}{b_0+b_1x+b_2y}$$

where the coefficients are easily calculated from equations (3.18).

The equations for total magnetic and quadrupole moments are expressed similar as [134].

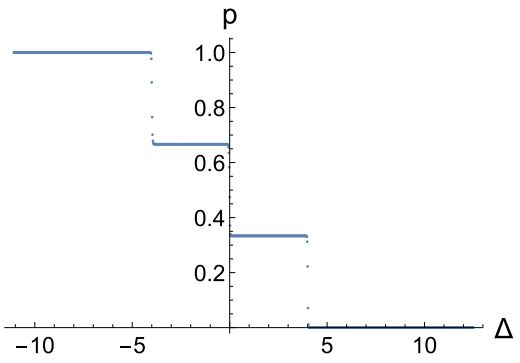

Figure 3.9: Quantum Ising-Hesenberg spin-1 quadrupole moment(p) for $J = 2, J_1 = 1, h = 0, T = 0.01$.

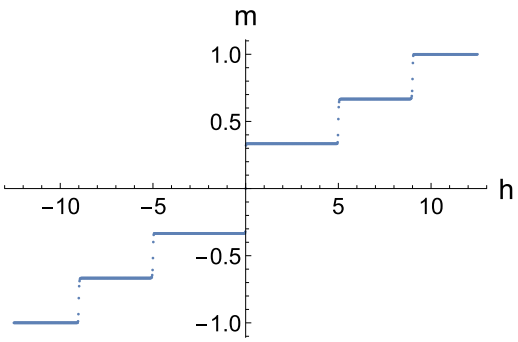

Figure 3.10: Quantum Ising-Hesenberg spin-1 magnetic moment(m) for $J = 2, J_1 = 1, \Delta = 1, T = 0.01$.

In the second part of this section we will focus on the thermodynamical equilibrium description of the spin-1 Ising/Ising-Heisenberg model on a diamond chain, by studying infinite-size systems. Lyapunov exponents have a crucial role in the study of "stability" or "instability" of systems. Lyapunov exponents are the growth rate of an infinitesimal perturbation on a reference trajectory. The following values of maximal Lyapunov exponents can be observed during the investigation ($\lambda = max(\lambda_i)$).

$\lambda < 0$ negative Lyapunov exponents show that the system is dissipative or non-conservative. The systems with more negative values of Lyapunov exponent are more stabile. If $\lambda = -\infty$ means that we have superstable fixed and superstable periodic points. $\lambda = 0$ corresponding to neutral fixed point. At this value of Lyapunov exponents the second-order phase transition takes place. $\lambda > 0$ corresponding to unstable and chaotic systems. In general case if we have a N dimensional map the $i-th$ Lyapunov exponent is calculated with the following equation

$$\lambda_i = \lim_{n\to\infty} \frac{\log H_i}{n}, \quad \mathbf{H} = J(x_0)J(x_1)...J(x_n) \tag{3.20}$$

where H_i is the $i-th$ eigenvalue of $\mathbf{H}$ and $J(x_k)$ is the Jacobian matrix of our N dimensional map after k iterations from the initial point x_0. In some cases when the eigenvalues of $\mathbf{H}$ are complex numbers and its reasonable to use $\mathbf{H}^\dagger\mathbf{H}$ ($\dagger$ denotes the transpose operator) instead of $\mathbf{H}$. In that case Lyapunov

exponents will have $\lambda_i = \lim_{n\to\infty} \frac{\log H_i}{2n}$ form.

Superstable points are particulary interesting studying maximal Lyapunov exponent in classical and quantum cases. In this aspect the above mentioned model have many similarities as well as fundamental differences. There is a superstable point in the spin-1 Ising model at $h = 0$, $J = 2$, $J_1 = 1$, $T \to 0$ and $\Delta > 0$. By computational research it's shown that for many antiferromagnetic configurations there is a superstable point if $\Delta > 0$ which vanishes for $\Delta < 0$ configurations. Ising-Heisenberg models behavior is simular, many antiferromagnetic configurations have superstable points but unlike the Ising model here are two superstable points and they vanish if approximately $\Delta < -1.75$ (this point is for $h = 0$, $J = 2$, $J_1 = 1$ configuration). The fact that there is a magnetization plateau around supercritical points in the classical (see Figures 3.8, 3.11) and quantum (see Figures 3.10, 3.12) cases is of great importance.

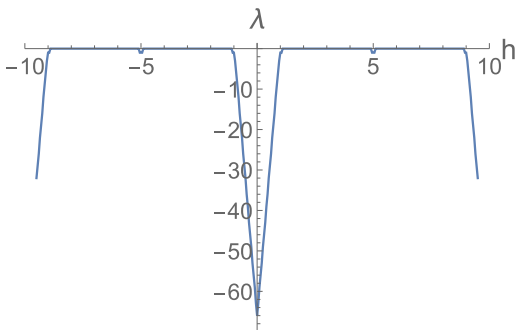

Figure 3.11: Classical Ising spin-1 maximal Lyapunov exponent for $J = 2, J_1 = 1, \Delta = 1, T = 0.03$.

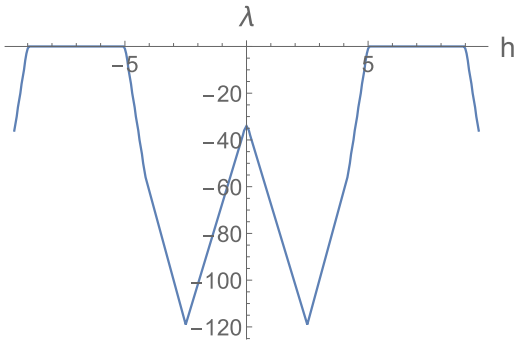

Figure 3.12: Quantum Ising-Hesenberg spin-1 maximal Lyapunov exponent for $J = 2, J_1 = 1, \Delta = 1, T = 0.03$.

3.5 Conclusions

In this paper we study symmetric IsingHubbard, spin-1 Ising and Ising-Heisenberg models on a diamond chain using transfer matrix and dynamical system methods for antiferromagnetic case. The behavior of the magnetization plateaus and thermal quantum entanglement are observed. It's detected the behavior of maximal Lyapunov exponent curves and superstable points connections with magnetization plateaus at $T \to 0$ in classical and quantum cases.

Chapter 4

Super stable cycles and magnetization plateau for spin-1 Ising model on diamond-like decorated Bethe lattice

4.1 Introduction

The dynamical approach represents an essential tool in the theory of phase transitions and criticality [135, 136] and it greatly enhanced the understanding of phase structure and critical properties of spin models. The method is widely used to investigate exact solution of spin models on hierarchical lattices, which are good approximations for real ones (the so called Bethe-Peierls approximation). This technique can also be applied to the generalized Bethe (Husimi) lattice, to describe properties of frustrated systems with multisite interactions, and RNA-like [93, 94, 100, 137]. Its worth mentioning the works on the family of non-linear maps exhibiting quite a complicated behavior, including period doubling cascade, chaos and periodic windows [138, 139].

Hida has theoretically predicted an appearance of the magnetization plateau for the ferromagnetic-antiferromagnetic Heisenberg chain of $3CuCl_2 - 2$ dioxane compound, which consists of the antiferromagnetic coupled ferromagnetic trimers [140].

Using dynamical system method of one-dimensional rational mapping allows us to research the mag-

netization plateaus, bifurcation points and one period doubling of solid and fluid ^3He films, depending on the values of the exchanging parameters and magnetic field [141–143].

The other major technique for studying magnetization plateau is the transfer matrix method at low dimensional systems and on a diamond chain [31, 91, 92, 99].

The Bethe lattice even after many years of its introduction presents an important case of study in many fields of physics and mathematics. The Bethe lattice was originally introduced in order to explain the phase separation and superfluidity in the mixtures and later developed to describe other multi-component physical systems, such as metamagnets, liquid crystal mixtures, microemulsions, semiconductors, etc. [128].

In this paper we study the spin-1 Ising model on a diamond-like decorated Bethe lattice (see Fig 4.1) using a dynamical approach.

The diamond chain with Ising or Ising-Heisenberg models is widely used in approximations for atoms of homometallic magnetic complex $[Ni_3(C_4H_2O_4)_2-(\mu_3-OH)_2(H_2O)_4]_n\cdot(2H_2O)_n$ and the molecular compound $[Ni_8(\mu_3-OH)_4(OMe)_2(O_3PR_1)_2(O_2C^tBu)_6(HO_2C^tBu)_8]$ as well for $Cu_3(CO_3)_2(OH)_2$-known as natural azurite (Copper Carbonate Hydroxide) which can be well described by using the quantum antiferromagnetic Heisenberg model on a generalized diamond chain [7, 8, 104–106, 110].

The aim of this paper is to study the dynamical approach, and notably superstability in the above mentioned models. A remarkable feature of these systems is their exact solvability through recurrence relations techniques; within this method, as we already mentioned, statistical properties of a system are associated to one or multidimensional rational mappings. We show a connection of superstable points and Lyapunov exponents to magnetic plateaus. In both antiferromagnetic and ferromagnetic cases the model exhibits a complex behavior, featuring superstable points and cycles, and magnetic plateaus. In the next section I give a brief description of the spin-1 Ising on Bethe diamond lattice and describe how the dynamical approach allows a detailed analysis of physical properties. Section 3 I describe the stability features of the dynamical mappings derived for such models, and their connections with magnetization. Finally, in Section 4, I conclude with some general remarks concerning the results.

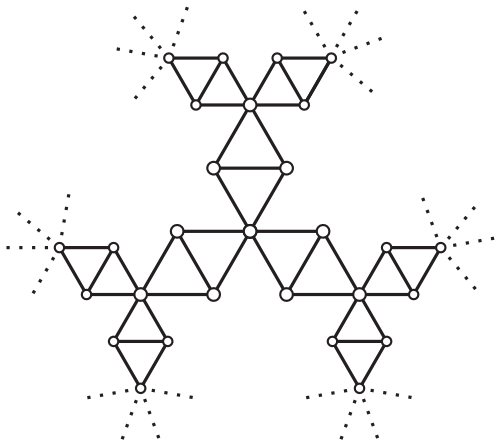

Figure 4.1: The structure of the diamond-like decorated Bethe lattice for q=3. White circles denote Ising spins.

4.2 Models and their dynamic solutions

The spin-1 Ising model on a Bethe-diamond lattice (see Fig 4.1) is defined by the following Hamiltonian, written in terms of block contributions:

$$\begin{aligned} H &= \sum_{\langle i,j\rangle}^{N} H_{i,j} = \sum_{\langle i,j\rangle}^{N} (J(S_{a,i,j}S_{b,i,j}) + K(S_{a,i,j}S_{b,i,j})^2 + J_1(\mu_i+\mu_j)(S_{a,i,j}+S_{b,i,j}) \\ &+ K_1({\mu_i}^2+{\mu_j}^2)(S^2_{a,i,j}+S^2_{b,i,j}) + \Delta(S^2_{a,i,j}+S^2_{b,i,j}) + \Delta_1\frac{{\mu_i}^2+{\mu_j}^2}{q} \\ &- h(S_{a,i,j}+S_{b,i,j}) - h_1\frac{\mu_i+\mu_j}{q}) \end{aligned} \tag{4.1}$$

In the Hamiltonian $\langle i,j\rangle$ denotes a summation over all nearest-neighbour diamond blocks and $S_{a,i,j}$, $S_{b,i,j}$, μ_i, μ_j are classical Ising spins who take the values $\pm 1, 0$. The parameter J accounts for the interactions between the nearest-neighbouring interstitial spins (i.e. $S_{a,i,j}$ - $S_{b,i,j}$) and J_1 is the interactions parameter for nearest-neighbouring nodal-interstitial spins (i.e. μ_i - $S_{a,i,j}$). Analogously, K and K_1 govern quadratic interactions. Δ and Δ_1 are the single-ion anisotropy parameters (crystal fields), h and h_1 represent contributions of a longitudinal external magnetic field, interacting with the interstitial and nodal spins correspondingly. q is a lattice coordination number. In further calculations we assume that $K = J$, $K_1 = J_1$, $\Delta = \Delta_1$, $h = h_1$. Taking into account the shell structure of the Bethe lattice (4.1) one can express the partition function Z of the model on the finite lattice in the following

formula:

$$Z = \sum_{\mu_i} e^{\beta H} = \sum_{\mu_0} e^{-\frac{-h_1\mu_0+\Delta_1{\mu_0}^2}{T}} g_n(\mu_0)^q \tag{4.2}$$

where μ_0 denotes the central spin and $g_n(\mu_0)$ is a contribution to the partition function of one lattice branch, starting from the central site with fixed spin value μ_0. $g_n(\mu_0)$ is connected with $g_{n-1}(\mu_1)$ in the following way:

$$\begin{aligned} g_n(\mu_0) &= \sum_{\mu_0}(J(S_{a,0,1}S_{b,0,1}) + K(S_{a,0,1}S_{b,0,1})^2 + J_1(\mu_0+\mu_1)(S_{a,0,1}+S_{b,0,1}) \\ &+ K_1({\mu_0}^2+{\mu_1}^2)(S^2_{a,0,1}+S^2_{b,0,1}) + \Delta(S^2_{a,0,1}+S^2_{b,0,1}) + \Delta_1\frac{{\mu_0}^2+{\mu_1}^2}{q} \\ &- h(S_{a,0,1}+S_{b,0,1}) - h_1\frac{\mu_0+\mu_1}{q}) \end{aligned} \tag{4.3}$$

The single site magnetic and quadrupole moments can be written in the form.

$$m_\mu = \langle\mu_i\rangle = \frac{\sum_{\mu_i,S_{a,i,j},S_{b,i,j}}(\mu_i)e^{-\beta H}}{Z} \tag{4.4}$$

$$m_S = \langle S_{a,i,j}+S_{b,i,j}\rangle = \frac{\sum_{\mu_i,S_{a,i,j},S_{b,i,j}}(S_{a,i,j}+S_{b,i,j})e^{-\beta H}}{Z} \tag{4.5}$$

$$p_\mu = \langle{\mu_i}^2\rangle = \frac{\sum_{\mu_i,S_{a,i,j},S_{b,i,j}}({\mu_i}^2)e^{-\beta H}}{Z} \tag{4.6}$$

$$p_S = \langle{S_{a,i,j}}^2+{S_{b,i,j}}^2\rangle = \frac{\sum_{\mu_i,S_{a,i,j},S_{b,i,j}}({S_{a,i,j}}^2+{S_{b,i,j}}^2)e^{-\beta H}}{Z} \tag{4.7}$$

where I have set $k_B = 1$. The total magnetization and quadrupole moment per site are given by the following expressions:

$$m = \frac{m_\mu+2\mu_s}{3}, \qquad p = \frac{p_\mu+2p_s}{3} \tag{4.8}$$

Introducing new notations.

$$x_n = \frac{g_n(+)}{g_n(0)}, \qquad y_n = \frac{g_n(-)}{g_n(0)} \tag{4.9}$$

By inserting the values of $g_n(\mu_0)$ in the above equation we get a set of recursion functions.

$$x_{n+1} = f_1(x_n, y_n), \qquad y_{n+1} = f_2(x_n, y_n) \tag{4.10}$$

where $f_1(x,y)$ and $f_2(x,y)$ have the following form:

$$f_1(x,y) = \frac{a_0 + a_1 x^{q-1} + a_2 y^{q-1}}{c_0 + c_1 x^{q-1} + c_2 y^{q-1}} \qquad \frac{b_0 + b_1 x^{q-1} + b_2 y^{q-1}}{c_0 + c_1 x^{q-1} + c_2 y^{q-1}} \tag{4.11}$$

where

$$\begin{aligned}
a_0 &= 1 + 2e^{-\frac{h+\Delta-J_1+K_1}{T}} + 2e^{-\frac{-h+\Delta+J_1+K_1}{T}} + 2e^{-\frac{-J+K+2\Delta+2K_1}{T}} + e^{-\frac{2h+J+K+2\Delta-2J_1+2K_1}{T}} \\
&+ e^{-\frac{-2h+J+K+2\Delta+2J_1+2K_1}{T}} \\
a_1 &= e^{-\frac{\Delta_1-h_1}{T}} + 2e^{-\frac{h+\Delta-h_1-2J_1+2K_1+\Delta_1}{T}} + 2e^{-\frac{-h+\Delta-h_1+2J_1+2K_1+\Delta_1}{T}} + 2e^{-\frac{-J+K+2\Delta-h_1+4K_1+\Delta_1}{T}} \\
&+ e^{-\frac{2h+J+K+2\Delta-h_1-4J_1+4K_1+\Delta_1}{T}} + e^{-\frac{-2h+J+K+2\Delta-h_1+4J_1+4K_1+\Delta_1}{T}} \\
a_2 &= e^{-\frac{h_1+\Delta_1}{T}} + 2e^{-\frac{-h+\Delta+h_1+2K_1+\Delta_1}{T}} + 2e^{-\frac{h+\Delta+h_1+2K_1+\Delta_1}{T}} + 2e^{-\frac{-J+K+2\Delta+h_1+4K_1+\Delta_1}{T}} \\
&+ e^{-\frac{-2h+J+K+2\Delta+h_1+4K_1+\Delta_1}{T}} + e^{-\frac{2h+J+K+2\Delta+h_1+4K_1+\Delta_1}{T}}
\end{aligned}$$

$$\begin{aligned}
b_0 &= 1 + 2e^{-\frac{-h+\Delta-J_1+K_1}{T}} + 2e^{-\frac{h+\Delta+J_1+K_1}{T}} + 2e^{-\frac{-J+K+2\Delta+2K_1}{T}} + e^{-\frac{-2h+J+K+2\Delta-2J_1+2K_1}{T}} \\
&+ e^{-\frac{2h+J+K+2\Delta+2J_1+2K_1}{T}} \\
b_1 &= e^{-\frac{\Delta_1-h_1}{T}} + 2e^{-\frac{-h+\Delta-h_1+2K_1+\Delta_1}{T}} + 2e^{-\frac{h+\Delta-h_1+2K_1+\Delta_1}{T}} + 2e^{-\frac{-J+K+2\Delta-h_1+4K_1+\Delta_1}{T}} \\
&+ e^{-\frac{-2h+J+K+2\Delta-h_1+4K_1+\Delta_1}{T}} + e^{-\frac{2h+J+K+2\Delta-h_1+4K_1+\Delta_1}{T}} \\
b_2 &= e^{-\frac{h_1+\Delta_1}{T}} + 2e^{-\frac{-h+\Delta+h_1-2J_1+2K_1+\Delta_1}{T}} + 2e^{-\frac{h+\Delta+h_1+2J_1+2K_1+\Delta_1}{T}} + 2e^{-\frac{-J+K+2\Delta+h_1+4K_1+\Delta_1}{T}} \\
&+ e^{-\frac{-2h+J+K+2\Delta+h_1-4J_1+4K_1+\Delta_1}{T}} + e^{-\frac{2h+J+K+2\Delta+h_1+4J_1+4K_1+\Delta_1}{T}}
\end{aligned}$$

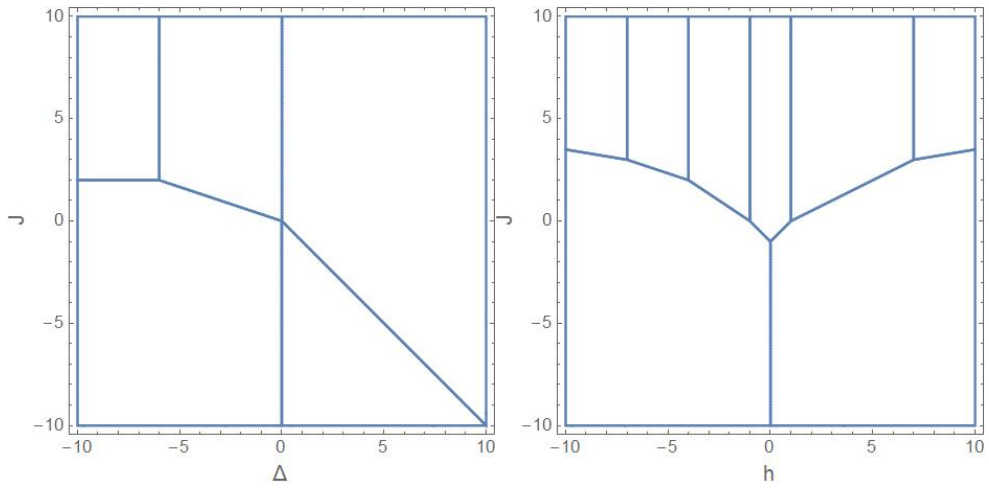

(a) $h = 0$ (b) $\Delta = 1$

Figure 4.2: Ground States diagram for $J_1 = 1$

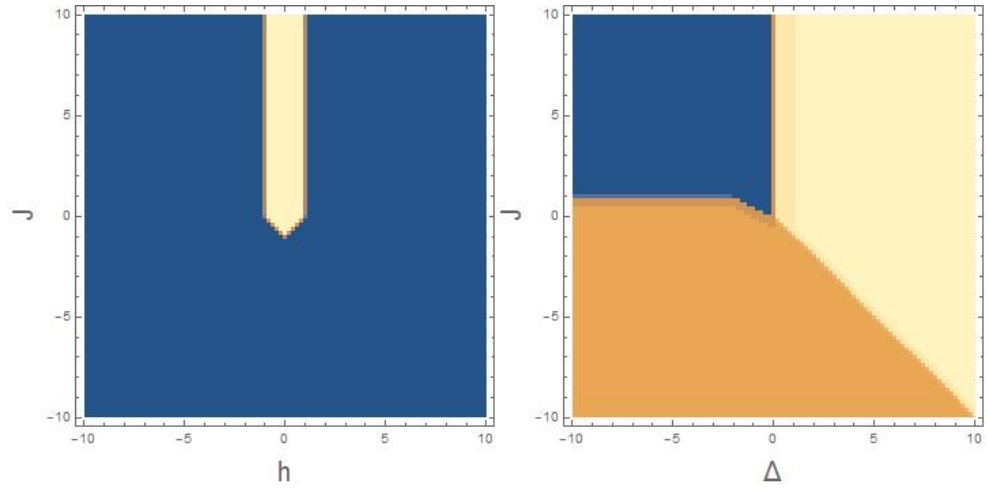

(a) $h = 0$ (b) $\Delta = 1$

Figure 4.3: Fixed Stable points for $J_1 = 1$

$$
\begin{aligned}
c_0 &= 1 + 2e^{-\frac{\Delta - h}{T}} + 2e^{-\frac{h+\Delta}{T}} + 2e^{-\frac{-J+K+2\Delta}{T}} + 2e^{-\frac{-2h+J+K+2\Delta}{T}} + e^{-\frac{2h+J+K+2\Delta}{T}} \\
c_1 &= e^{-\frac{\Delta_1 - h_1}{T}} + 2e^{-\frac{h+\Delta-h_1-J_1+K_1+\Delta_1}{T}} + 2e^{-\frac{-h+\Delta-h_1+J_1+K_1+\Delta_1}{T}} + 2e^{-\frac{-J+K+2\Delta-h_1+2K_1+\Delta_1}{T}} \\
&+ e^{-\frac{2h+J+K+2\Delta-h_1-2J_1+2K_1+\Delta_1}{T}} + e^{-\frac{-2h+J+K+2\Delta-h_1+2J_1+2K_1+\Delta_1}{T}} \\
c_2 &= e^{-\frac{h_1+\Delta_1}{T}} + 2e^{-\frac{-h+\Delta+h_1-J_1+K_1+\Delta_1}{T}} + 2e^{-\frac{h+\Delta+h_1+J_1+K_1+\Delta_1}{T}} + 2e^{-\frac{-J+K+2\Delta+h_1+2K_1+\Delta_1}{T}} \\
&+ e^{-\frac{-2h+J+K+2\Delta+h_1-2J_1+2K_1+\Delta_1}{T}} + e^{-\frac{2h+J+K+2\Delta+h_1+2J_1+2K_1+\Delta_1}{T}}
\end{aligned}
\tag{4.12}
$$

By using the recursion relations, the calculations of magnetic and quadrupole moments are straightforward. The quadrupole and magnetic moments are shown in Fig 4.5a and 4.5b.

4.3 Lyapunov exponents and superstable points

Lyapunov exponents quantify the growth rate of an infinitesimal perturbation on a reference trajectory, and they provide a measure of the degree of "instability" of the system: a positive maximum Lyapunov exponent corresponds to chaotic, unstable states, while a negative maximum Lyapunov exponent signals stable states. Such exponents are computed from dynamical recursion equations: a zero maximum Lyapunov exponents is the dynamic counterpart of a second-order phase transition.
We recall that if we have a dimensional map then a spectrum of exponents is present; the Lyapunov exponent is calculated by the following equation (see [108, 112, 114, 115, 144, 145])

$$\lambda_i = \lim_{n\to\infty} \frac{\log H_i}{2n}, \qquad \mathbf{H} = J(x_0)J(x_1)\ldots J(x_n) \tag{4.13}$$

where H_i is the i-th eigenvalue of $\mathbf{H}^\dagger\mathbf{H}$ and $J(x_k)$ is the Jacobian matrix of our N dimensional map after k iterations from the initial point x_0.
We used a standard (Gram-Schmidt) numerical procedure to compute both Lyapunov exponents for our 2 dimensional recursion relations. We consider a point a superstable if it's maximum lyapunov exponent tends to minus infinity when the temperature goes to zero (see Fig. 4.4). Our numerical investigation shows the existence of superstable for $\Delta > 0$ when $J > 0$ (antiferomagnetic) cases and $\Delta > 0$ when , $J < 0$ & $|J| < 0$ (feromagnetic) cases. This region coincides with the a phase in the ground states diagram as well as with a region in fixed stable points diagram (see Fig. 4.2 and 4.3). The three way connection of fixed stable points, ground states and superstable points implies a fundamental property of the system with the specific regions. It's also worth noticing the existence of magnetisation plateaus in the region surrounding superstable point.

4.4 Discussion and conclusions

In the present work, I investigated the connections between stability and magnetic properties of the spin-1 Ising model on the diamond-like decorated Bethe lattice. The dynamical solution of the

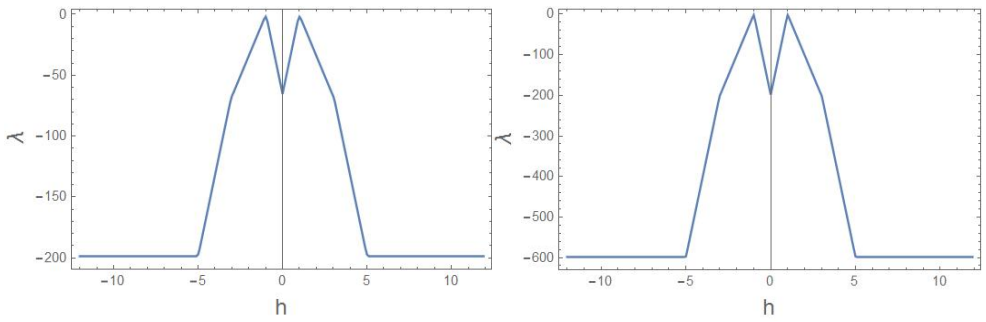

(a) $T = 0.03$ (b) $T = 0.01$

Figure 4.4: maximum Lyapunov exponents for $J = 1$, $J_1 = 1$, $\Delta = 1$

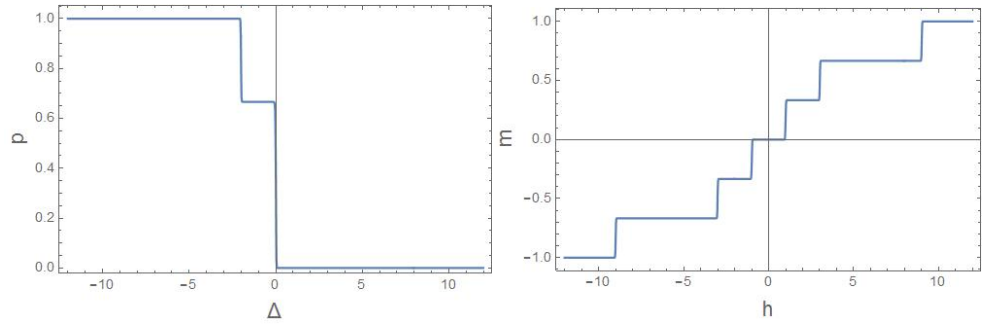

(a) $h = 0$ (b) $\Delta = 1$

Figure 4.5: quadrupole moment and magnetization for $J = 1$, $J_1 = 1$, $T = 0.01$

model is obtained by using the recursion relations method. The Lyapunov exponents, magnetic and quadrupole moments, superstable points and cycles of the system at $T \to 0$ have been studied. Furthermore the paper shows connection between ground states and stable fixed points suggests a non-trivial relation between them. Finally we believe its implying a more general connection between magnetization, stable point and superstable points independent of the lattice.

Chapter 5

Classical limit theorems and high entropy MIXMAX random number generator

5.1 *Introduction*

Our intention in this article is to consider the behaviour of deterministic Anosov C-systems in parallel with the classical limit theorems of probability theory, demonstrating that they possess the properties which are inherent to the independent and identically distributed random variables defined in probability theory.

We investigate the interrelation between the distribution of stochastic fluctuations of independent random variables in probability theory and the distribution of time averages in deterministic Anosov C-systems. On the one hand, in probability theory, our interest dwells on three basic topics: the laws of large numbers, the central limit theorem and the law of the iterated logarithm for sequences of real-valued random variables [146–158] . On the other hand we have chaotic, uniformly hyperbolic Anosov C-systems defined on tori which have mixing of all orders and nonzero Kolmogorov entropy [76, 77, 79–86, 88, 159–163]. These extraordinary ergodic properties of Anosov C-systems ensure that the above classical limit theorems for sums of independent random variables in probability theory are fulfilled by the time averages for the sequences generated by the C-systems [164–167]. The MIXMAX generator of pseudorandom numbers represents the homogeneous C-system for which the

classical limit theorems are fulfilled [77, 86, 88, 162, 163].

The present paper is organised as follows. In section two we shall overview the classical limit theorems in probability theory. In section three the basic properties of the Anosov C-systems will be defined, their spectral properties and the entropy will be presented. In section four a parallel between the classical limit theorems of probability theory and behaviour of deterministic dynamical C-systems will be derived and the mapping dictionary between the two systems will be established. We shall analyse the law of large numbers, the central limit theorem and law of the iterated logarithm in the case of C-system MIXMAX generator of pseudorandom numbers. The C-system nature of the MIXMAX generator provides well define mathematical background and guaranty the uniformity of generated sequences.

5.2 *Classical Limit Theorems in Probability Theory*

Consider an infinite sequence of *independent and identically distributed random variables* $\xi_1(x), \xi_2(x), \ldots$ on the interval $0 \leq x \leq 1$ having finite mean values $\mathbf{M}\xi_k = \mu$ and finite variance $\sigma^2 = \mathbf{M}(\xi_k - \mu)^2$ ($0 < \sigma^2 < \infty$) [146]. One of the fundamental questions of interest in probability theory is the limiting behaviour of the sum [146–150, 152, 158]

$$S_n = \xi_1 + \xi_2 + ... + \xi_n = \sum_{k=1}^{n} \xi_k \tag{5.1}$$

as $n \to \infty$. By the classical *central limit theorem* the difference between the average S_n/n and μ multiplied by the factor $\sqrt{n}$ *converges in probability* to the normal distribution $\Phi(\frac{z}{\sigma})$

$$\mathbf{P}\left\{ \sqrt{n}(\frac{S_n}{n} - \mu) < z \right\} \;\; \to \;\; \frac{1}{\sqrt{2\pi\sigma^2}} \int_{-\infty}^{z} e^{-\frac{y^2}{2\sigma^2}}\, dy \qquad \text{for every z.} \tag{5.2}$$

The estimates of the convergence rate in the above central limit theorem were obtained by Lyapunov, Berry, Esseen and others [153–157]. For independent and identically distributed random variables

having finite absolute third moments $\chi^3 = \mathbf{M}\xi_k^3 < \infty$ it has the form:

$$\sup_z |\mathbf{P}\left\{ \sqrt{n}(\frac{S_n}{n} - \mu) < z \right\} - \Phi(\frac{z}{\sigma})| \leq \frac{1}{\sqrt{n}}\Big(\frac{\chi}{\sigma}\Big)^3 . \tag{5.3}$$

By the Kolmogorov *strong law of large numbers* the average S_n/n converges *almost surely* to the common mean value μ of the random variables $\xi_k(x)$, that is

$$\mathbf{P}\left\{ \lim_{n\to\infty} \frac{S_n}{n} = \mu \right\} = 1 . \tag{5.4}$$

Under the same conditions as in the above theorems Petrov [158] has derived the estimates of the order of growth of the sums S_n (5.1). The following growth estimates take place

$$\begin{aligned}
\mathbf{P}\left\{ \lim_{n\to\infty} \frac{S_n - \mu n}{n^{\frac{1}{2}+\varepsilon}} = 0 \right\} &= 1 , \\
\mathbf{P}\left\{ \lim_{n\to\infty} \frac{S_n - \mu n}{n^{\frac{1}{2}}(\ln n)^{\frac{1}{2}+\varepsilon}} = 0 \right\} &= 1 , \\
\mathbf{P}\left\{ \lim_{n\to\infty} \frac{S_n - \mu n}{n^{\frac{1}{2}}\ln n^{\frac{1}{2}}(\ln\ln n)^{\frac{1}{2}+\varepsilon}} = 0 \right\} &= 1 , \\
&\cdots\cdots\cdots\cdots
\end{aligned} \tag{5.5}$$

for arbitrary $\varepsilon > 0$. This result means that the random variables $S_n - \mu n$ cannot grow faster than $n^{\frac{1}{2}+\varepsilon}$ or $n^{\frac{1}{2}}(\ln n)^{\frac{1}{2}+\varepsilon}$ or $\ln n^{\frac{1}{2}}(\ln\ln n)^{\frac{1}{2}+\varepsilon}$ and so on. The theorem on the *law of the iterated logarithm* for a sequence of random variables $\{\xi_k\}$ involve conditions under which the sequence $\lim_{n\to\infty}\sup\frac{S_n-\mu n}{\sqrt{2n\ln\ln n}} = \sigma$ converges almost surely. This relation strengthens the estimates provided by the strong law of large numbers (5.4) and (5.5). For the independent and identically distributed random variables (5.1) the following Kolmogorov *theorem of the iterated logarithm* take place [147–149]

$$\mathbf{P}\left\{ \lim_{n\to\infty}\sup\frac{S_n - \mu n}{\sqrt{2n\ln\ln n}} = \sigma \right\} = 1, \quad \mathbf{P}\left\{ \lim_{n\to\infty}\inf\frac{S_n - \mu n}{\sqrt{2n\ln\ln n}} = -\sigma \right\} = 1 , \tag{5.6}$$

that is a maximal possible growth of the sum is $\sigma\sqrt{2n\ln\ln n}$. In order to gain an intuitive understanding of this result it is worth to calculate the probability of large fluctuations of the sum S_n us-

ing the central limiting theorem (5.2). It follows from (5.2) that for the arbitrary positive number b, $z = \sigma\, b\sqrt{2\ln\ln n}$ and large n take place the following relation

$$\mathbf{P}\left\{ \sqrt{n}(\frac{S_n}{n} - \mu) \geq \sigma\, b\sqrt{2\ln\ln n} \right\} \rightarrow 1 - \frac{1}{\sqrt{2\pi\sigma^2}} \int_{-\infty}^{\sigma\, b\sqrt{2\ln\ln n}} e^{-\frac{y^2}{2\sigma^2}} dy\,, \tag{5.7}$$

where the right hand side has the asymptotic $1/2b(\pi\ln\ln n)^{1/2}(\ln n)^{b^2}$ and therefore

$$\frac{1}{(\ln n)^{(1+\delta)b^2}} \leq \mathbf{P}\left\{ \frac{S_n(x) - \mu n}{\sqrt{2n\ln\ln n}} \geq b\,\sigma \right\} \leq \frac{1}{(\ln n)^{b^2}}\,. \tag{5.8}$$

Considering the subsequence $n = q^m$, where q is a fixed integer, one can derive from (5.8) the celebrated law of the iterated logarithm (5.6) [147–150, 152, 158]. The law of the iterated logarithm is a refinement of the law of large numbers (5.4) and specifies the global behaviour of the asymptotic sequence of the sum S_n since the quantity in the limit in (5.6) depends not only on single n but the totality of the remainder of the sum. Using the central limiting theorem (5.2) now for the fluctuations in the interval $(-\varepsilon\sqrt{2\ln\ln n}, +\varepsilon\sqrt{2\ln\ln n})$ one can get that

$$\mathbf{P}\left\{ |\frac{S_n(x) - \mu n}{\sqrt{2n\ln\ln n}}| < \varepsilon \right\} \rightarrow \frac{1}{\sqrt{2\pi\sigma^2}} \int_{-\sigma\,\varepsilon\sqrt{2\ln\ln n}}^{\sigma\,\varepsilon\sqrt{2\ln\ln n}} e^{-\frac{y^2}{2\sigma^2}} dy \rightarrow 1, \tag{5.9}$$

meaning that the sum (5.1) scaled by the factor $\sqrt{2n\ln\ln n}$ is less than any $\varepsilon > 0$ with probability approaching one, but will be occasionally visiting points in the interval $(-\sigma, \sigma)$ in accordance with the theorem (5.6).

Our goal is to compare the asymptotic behaviour of the sum S_n which have been establish in the above limit theorems in probability theory with the asymptotic behaviour of the corresponding quantities defined for deterministic dynamical C-systems and specifically for the C-system which have been implemented into the MIXMAX generator [77, 86, 88, 162, 163].

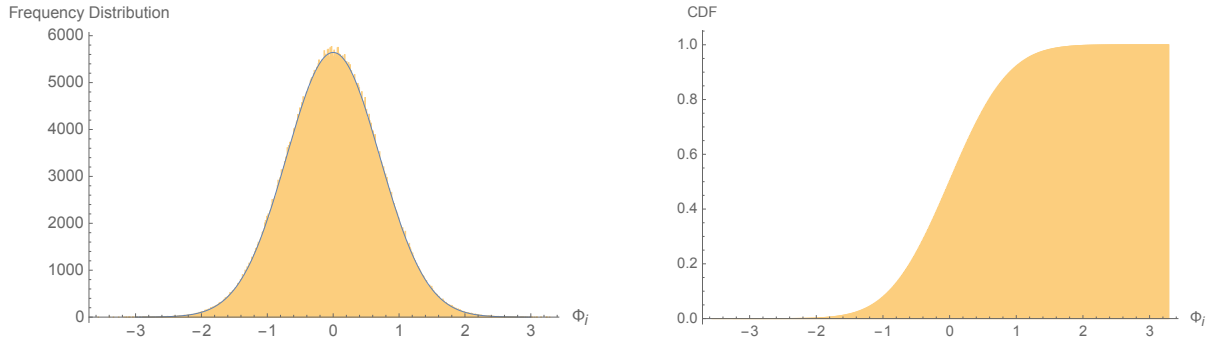

(a) (b)

Figure 5.1: a)The frequency distribution histogram for the underlying variable $\phi_i(f,n)$ in (5.23). The dimension of the C-system generator is $N = 17$, the iteration time is $n = 10^4$, the bins are of equal size $\varepsilon = 0.01$ and the total number of phase space points x_i is $I = 10^6$. The function $f(x) = \cos 2\pi(x_1 + ... + x_{17})$. The mean value is $\langle\phi\rangle = 0.000470253$ and the standard deviation $\langle\phi^2\rangle = \sigma_f^2 = 0.499867$. b) The p-value of the cumulative distribution function (CDF) for the Kolmogorov-Smirnov test is $p = 0.909337$.

5.3 *Classical Limit Theorems and Deterministic C-systems*

With that aim let us now consider the statistical properties of deterministic dynamical C-systems. The hyperbolic Anosov C-systems defined on a torus have *mixing of all orders and nonzero Kolmogorov entropy* [76, 77, 79–85, 159–161, 163]. The statistical properties of a C-system defined by the map $\{\forall\, x \in \mathcal{M} : x \to x_n = T^n x\}$ are characterised by the behaviour of the correlation functions of observables $\{f(x)\}$ on the phase space $\mathcal{M}$

$$D_n(f,g) = \langle f(x)g(T^n x)\rangle - \langle f(x)\rangle\langle g(x)\rangle, \tag{5.10}$$

where T denotes the Anosov C-system and $\langle....\rangle$ the phase space averages [77, 86, 88, 161, 162, 168, 169]. These correlation functions decay exponentially, meaning that the observables on the phase space become independent and uncorrelated exponentially fast [170–182]. For the C-systems defined on the N-dimensional torus (5.19) the upper bound on the exponential decay of the correlation functions is universal and is defined by the value of the system entropy $h(T)$ [163] :

$$|D_n(f,g)| \leq C\, e^{-nh(T)\nu}, \tag{5.11}$$

where $C = C(f,g)$ and $\nu = \nu(f,g)$ depend only on the observables and are positive numbers. This result allows to define the *decorrelation time* τ_0 for the observable $f(x)$ as [163]

$$\tau_0 = \frac{1}{h(T)\nu_f} , \tag{5.12}$$

where $\nu_f = \nu(f,f)$. The index ν_f is increasing linearly $\nu_f = 2pN$ with the dimension N of the C-system, where p is the order of smoothness of the function $f(x)$ [163]. The entropy $h(T)$ is also increases linearly $h(T) = \frac{2}{\pi}N$ (5.22) [162], therefore [163]

$$\tau_0 = \frac{\pi}{4pN^2} \ . \tag{5.13}$$

This result justifies the statistical/probabilistic description of the C-systems [161] and have important consequences in the form of the law of large numbers and central limit theorem for Anosov C-systems [164–167]. The time average of the observable $f(x)$ on $\mathcal{M}$

$$\bar{f}_n(x) = \frac{1}{n}\sum_{k=0}^{n-1} f(T^k x) \tag{5.14}$$

behaves as a superposition of quantities which are statistically independent, therefore [76, 164]

$$\lim_{n\to\infty} \bar{f}_n(x) = \langle f \rangle \tag{5.15}$$

and the fluctuations of the time averages (5.14) from the phase space average $\langle f \rangle$ multiplied by $\sqrt{n}$ have at large $n \to \infty$ the Gaussian distribution [164–167, 183]:

$$\lim_{n\to\infty} m\left\{ x : \sqrt{n}\left(\bar{f}_n(x) - \langle f \rangle \right) < z \right\} = \frac{1}{\sqrt{2\pi\sigma_f^2}} \int_{-\infty}^{z} e^{-\frac{y^2}{2\sigma_f^2}} dy \ , \tag{5.16}$$

where m is the invariant measure on the phase space $\mathcal{M}$ and the value of the standard deviation σ_f is a sum

$$\sigma_f^2 = \langle f^2(x) \rangle - \langle f(x) \rangle^2 + 2\sum_{n=1}^{+\infty} [\langle f(T^n x) f(x) \rangle - \langle f(x) \rangle^2]. \tag{5.17}$$

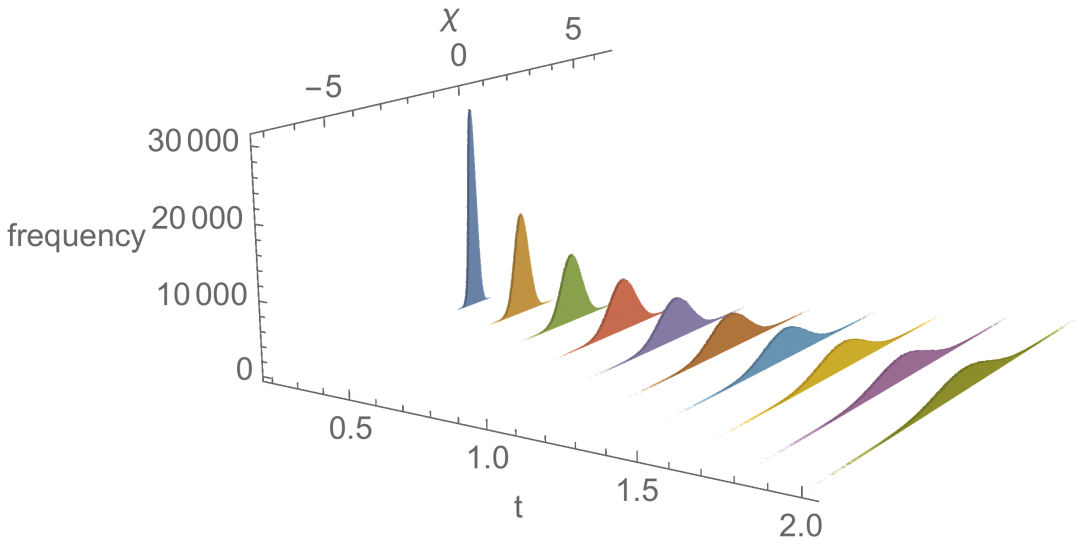

Figure 5.2: The frequency distribution histogram for the variable $\chi_i(t)$ defined in (5.25). The "time" interval is taken as $[0.2, 2]$. The other parameters are the same as in Fig. 5.1.

These results allow to trace a parallel between the classical limit theorems of probability theory and behaviour of deterministic dynamical C-systems. The theorems (5.15) and (5.16) which taking place for the deterministic C-systems are in fine analogy with the theorems (5.4) and (5.2) in probability theory. This analogy can be made explicit if one use the dictionary:

$$\begin{aligned} \xi_k(x) &\iff f(T^k x), \\ S_n(x) &\iff \sum_{k=0}^{n-1} f(T^k x), \\ \frac{S_n(x)}{n} &\iff \frac{1}{n}\sum_{k=0}^{n-1} f(T^k x). \end{aligned} \tag{5.18}$$

In the next section we shall consider the fine examples of the C-systems defined on the tori. These systems represent a large class of C-systems which can be easily realised on a computer platform in the form of computer algorithms. These algorithms are used to generate pseudorandom numbers of high quality and represent the called MIXMAX pseudorandom number generators [77, 86, 88, 184–186]. In particular it passes all empirical *U01 tests* [187].

5.4 *MIXMAX C-systems Generator*

The linear automorphisms of the unit hypercube $\mathcal{M}^N$ in Euclidean space E^N with coordinates $(x_1,...,x_N)$ [76, 77, 86, 88] is defined as follows:

$$x_i^{(k+1)} = \sum_{j=1}^{N} T_{ij} x_j^{(k)} \mod 1, \qquad k = 0,1,2,... \tag{5.19}$$

where the components of the vector $x^{(k)}$ are $x^{(k)} = (x_1^{(k)},...,x_N^{(k)})$. The phase space $\mathcal{M}^N$ of the systems (5.19) can also be considered as the N-dimensional torus [76, 77, 86, 88]. The operator T acts on the initial vector $x^{(0)}$ and produces a phase space trajectory $x^{(n)} = T^n x^{(0)}$ on a torus. The C-system is defined by the integer matrix T which has a determinant equal to one $\mathrm{Det}T = 1$ and has no eigenvalues on the unit circle [76]:

$$1)\ \mathrm{Det}T = \lambda_1 \lambda_2 ... \lambda_N = 1, \quad 2)\ |\lambda_i| \neq 1, \quad \forall\ i. \tag{5.20}$$

The measure $dm = dx_1...dx_N$ is invariant under the action of T. The conditions (5.20) guarantee that T represents Anosov C-system [76] and therefore as such it is a Kolmogorov K-system [79–81, 84, 85] with mixing of all orders and of nonzero entropy. The C-system (5.19) has a nonzero Kolmogorov entropy $h(T)$ [76, 81–83, 85, 88]:

$$h(A) = \sum_{|\lambda_\beta|>1} \ln|\lambda_\beta|. \tag{5.21}$$

We shall consider a family of matrix operators T of dimension N introduced in [86]. The operators T fulfill the C-condition (5.20) and represents a C-system [77, 86, 162] with entropy:

$$h(A) = \sum_{\beta} \ln|\lambda_\beta| \approx \frac{2}{\pi} N \tag{5.22}$$

which is increases linearly with the dimension N of the matrix. Our aim is to study the asymptotic behaviour of the sum S_n as $n \to \infty$ for the pseudorandom number generator MIXMAX [86, 162] which is defined by the equations (5.19).

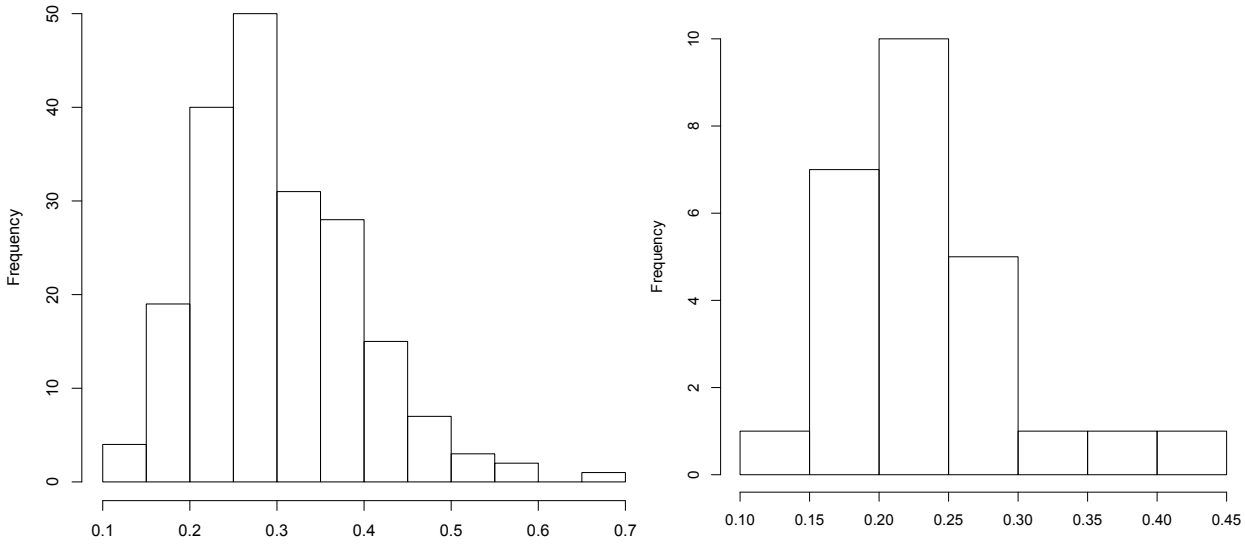

Figure 5.3: Two histograms of the variable $\Gamma_n = S_n/\sqrt{2n\ln\ln n}$ in (5.27). The dimension of the C-system generator is $N = 240$ and the iteration time $n = 10^9$. The total number of phase space points x_i is $I = 200$. Here in S_n data we have subtracted the term μn. The sum S_n grows approximately as $\sigma\sqrt{n}$. The standard deviation for the observable $f(x) = x$ is equal to $\sigma = 1/\sqrt{12}$. The distribution function of the supremum of the Γ_n is calculated for the values n in the interval $n \in [m, 10^9]$ for $m = 15$ and $m = 10^5$. As one can see the distribution of Γ_n for the supremum values (5.28) is tightens towards $\sigma = 1/\sqrt{12} \approx 0.27$ in accordance with the Kolmogorov law of the iterated logarithm (5.6). On the first histogram, at $m = 15$, there are 65 events smaller and 85 events larger than σ. On the second histogram, at $m = 10^5$, there are 8 events smaller and 8 events larger than σ.

In order to study the asymptotic behaviour in equation (5.16) as $n \to \infty$ we shall consider first the following variable

$$\phi_i(f,n) = \sqrt{n}\Big(\frac{1}{n}\sum_{k=0}^{n-1} f(T^k x_i) - \langle f \rangle\Big) \tag{5.23}$$

which depends on initial phase space vector x_i of the N-dimensional unit hypercube $\mathcal{M}^N$, the function $f(x)$ and the number of iterations n. In order to calculate the number of vectors $x_i, i = 1,...,I$ which fulfill the inequality $\phi_i(f,n) < z$ we shall construct the frequency distribution of the underlying variable $\phi_i(f,n)$. The bins will be taken of equal size ε. The Fig. 5.1 represents the distribution function calculated for the MIXMAX generator of size $N = 17$ and the comparison with the Gaussian distribution

$$\rho(\phi) = \frac{I\varepsilon}{\sqrt{2\pi\sigma_f^2}}\, e^{-\frac{\phi^2}{2\sigma_f^2}}, \tag{5.24}$$

shown on the Fig.5.1 as a solid blue line. We have used the Kolmogorov-Smirnov test to calculate the p-value. The p-value of the cumulative distribution function (CDF) for the Kolmogorov-Smirnov test here was $p = 0.909337$. The null hypothesis that the data is distributed according to the normal distribution is not rejected at the 0.1% level based on the Kolmogorov-Smirnov test.

Introducing a new parameter $t = p/n$, where p is an integer number $p \in \mathcal{Z}$ and the alternative variable

$$\chi_i(t) = t\sqrt{n}\Big(\frac{1}{tn}\sum_{k=0}^{tn-1} f(T^k x_i) - \langle f \rangle\Big) \tag{5.25}$$

we can find the distribution function for the variable χ. It was proven that the variable χ is described in accordance with the Wiener-Feynman process [172]

$$\rho(\chi,t) = \frac{I\varepsilon}{\sqrt{2\pi\sigma_f^2 t}}\, e^{-\frac{\chi^2}{2\sigma_f^2 t}}. \tag{5.26}$$

On Fig. 5.2 one can see that with the increasing "time" t the distribution evolve as in (5.26). The useful analogy will be if one consider $I\varepsilon$ as the number of "particle" at the initial time of the diffusion and $D = \sigma_f^2$ as the diffusion coefficient.

Considering the central limit theorem we were performing iterations for the relatively small

values of $n \approx 10^4$. In order to study the large fluctuations of the sum S_n described by the law of the iterated logarithm we generated sequences of increasing length $n = 10^7 - 10^9$ and then constructed the distribution function of the maximum values of the variable

$$\Gamma_n(x) = \frac{\sum_{k=0}^{n-1} f(T^k x) - \langle f \rangle \, n}{\sqrt{2n \ln \ln n}} \tag{5.27}$$

at the tail of the sequences in accordance with the definition of the limit superior

$$\overline{\lim}\, \Gamma := \lim_{m \to \infty} \left(\sup_{n \geq m} \Gamma_n \right). \tag{5.28}$$

We illustrated the distribution function for the values n in the interval $n \in [m, 10^9]$ for $m = 15$ and $m = 10^5$ on Fig. 5.3. As one can see the distribution of the supremum values is tightens towards $\sigma = 1/\sqrt{12}$.

Chapter 6

Frontal Cellular Automata for the Study of Non-Equilibrium Lattice Models

6.1 Introduction

The Abelian sandpile model(ASM) [188, 189] also known as the Bak Tang Wiesenfeld(BTW model originally proposed by Bak [29] is a dynamical system with essential properties of self-organized criticality (SOC). The characterization of the SOC state has two aspects, dynamical and structural. The first one, implies a description of avalanches, their duration, mass, linear extent, perimeter, etc. The structural characteristics of the sandpile are fractional numbers of sites having a given height and correlations between heights at different sites in a typical allowed configuration. The model is a cellular automata, which allows using CA algorithms for research.

The most natural formulation of a 2D lattice ASM is in terms of discrete height variables, take on four integral values 1 to 4 and are located at the sites of a grid. The configuration of the sandpile, formed by the values of the heights, evolves under a stochastic dynamics, which eventually reaches a stationary regime, where the configurations are weighted according to an invariant measure.

The height properties have been calculated for an infinite lattice, also for upper half plane and various other elementary boundaries [190–195]. In this paper we take fractals as boundaries taking into account their self repeating nature.

ASM is strongly correlated with the rotor-router model and loop-erased random walks. The researches of the late decades showed the connection between the ASM and diverse phenomena such as: earthquakes, luminosity of stars, river flows, coagulation, relaxation phenomena in magnets, and neural networks. Another interesting feature is its connection to conformal field theory (CFT) models. In particular, for 2D ASM, the associated conformal field theory is suggested to be symplectic fermions with central charge c=-2. Furthermore, some operators in the logarithmic conformal field theories(LCFT) model which correspond to different clusters in ASM are found. LCFT are believed to describe the continuum limit of certain non-equilibrium lattice models, like dense polymers, sandpile models, dimer models and percolation , as well as the infinite series of the lattice models recently defined.

6.2 Cellular Automata

Cellular automata are consisted of a grid whose nodes are finite automata. Each node has a finite set of states and transition rules which depending on the node, the state of the node, the state of its neighbors and the moment of time change the state of the node. In the general case the neighbors of a node can be chosen arbitrarily. The general CA is a loosely defined model which allows representing a great number of models and systems as CAs. In our case we assume that the CA is frontal cellular automaton. The difference in general CAs and FCAs is in their transition rules and the number of active nodes (if a node acted by a transition rule changes its state it's named active). A general FCAs transition rules do not depend on the time, also the number of active nodes is far smaller then the number of nodes. The latter criterion ensures a much faster speed in comparison to general CAs. The following is the classical algorithm for FCAs relaxation.

6.3 Abelian sandpile model

We denote by $G = (V,E)$ a directed finite graph where V is the set of vertices and E is the set of directed edges. In this model we allow self loops and multiple edges. We denote by $E(v)$ and d_v(out

Algorithm 1 The relaxation of the asynchronous frontal cellular automata

```
1: for all x ∈ V do
2:     if x.isUnstable() then
3:         stack.push(x)
4:         bitmap[x] ← 1
5:     else
6:         bitmap[x] ← 0
7:     end if
8: end for

9: while stack.containsElement() do
10:    x ← stack.pop()
11:    bitmap[x] ← 0
12:    while x.isUnstable() do
13:        computeNewValue(x)
14:        for all y ∈ adj[x] do
15:            sendMessage(x, y)
16:            if y.isUnstable() ∧ bitmap[y] = 0 then
17:                stack.push(y)
18:                bitmap[y] ← 1
19:            end if
20:        end for
21:    end while
22: end while
```

degree) the set of edges whose first or second component is v and the number of edges whose first component is vertex v accordingly. A vertex is a sink if its $d_v = 0$.

We label the vertices of G by $v_1, v_2, ..., v_n$ ($|V| = n$). The Laplacian Δ of G will be an $n \times n$ matrix with the following components:

$$\Delta_{ij} = \begin{cases} -a_{ij} & \text{for } i \neq j \\ & \qquad i, j \in 1, 2, ..., n, \\ d_i - a_{ii} & \text{for } i = j \end{cases}$$

where a_{ij} is the number of (v_i, v_j) edges.

We associate every vertex with, a non negative integer $h(v)$ which is the number of sand grains on the vertex (if it is a sink, we consider it to be always 0). A configuration or state of sand piles is an one line (or row) matrix of all $h(v)$. We denote it by $h = \{h(v_1), h(v_2), h(v_3), ..., h(v_n)\}$. The sand piles are in a stable configuration if for any $h(v) < d_v$. If for the given vertex v, the height $h(v) > d_v$ then we consider this vertex as active and in that case we can topple it. The new configuration after toppling

will be $h' = h - \Delta_v$, where Δ_v is a row associated to the vertex v in the Laplacian matrix. We say there is a path from v_i to v_j if there exists a sequence of $e_i, e_{i+1}, ..., e_j$, where for every non ending edge his second component is equal to the firs component of the next edge. If for every vertex there is a path to a sink then this state can always be toppled to a stable state. We refer such graphs to be graphs with global sink and from here we will deal with such graphs.

We denote by E_{v_i} the sand grain addition operator which acts on the state as follows: $E_{v_i}h$ is equal to the stabilized $h = \{h(v_1), h(v_2), h(v_3), ..., h(v_i + 1), ..., h(v_n)\}$. It's proven that in the sandpile models with a global sink the sand grain addition operator is commutative, this property is called the abelian property and a sandpile model with this property abelian sandpile model.

The number of stable configurations is $\prod_i \Delta_{ii}$, $i \in 1, 2, 3..., n$ where the product is over all non-sink vertices i. If a stable configuration can be reached from any configuration by using the operator E_v then we say it's a recurrent configuration [188]. The number of recurrent configurations is $\det\Delta$. The recurrent configurations form a group. A natural question arises: what is the probability of a concrete vertex having a concrete number of sand grains if it's in a recurrent configuration? The most trivial method is to generate all the stable configurations, then separate recurrent configurations and calculate the above mentioned probabilities. Generating stable configurations isn't difficult. If σ is a recurrent configuration, then $(\sigma + \varepsilon)^\circ = \sigma$ equation is true, where $\varepsilon = (2\delta) - (2\delta)^\circ$. Here the δ configuration is given by $\delta(v) = d_v$, and with this formula we can determine if it is stable or not. For a 100×100 quadratic lattice the number of stable configurations will be 4^{10000} which is far grater than the number of elementary particles in the observed universe (10^{86}). A solution to this dilemma might be a statistical approach where we don't generate all stable configurations but only a randomly chosen subset. The second problem is connected to $(\sigma + \varepsilon)^\circ = \sigma$ equation which computes relatively slow and for large lattices is unusable. Fortunately, there is a one to one mapping between recurrent configurations and spanning trees.

6.4 Loop erased random walk and Wilson's method

Wilson's method [196] is a way to generate spanning trees on a given graph. We choose this particular method due to uniform generation of the trees, also the resolution is computationally and resource efficient. A walk in $G(V,E)$ is a sequence of vertices $v_0, v_1, ...$ where for any v_i and v_{i+1} there is an (v_i, v_{i+1}) edge. We define a path as a walk where all vertices are distinct. Lawler [197] defined the loop-erasure $LE(v)$ operator as the path obtained by deleting the cycles in chronological order from walk v as follows:

$$LE(v) = (v_{s(0)}, v_{s(1)}, ..., v_{s(J)}),$$

where $s(0) = 0$ and for $j \geq 0$,

$$s(j+1) = 1 + max\{i | v_i = v_{s(j)}\}$$

A loop erased random walk is obtained by using the operation LE on a random walk.

The following is Wilson's method. Let $G = (V,E)$ be a finite connected graph. Pick up any vertex $r \in V$, and name it as "root". We define a growing sequence of subtrees $T(i), i \geq 0$. We let $T(0) := \{r\}$ and we let $< v_1, v_2, ..., v_{n-1}, r >$ be an enumeration of V. Suppose $T(i)$ has been generated. Start a LORW at v_{i+1} and stop when it hits $T(i)$

$$T(i+1) := T(i) \cup \text{LE walk from } v_{i+1} \text{ to} T(i)).$$

6.5 Height probabilities of a fractal bounded lattice

We use as boundaries two kinds of fractals. These are created by acting on a square graphs vertices with fractal operations. The deforming operation which creates fractals we name fractal operation. The fractal operations we used are illustrated in the following figure: We used four lattices, two of 500×500 and two of 150×150 with $4, 3$ fractal operations on a square as boundaries, respectively. We denote the number of adjacent vertices of v whose unique path to the root passes through v

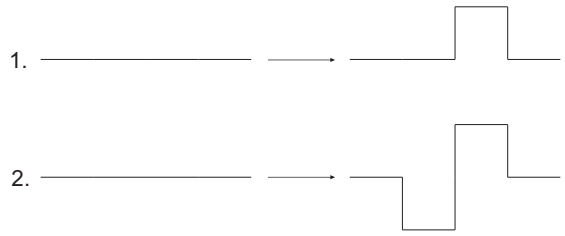

Figure 6.1: Illustration of the two fractal operations.

by $pred_v$, and name it the number of predecessors of v. Its proven that after a sufficient times of experiments the probability for vertex v to have i ($i \in \{0-3\}$) number of predecessors is the same as the probability p_v of having i number of sand grains. Since the number of predecessors depends on only neighboring vertices then if we are interested in only vertex v probabilities we can generate only the subtrees which have the vertex v and its neighbors. According to Wilson's method, the sub tree T for vertex v can be generated in the following process: $T(1) \leftarrow v$

$T(2) \leftarrow$ the upper adjacent vertex of v

$T(3) \leftarrow$ the left adjacent vertex of v

$T(4) \leftarrow$ the lower adjacent vertex of v

$T(5) \leftarrow$ the right adjacent vertex of v

Considering the fact that vertices whose distance is more than 4 or 5 have constant probabilities, we calculated the near border vertices with fare more accuracy (1.6 billion times) in comparison to further away vertices (100 million times).

6.6 Conclusion

As was expected the further away vertices don't depend on the distance from the border, therefore have constant probabilities. The state is different for near border vertices which have a logarithmic dependance on the distance from the border. We try to find a dependence between this logarithmic

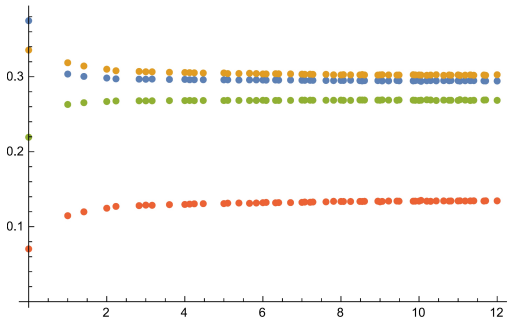

Figure 6.2: Illustration of the dependence of probabilities p_i from the distance from boundary. Here blue=0, orange=1, green=2, red=3 is the number of predecessors.

expression and the dimension of fractal boundaries. Despite their complicated shapes, the fractals have a very weak effect on the probabilities. The results for all four lattices are almost the same and furthermore we experimented with other fractals as boundaries and the results indicate the same. We think that considering the almost invisible effect of 2D fractals numerous experiments are needed to evaluate the height probabilities. The latter is a considerable difficulty taking into account that the size of the lattice grows with the dimension of fractals.

Bibliography

[1] Stephen G Brush. History of the lenz-ising model. *Reviews of modern physics*, 39(4):883, 1967.

[2] G. Bouzerar, A. P. Kampf, and G. I. Japaridze. Elementary excitations in dimerized and frustrated heisenberg chains. *Physical Review B*, 58(6):3117–3123, aug 1998.

[3] H.M. Babujian. Exact solution of the one-dimensional isotropic heisenberg chain with arbitrary spins s. *Physics Letters A*, 90(9):479–482, aug 1982.

[4] H.M. Babujian. Exact solution of the isotropic heisenberg chain with arbitrary spins: Thermodynamics of the model. *Nuclear Physics B*, 215(3):317–336, feb 1983.

[5] L.A. Takhtajan. The picture of low-lying excitations in the isotropic heisenberg chain of arbitrary spins. *Physics Letters A*, 87(9):479–482, feb 1982.

[6] Kazuo Hida. Magnetic properties of the spin-1/2 ferromagnetic-ferromagnetic-antiferromagnetic trimerized heisenberg chain. *Journal of the Physical Society of Japan*, 63(6):2359–2364, jun 1994.

[7] H. Kikuchi, Y. Fujii, M. Chiba, S. Mitsudo, T. Idehara, T. Tonegawa, K. Okamoto, T. Sakai, T. Kuwai, and H. Ohta. Experimental observation of the1/3magnetization plateau in the diamond-chain CompoundCu3(CO3)2(OH)2. *Physical Review Letters*, 94(22), jun 2005.

[8] K. C. Rule, A. U. B. Wolter, S. Süllow, D. A. Tennant, A. Brühl, S. Köhler, B. Wolf, M. Lang, and J. Schreuer. Nature of the spin dynamics and1/3magnetization plateau in azurite. *Physical Review Letters*, 100(11), mar 2008.

[9] G I Japaridze and E Pogosyan. Magnetization plateau in the spin ladder with alternating rung exchange. *Journal of Physics: Condensed Matter*, 18(40):9297–9306, sep 2006.

[10] Harald Jeschke, Ingo Opahle, Hem Kandpal, Roser Valentí, Hena Das, Tanusri Saha-Dasgupta, Oleg Janson, Helge Rosner, Andreas Brühl, Bernd Wolf, Michael Lang, Johannes Richter, Shijie Hu, Xiaoqun Wang, Robert Peters, Thomas Pruschke, and Andreas Honecker. Multistep approach to microscopic models for frustrated quantum magnets: The case of the natural mineral azurite. *Physical Review Letters*, 106(21), may 2011.

[11] Hamid Arian Zad and Nerses Ananikian. Phase transitions and thermal entanglement of the distorted ising–heisenberg spin chain: topology of multiple-spin exchange interactions in spin ladders. *Journal of Physics: Condensed Matter*, 29(45):455402, oct 2017.

[12] V V Hovhannisyan, J Strečka, and N S Ananikian. Exactly solvable spin-1 ising–heisenberg diamond chain with the second-neighbor interaction between nodal spins. *Journal of Physics: Condensed Matter*, 28(8):085401, feb 2016.

[13] N. Ananikian, H. Lazaryan, and M. Nalbandyan. Magnetic and quantum entanglement properties of the distorted diamond chain model for azurite. *The European Physical Journal B*, 85(7), jun 2012.

[14] T. A. Arakelyan, V. R. Ohanyan, L. N. Ananikyan, N. S. Ananikian, and M. Roger. Multisite-interaction ising model approach to the solid3hesystem on a triangular lattice. *Physical Review B*, 67(2), jan 2003.

[15] V.R. Ohanyan and N.S. Ananikian. Magnetization plateaus in the ferromagnetic–ferromagnetic–antiferromagnetic ising chain. *Physics Letters A*, 307(1):76–84, jan 2003.

[16] Luigi Amico, Rosario Fazio, Andreas Osterloh, and Vlatko Vedral. Entanglement in many-body systems. *Reviews of Modern Physics*, 80(2):517–576, may 2008.

[17] Ryszard Horodecki, Pawel Horodecki, Michal Horodecki, and Karol Horodecki. Quantum entanglement. *Reviews of Modern Physics*, 81(2):865–942, jun 2009.

[18] Subir Sachdev. *Quantum phase transitions*. Cambridge University Press, Cambridge New York, 2011.

[19] E. Schrödinger and M. Born. Discussion of probability relations between separated systems. *Mathematical Proceedings of the Cambridge Philosophical Society*, 31(04):555, oct 1935.

[20] G. I. Japaridze and S. Mahdavifar. Magnetic phase diagram of the dimerized spin s = 1/2 ladder. *The European Physical Journal B*, 68(1):59–66, mar 2009.

[21] D. C. Cabra, G. L. Rossini, A. Ferraz, G. I. Japaridze, and H. Johannesson. Half-metal phases in a quantum wire with modulated spin-orbit interaction. *Physical Review B*, 96(20), nov 2017.

[22] Otfried Gühne and Géza Tóth. Entanglement detection. *Physics Reports*, 474(1-6):1–75, apr 2009.

[23] Artur K. Ekert. Quantum cryptography based on bell's theorem. *Physical Review Letters*, 67(6):661–663, aug 1991.

[24] Charles H. Bennett, Gilles Brassard, Claude Crépeau, Richard Jozsa, Asher Peres, and William K. Wootters. Teleporting an unknown quantum state via dual classical and einstein-podolsky-rosen channels. *Physical Review Letters*, 70(13):1895–1899, mar 1993.

[25] Robert Raussendorf and Hans J. Briegel. A one-way quantum computer. *Physical Review Letters*, 86(22):5188–5191, may 2001.

[26] K. C. Lee, M. R. Sprague, B. J. Sussman, J. Nunn, N. K. Langford, X.-M. Jin, T. Champion, P. Michelberger, K. F. Reim, D. England, D. Jaksch, and I. A. Walmsley. Entangling macroscopic diamonds at room temperature. *Science*, 334(6060):1253–1256, dec 2011.

[27] Dong E. Liu, Shailesh Chandrasekharan, and Harold U. Baranger. Quantum phase transition and emergent symmetry in a quadruple quantum dot system. *Physical Review Letters*, 105(25), dec 2010.

[28] Kenn Kubo and Tsutomu Momoi. Magnetic ground-state phase diagram of a multiple-spin exchange model on the triangular lattice. *Physica B: Condensed Matter*, 329-333:142–143, may 2003.

[29] Per Bak, Chao Tang, and Kurt Wiesenfeld. Self-organized criticality: An explanation of the 1/f noise. *Physical review letters*, 59(4):381, 1987.

[30] N. Ananikian, R. Artuso, and H. Poghosyan. Superstable cycles and magnetization plateaus for antiferromagnetic spin-1 ising and ising–heisenberg models on diamond chains. *Physica A: Statistical Mechanics and its Applications*, 503:892–904, aug 2018.

[31] Nerses Ananikian, Č Burdík, L Ananikyan, and H Poghosyan. Magnetization plateaus and thermal entanglement of spin systems. In *Journal of Physics: Conference Series*, volume 804, page 012002. IOP Publishing, 2017.

[32] Hayk Poghosyan. Super stable cycles and magnetization plateau for spin-1 ising model on diamond-like decorated bethe lattice. *Armenian Journal of Physics*, 10(3):92–98, 2017.

[33] Hayk Poghosyan, Konstantin Savvidy, and George Savvidy. Classical limit theorems and high entropy mixmax random number generator. *Chaotic Modeling and Simulation*, page 7989, 2018.

[34] Hayk Poghosyan and Vahagn Poghosyan. Frontal cellular automata for the study of non-equilibrium lattice models. In *Computer Science and Information Technologies (CSIT), 2015*, pages 44–46. IEEE, 2015.

[35] V V Papoyan and R R Shcherbakov. Abelian sandpile model on the husimi lattice of square plaquettes. *Journal of Physics A: Mathematical and General*, 28(21):6099–6107, nov 1995.

[36] J.G. Brankov, Vl.V. Papoyan, V.S. Poghosyan, and V.B. Priezzhev. The totally asymmetric exclusion process on a ring: Exact relaxation dynamics and associated model of clustering transition. *Physica A: Statistical Mechanics and its Applications*, 368(2):471–480, aug 2006.

[37] Vl. V. PAPOYAN and R. R. SHCHERBAKOV. DISTRIBUTION OF HEIGHTS IN THE ABELIAN SANDPILE MODEL ON THE HUSIMI LATTICE. *Fractals*, 04(01):105–110, mar 1996.

[38] RJ Baxter. Exactly solved models in statistical physics. *Academic, New York*, page 3, 1982.

[39] Kersen Huang. Statistical mechanics, john wily & sons. *New York*, 1963.

[40] L D Landau and E.M. Lifshitz. *Statistical Physics, Third Edition, Part 1: Volume 5 (Course of Theoretical Physics, Volume 5)*. Butterworth-Heinemann, 1980.

[41] Gibbs J Willard. Elementary principles in statistical mechanics. *The Rational Foundation of Thermodynamics, New York, Charles Scribners sons and London, Edward Arnold*, 1902.

[42] John Cardy. *Scaling and renormalization in statistical physics*, volume 5. Cambridge university press, 1996.

[43] R. Peierls and M. Born. On ising's model of ferromagnetism. *Mathematical Proceedings of the Cambridge Philosophical Society*, 32(03):477, oct 1936.

[44] Roger E Mills, Edgar Ascher, and Robert Isaac Jaffee. Critical phenomena in alloys, magnets, and superconductors. *Battelle Institute materials science colloquia*, 1971.

[45] Lars Onsager. Crystal statistics. i. a two-dimensional model with an order-disorder transition. *Physical Review*, 65(3-4):117, 1944.

[46] B McCoy and TT Wu. Two dimensional ising models, harvard u. *Press. Cambridge, Mass*, 1973.

[47] A Brooks Harris. Effect of random defects on the critical behaviour of ising models. *Journal of Physics C: Solid State Physics*, 7(9):1671, 1974.

[48] Cyril Domb. On the theory of cooperative phenomena in crystals. *Advances in Physics*, 9(35):245–361, 1960.

[49] Cyril Domb. *Phase transitions and critical phenomena*, volume 19. Elsevier, 2000.

[50] Bruria Kaufman. Crystal statistics: Ii. partition function evaluated by spinor analysis. iii. short-range order in a binary ising lattice. 1950.

[51] Ernst Ising. Beitrag zur theorie des ferromagnetismus. *Zeitschrift für Physik*, 31(1):253–258, 1925.

[52] Domb Cyril. The critical point, 1996.

[53] Pierre Curie. *Propriétés magnétiques des corps a diverses températures*. Number 4. Gauthier-Villars et fils, 1895.

[54] Pierre Weiss. L'hypothèse du champ moléculaire et la propriété ferromagnétique. *J. Phys. Theor. Appl.*, 6(1):661–690, 1907.

[55] Bruria Kaufman. Crystal statistics. ii. partition function evaluated by spinor analysis. *Physical Review*, 76(8):1232, 1949.

[56] Elliott W Montroll, Renfrey B Potts, and John C Ward. Correlations and spontaneous magnetization of the two-dimensional ising model. *Journal of Mathematical Physics*, 4(2):308–322, 1963.

[57] Tai Tsun Wu. Theory of toeplitz determinants and the spin correlations of the two-dimensional ising model. i. *Physical Review*, 149(1):380, 1966.

[58] Tai Tsun Wu, Barry M McCoy, Craig A Tracy, and Eytan Barouch. Spin-spin correlation functions for the two-dimensional ising model: Exact theory in the scaling region. *Physical Review B*, 13(1):316, 1976.

[59] Hendrik A Kramers and Gregory H Wannier. Statistics of the two-dimensional ferromagnet. part i. *Physical Review*, 60(3):252, 1941.

[60] Paul Ehrenfest. Phase changes in the ordinary and extended sense classified according to the corresponding singularities of the thermodynamic potential. In *Proc Acad Sci Amsterdam*, volume 36, pages 153–157, 1933.

[61] Debra Daugherty. *Elaborating the crystal concept: scientific modeling and ordered states of matter*. The University of Chicago, 2007.

[62] George E Uhlenbeck. Some historical and critical remarks about the theory of phase transitions. *Science of Matter: Festschrift in Honor of Professor Ta-You Wu. Gordon & Breach, New York*, 1978.

[63] D Ruelle. Statistical mechanics, rigorous results, benjamin. *New York, USA*, 1969.

[64] Robert B Griffiths. Peierls proof of spontaneous magnetization in a two-dimensional ising ferromagnet. *Physical Review*, 136(2A):A437, 1964.

[65] JM Luck. A classification of critical phenomena on quasi-crystals and other aperiodic structures. *EPL (Europhysics Letters)*, 24(5):359, 1993.

[66] br¿ JW Essam. Phase transitions and critical phenomena. *Phase Transit. Crit. Phenomena*, 2:1583–1585, 1972.

[67] T. P. Eggarter. Cayley trees, the ising problem, and the thermodynamic limit. *Phys. Rev. B*, 9:2989–2992, Apr 1974.

[68] Michio Kurata, Ryoichi Kikuchi, and Tatsuro Watari. A theory of cooperative phenomena. iii. detailed discussions of the cluster variation method. *The Journal of Chemical Physics*, 21(3):434–448, 1953.

[69] Shigetoshi Katsura and Makoto Takizawa. Bethe lattice and the bethe approximation. *Progress of Theoretical Physics*, 51(1):82–98, 1974.

[70] H. A. Bethe. Statistical theory of superlattices. *Proceedings of the Royal Society A: Mathematical, Physical and Engineering Sciences*, 150(871):552–575, jul 1935.

[71] M. Ostilli. Cayley trees and bethe lattices: A concise analysis for mathematicians and physicists. *Physica A: Statistical Mechanics and its Applications*, 391(12):3417 – 3423, 2012.

[72] Hirotsugu Matsuda. Infinite susceptibility without spontaneous magnetization: Exact properties of the ising model on the cayley tree. *Progress of Theoretical Physics*, 51(4):1053–1063, 1974.

[73] E Müller-Hartmann and J Zittartz. New type of phase transition. *Physical Review Letters*, 33(15):893, 1974.

[74] YK Wang and FY Wu. Multi-component spin model on a cayley tree. *Journal of Physics A: Mathematical and General*, 9(4):593, 1976.

[75] Loïc Turban. s-state potts model on a cayley tree. *Physics Letters A*, 78(4):404–406, 1980.

[76] Dmitry Victorovich Anosov. Geodesic flows on closed riemannian manifolds of negative curvature. *Trudy Matematicheskogo Instituta Imeni VA Steklova*, 90:3–210, 1967.

[77] G.K Savvidy and N.G Ter-Arutyunyan-Savvidy. On the monte carlo simulation of physical systems. *Journal of Computational Physics*, 97(2):566–572, dec 1991.

[78] N.Z Akopov, G.K Savvidy, and N.G Ter-Arutyunyan-Savvidy. Matrix generator of pseudorandom numbers. *Journal of Computational Physics*, 97(2):573–579, dec 1991.

[79] Andrei Nikolaevich Kolmogorov. A new metric invariant of transient dynamical systems and automorphisms in lebesgue spaces. *Dokl. Akad. Nauk SSSR (NS)*, 119(861-864):2, 1958.

[80] Andrei Nikolaevich Kolmogorov. Entropy per unit time as a metric invariant of automorphism. *Dokl. Akad. Nauk SSSR (NS)*, 124(754-755):1, 1959.

[81] Ya Ge Sinai. On the notion of entropy of a dynamical system. *Dokl. Akad. Nauk. SSSR*, 124:768, 1959.

[82] Vladimir Igorevich Arnol'd, Aleksandr Aleksandrovich Kirillov, and Yakov Grigor'evich Sinai. Dynamical systems at the stockholm mathematical congress. *Uspekhi Matematicheskikh Nauk*, 18(2):189–196, 1963.

[83] AL Genis. Metric properties of endomorphisms of an r-dimensional torus. *Dokl. Akad. Nauk SSSR*, 138(5):991–993, 1961.

[84] Vladimir Abramovich Rokhlin. On endomorphisms of compact commutative groups. *Izvestiya Rossiiskoi Akademii Nauk. Seriya Matematicheskaya*, 13(4):329–340, 1949.

[85] Vladimir Abramovich Rokhlin. On the entropy of an automorphism of a compact commutative group. *Theory of Probability & Its Applications*, 6(3):322–323, 1961.

[86] Konstantin G. Savvidy. The MIXMAX random number generator. *Computer Physics Communications*, 196:161–165, nov 2015.

[87] G. G. Athanasiu, E. G. Floratos, and G. K. Savvidy. K-system generator of pseudorandom numbers on galois field. *International Journal of Modern Physics C*, 08(03):555–565, jun 1997.

[88] G. K. Savvidy. Anosov c-systems and random number generators. *Theoretical and Mathematical Physics*, 188(2):1155–1171, aug 2016.

[89] Steven H. Strogatz. *Nonlinear Dynamics and Chaos: With Applications to Physics, Biology, Chemistry, and Engineering (Studies in Nonlinearity)*. Westview Press, 2014.

[90] Steve Smale. *The Mathematics of Time: Essays on Dynamical Systems, Economic Processes, and Related Topics*. Springer-Verlag, 2013.

[91] Onofre Rojas, S. M. de Souza, Vadim Ohanyan, and Martiros Khurshudyan. Exactly solvable mixed-spin ising-heisenberg diamond chain with biquadratic interactions and single-ion anisotropy. *Physical Review B*, 83(9), mar 2011.

[92] N.S. Ananikian, J. Strečka, and V. Hovhannisyan. Magnetization plateaus of an exactly solvable spin-1 ising–heisenberg diamond chain. *Solid State Communications*, 194:48–53, sep 2014.

[93] Roberto F. S. Andrade and Daniel Cason. Ising model with long range correlated disorder on hierarchical lattices. *Physical Review B*, 81(1), jan 2010.

[94] Takatsugu Iharagi, Andrej Gendiar, Hiroshi Ueda, and Tomotoshi Nishino. Phase transition of the ising model on a hyperbolic lattice. *Journal of the Physical Society of Japan*, 79(10):104001, oct 2010.

[95] Lucia Čanová, Jozef Strečka, and Michal Jaščur. Geometric frustration in the class of exactly solvable ising–heisenberg diamond chains. *Journal of Physics: Condensed Matter*, 18(20):4967–4984, may 2006.

[96] M. S. S. Pereira, F. A. B. F. de Moura, and M. L. Lyra. Magnetocaloric effect in kinetically frustrated diamond chains. *Physical Review B*, 79(5), feb 2009.

[97] B. M. Lisnii. Distorted diamond ising-hubbard chain. *Low Temperature Physics*, 37(4):296–304, apr 2011.

[98] H.-J. Mikeska and C. Luckmann. Dynamics of a distorted diamond chain. *Physical Review B*, 77(5), feb 2008.

[99] Lucia Gálisová. Magnetic properties of the spin-1/2 ising-heisenberg diamond chain with the four-spin interaction. *physica status solidi (b)*, 250(1):187–195, sep 2012.

[100] N. S. Ananikian, L. N. Ananikyan, and L. A. Chakhmakhchyan. Cyclic period-3 window in antiferromagnetic potts and ising models on recursive lattices. *JETP Letters*, 94(1):39–43, sep 2011.

[101] Yong Peng, Ulrich H. E. Hansmann, and Nelson A. Alves. Solution effects and the order of the helix–coil transition in polyalanine. *The Journal of Chemical Physics*, 118(5):2374–2380, feb 2003.

[102] Walter Thirring. *A Course in Mathematical Physics 1 and 2*. Springer New York, 1992.

[103] J. P. Eckmann and D. Ruelle. Ergodic theory of chaos and strange attractors. *Reviews of Modern Physics*, 57(3):617–656, jul 1985.

[104] Sanjit Konar, Partha Sarathi Mukherjee, Ennio Zangrando, Francesc Lloret, and Nirmalendu Ray Chaudhuri. A three-dimensional homometallic molecular ferrimagnet. *Angewandte Chemie International Edition*, 41(9):1561–1563, 2002.

[105] V.S. Abgaryan, N.S. Ananikian, L.N. Ananikyan, and V.V. Hovhannisyan. Quantum transitions, magnetization and thermal entanglement of the spin-1 ising–heisenberg diamond chain. *Solid State Communications*, 224:15–20, dec 2015.

[106] Javeed Ahmad Sheikh, Amit Adhikary, Himanshu Sekhar Jena, Soumava Biswas, and Sanjit Konar. High nuclearity (octa-, dodeca-, and pentadecanuclear) metal (m = CoII, NiII) phosphonate cages: Synthesis, structure, and magnetic behavior. *Inorganic Chemistry*, 53(3):1606–1613, feb 2014.

[107] J Kang, C Lee, R K Kremer, and M-H Whangbo. Consequences of the intrachain dimer–monomer spin frustration and the interchain dimer–monomer spin exchange in the diamond-chain compound azurite cu 3 (CO 3) 2 (OH) 2. *Journal of Physics: Condensed Matter*, 21(39):392201, sep 2009.

[108] M. Howard Lee. Analytical study of the superstable 3-cycle in the logistic map. *Journal of Mathematical Physics*, 50(12):122702, dec 2009.

[109] M. Howard Lee. Solving for the fixed points of 3-cycle in the logistic map and toward realizing chaos by the theorems of sharkovskii and li—yorke. *Communications in Theoretical Physics*, 62(4):485–496, oct 2014.

[110] N. Ananikian and V. Hovhannisyan. Magnetic properties, lyapunov exponent and superstability of the spin- ising–heisenberg model on a diamond chain. *Physica A: Statistical Mechanics and its Applications*, 392(10):2375–2383, may 2013.

[111] N.S. Ananikian, S.K. Dallakian, N.Sh. Izmailian, and K.A. Oganessyan. Chaotic repellers in the antiferromagnetic ising model. *Physics Letters A*, 214(3-4):205–210, may 1996.

[112] N. Ananikian, R. Artuso, and L. Chakhmakhchyan. Superstable cycles for antiferromagnetic q-state potts and three-site interaction ising models on recursive lattices. *Communications in Nonlinear Science and Numerical Simulation*, 19(10):3671–3678, oct 2014.

[113] Arkady Pikovsky and Antonio Politi. *Lyapunov Exponents: A Tool to Explore Complex Dynamics*. Cambridge University Press, 2016.

[114] Giancarlo Benettin, Luigi Galgani, Antonio Giorgilli, and Jean-Marie Strelcyn. Lyapunov characteristic exponents for smooth dynamical systems and for hamiltonian systems: A method for computing all of them. part 1: Theory. *Meccanica*, 15(1):9–20, mar 1980.

[115] Giancarlo Benettin, Luigi Galgani, Antonio Giorgilli, and Jean-Marie Strelcyn. Lyapunov characteristic exponents for smooth dynamical systems and for hamiltonian systems: A method for computing all of them. part 2: Numerical application. *Meccanica*, 15(1):21–30, mar 1980.

[116] Bo Gu and Gang Su. Magnetism and thermodynamics of spin-12heisenberg diamond chains in a magnetic field. *Physical Review B*, 75(17), may 2007.

[117] K Takano, K Kubo, and H Sakamoto. Ground states with cluster structures in a frustrated heisenberg chain. *Journal of Physics: Condensed Matter*, 8(35):6405–6411, aug 1996.

[118] Onofre Rojas and S.M. de Souza. Spinless fermion model on diamond chain. *Physics Letters A*, 375(10):1295–1299, mar 2011.

[119] Onofre Rojas, S. M. de Souza, and N. S. Ananikian. Geometrical frustration of an extended hubbard diamond chain in the quasiatomic limit. *Physical Review E*, 85(6), jun 2012.

[120] Mikayel Nalbandyan, Hrachya Lazaryan, Onofre Rojas, Sergio Martins de Souza, and Nerses Ananikian. Magnetic, thermal, and entanglement properties of a distorted ising-hubbard diamond chain. *Journal of the Physical Society of Japan*, 83(7):074001, jul 2014.

[121] J. Torrico, M. Rojas, S. M. de Souza, Onofre Rojas, and N. S. Ananikian. Pairwise thermal entanglement in the ising-XYZ diamond chain structure in an external magnetic field. *EPL (Europhysics Letters)*, 108(5):50007, dec 2014.

[122] N S Ananikian, L N Ananikyan, L A Chakhmakhchyan, and Onofre Rojas. Thermal entanglement of a spin-1/2 ising–heisenberg model on a symmetrical diamond chain. *Journal of Physics: Condensed Matter*, 24(25):256001, may 2012.

[123] L Chakhmakhchyan, N Ananikian, L Ananikyan, and Č Burdík. Thermal entanglement of the spin-1/2 diamond chain. *Journal of Physics: Conference Series*, 343:012022, feb 2012.

[124] V.S. Abgaryan, N.S. Ananikian, L.N. Ananikyan, and V. Hovhannisyan. Entanglement, magnetic and quadrupole moments properties of the mixed spin ising–heisenberg diamond chain. *Solid State Communications*, 203:5–9, feb 2015.

[125] J. Torrico, M. Rojas, S.M. de Souza, and Onofre Rojas. Zero temperature non-plateau magnetization and magnetocaloric effect in an ising-XYZ diamond chain structure. *Physics Letters A*, 380(43):3655–3660, oct 2016.

[126] Jie Qiao and Bin Zhou. Thermal entanglement of the ising–heisenberg diamond chain with dzyaloshinskii–moriya interaction. *Chinese Physics B*, 24(11):110306, nov 2015.

[127] N.S. Ananikian and S.K. Dallakian. Multifractal approach to three-site antiferromagnetic ising model. *Physica D: Nonlinear Phenomena*, 107(1):75–82, aug 1997.

[128] AZ Akheyan and NS Ananikian. Global bethe lattice consideration of the spin-1 ising model. *Journal of Physics A: Mathematical and General*, 29(4):721, 1996.

[129] A.R. Avakian, N.S. Ananikyan, and N.Sh. Izmailyan. A spin-1 model on the bethe lattice. *Physics Letters A*, 150(3-4):163–165, nov 1990.

[130] N. Ananikian, L. Ananikyan, R. Artuso, and H. Lazaryan. Magnetization and lyapunov exponents on a kagome chain with multi-site exchange interaction. *Physics Letters A*, 374(40):4084–4089, sep 2010.

[131] Hrachya Lazaryan, Mikayel Nalbandyan, and Nerses Ananikian. Diamond chain with delocalized interstitial spins: Magnetization, thermal and entanglement properties. *International Journal of Modern Physics B*, 30(22):1650135, sep 2016.

[132] William K. Wootters. Entanglement of formation of an arbitrary state of two qubits. *Physical Review Letters*, 80(10):2245–2248, mar 1998.

[133] G. Vidal and R. F. Werner. Computable measure of entanglement. *Physical Review A*, 65(3), feb 2002.

[134] V.V. Hovhannisyan, N.S. Ananikian, and R. Kenna. Partition function zeros and magnetization plateaus of the spin-1 ising–heisenberg diamond chain. *Physica A: Statistical Mechanics and its Applications*, 453:116–130, jul 2016.

[135] PD Gujrati. Bethe or bethe-like lattice calculations are more reliable than conventional mean-field calculations. *Physical review letters*, 74(5):809, 1995.

[136] N Sh Ananikian, AR Avakian, and N Sh Izmailian. Phase diagrams and tricritical effects in the beg model. *Physica A: Statistical Mechanics and Its Applications*, 172(3):391–404, 1991.

[137] Reginaldo A Zara and Marco Pretti. Exact solution of a rna-like polymer model on the husimi lattice. *The Journal of chemical physics*, 127(18):11B610, 2007.

[138] T.D. Heinz georg schuster, deterministic chaos: An introduction, physik–verlag, weinheim 1986, 220 pages. *Laser and Particle Beams*, 5(01):166, feb 1987.

[139] Evelyn Sander and James A Yorke. A period-doubling cascade precedes chaos for planar maps. *Chaos: An Interdisciplinary Journal of Nonlinear Science*, 23(3):033113, 2013.

[140] Kazuo Hida. Magnetic properties of the spin-1/2 ferromagnetic-ferromagnetic-antiferromagnetic trimerized heisenberg chain. *Journal of the Physical Society of Japan*, 63(6):2359–2364, 1994.

[141] LN Ananikyan. The hexagonal recursive approximation with multisite-interaction ising model for the solid and fluid 3 he system. *International Journal of Modern Physics B*, 21(05):755–772, 2007.

[142] TA Arakelyan, VR Ohanyan, LN Ananikyan, NS Ananikian, and M Roger. Multisite-interaction ising model approach to the solid 3 he system on a triangular lattice. *Physical Review B*, 67(2):024424, 2003.

[143] LN Ananikian. Magnetic properties of 3 he on the recursive lattices. *Journal of Contemporary Physics (Armenian Academy of Sciences)*, 42(1):11–15, 2007.

[144] AS De Wijn, B Hess, and BV Fine. Lyapunov instabilities in lattices of interacting classical spins at infinite temperature. *Journal of Physics A: Mathematical and Theoretical*, 46(25):254012, 2013.

[145] Freddy Christiansen and Hans Henrik Rugh. Computing lyapunov spectra with continuous gram-schmidt orthonormalization. *Nonlinearity*, 10(5):1063, 1997.

[146] Alexander Kolmogoroff. *Grundbegriffe der wahrscheinlichkeitsrechnung*. Springer, 1933.

[147] Aleksandr Khintchine. über einen satz der wahrscheinlichkeitsrechnung. *Fundamenta Mathematicae*, 6(1):9–20, 1924.

[148] A Kolmogoroff. Über das gesetz des iterierten logarithmus. *Mathematische Annalen*, 101(1):126–135, 1929.

[149] Philip Hartman and Aurel Wintner. On the law of the iterated logarithm. *American Journal of Mathematics*, 63(1):169–176, 1941.

[150] B.V. Gnedenko and A. N. Kolmogorov. *Limit Distributions for Sums of Independent Random Variables*. Addison-Wesley, 1954.

[151] Valentin V. Petrov. *Sums of Independent Random Variables*. Springer Berlin Heidelberg, 1975.

[152] Yu. V. Prokhorov and V. Statulevičius, editors. *Limit Theorems of Probability Theory*. Springer Berlin Heidelberg, 2000.

[153] Alexandre Liapounoff. Sur une proposition de la théorie des probabilités. . , 13(4):359–386, 1900.

[154] Alexandre Liapounoff. Nouvelle forme du thorme sur la limite de probabilit. *Mmoires de l'Acadmie impriale des sciences de St. Ptersbourg*, 11, 1901.

[155] Andrew C Berry. The accuracy of the gaussian approximation to the sum of independent variates. *Transactions of the american mathematical society*, 49(1):122–136, 1941.

[156] Carl-Gustaf Esseen. *On the Liapounoff limit of error in the theory of probability*. Almqvist & Wiksell Stockholm, 1942.

[157] Carl-Gustav Esseen. Fourier analysis of distribution functions. a mathematical study of the laplace-gaussian law. *Acta Mathematica*, 77(1):1–125, 1945.

[158] V. V. Petrov. On the strong law of large numbers. *Theory of Probability & Its Applications*, 14(2):183–192, jan 1969.

[159] R Bowen. Equilibrium states and the ergodic theory of anosov diffeomorphisms. *Springer Lecture Notes in Math.*, 470:78–104, 1975.

[160] David Ruelle. *Thermodynamic formalism : the mathematical structures of equilibrium statistical mechanics*. Cambridge University Press, Cambridge, 2004.

[161] NS Krylov, AB Migdal, Ya G Sinai, and Yu L Zeeman. Works on the foundations of statistical physics by nikolai sergeevich krylov. *Works on the Foundations of Statistical Physics by Nikolai Sergeevich Krylov translsated by AB Migdal, Ya. G. Sinai and Yu. L. Zeeman. Princeton Series in Physics. Published by Princeton University Press, Princeton, New Jersey 1979.*, 1979.

[162] Konstantin Savvidy and George Savvidy. Spectrum and entropy of c-systems MIXMAX random number generator. *Chaos, Solitons & Fractals*, 91:33–38, oct 2016.

[163] George Savvidy and Konstantin Savvidy. Hyperbolic Anosov C-systems. Exponential Decay of Correlation Functions. 2017.

[164] VP Leonov. On the central limit theorem for ergodic endomorphisms of compact commutative groups. *Dokl. Akad. Nauk SSSR*, 135(2):258–261, 1960.

[165] N. I. Chernov. Limit theorems and markov approximations for chaotic dynamical systems. *Probability Theory and Related Fields*, 101(3):321–362, sep 1995.

[166] Yu. A. Rozanov. A central limit theorem for additive random functions. *Theory of Probability & Its Applications*, 5(2):221–223, jan 1960.

[167] M. Ratner. The central limit theorem for geodesic flows onn-dimensional manifolds of negative curvature. *Israel Journal of Mathematics*, 16(2):181–197, jun 1973.

[168] VG Gurzadian and GK Savvidy. Collective relaxation of stellar systems. *Astronomy and Astrophysics*, 160:203–210, 1986.

[169] G W Gibbons. The jacobi metric for timelike geodesics in static spacetimes. *Classical and Quantum Gravity*, 33(2):025004, dec 2015.

[170] P Collet, H Epstein, and G Gallavotti. Perturbations of geodesic flows on surface of constant negative curvature and their mixing properties. *Communications in Mathematical Physics*, 95(1):61–112, 1984.

[171] Calvin C Moore. Exponential decay of correlation coefficients for geodesic flows. In *Group representations, ergodic theory, operator algebras, and mathematical physics*, pages 163–181. Springer, 1987.

[172] NI Chernov. Ergodic and statistical properties of piecewise linear hyperbolic automorphisms of the 2-torus. *Journal of statistical physics*, 69(1):111–134, 1992.

[173] L-S Young. Decay of correlations for certain quadratic maps. *Communications in mathematical physics*, 146(1):123–138, 1992.

[174] Slobodan Simic. Lipschitz distributions and anosov flows. *Proceedings of the American Mathematical Society*, 124(6):1869–1877, 1996.

[175] Nikolai I Chernov. Markov approximations and decay of correlations for anosov flows. *Annals of mathematics*, 147(2):269–324, 1998.

[176] Dmitry Dolgopyat. On decay of correlations in anosov flows. *Annals of mathematics*, 147(2):357–390, 1998.

[177] Viviane Baladi and Masato Tsujii. Anisotropic hölder and sobolev spaces for hyperbolic diffeomorphisms. *Annales de l'institut Fourier*, 57(1):127–154, 2007.

[178] MASATO TSUJII. Decay of correlations in suspension semi-flows of angle-multiplying maps. *Ergodic Theory and Dynamical Systems*, 28(01), oct 2007.

[179] Masato Tsujii. Quasi-compactness of transfer operators for contact anosov flows. *Nonlinearity*, 23(7):1495, 2010.

[180] Masato Tsujii. Contact anosov flows and the fourier–bros–iagolnitzer transform. *Ergodic theory and dynamical systems*, 32(6):2083–2118, 2012.

[181] Frédéric Faure and Johannes Sjöstrand. Upper bound on the density of ruelle resonances for anosov flows. *Communications in mathematical physics*, 308(2):325, 2011.

[182] Frédéric Faure, Nicolas Roy, and Johannes Sjöstrand. Semi-classical approach for anosov diffeomorphisms and ruelle resonances. *arXiv preprint arXiv:0802.1780*, 2008.

[183] M Kac. On the distribution of values of sums of the type σ f (2kt). *Annals of Mathematics*, pages 33–49, 1946.

[184] Hepforge.org. `http://mixmax.hepforge.org`. `http://www.inp.demokritos.gr/~savvidy/mixmax.php`.

[185] Root. Release 6.04/06 on 2015-10-13.

[186] Geant/clhep. Release 2.3.1.1 on 2015-11-10.

[187] Pierre L'Ecuyer and Richard Simard. Testu01: Ac library for empirical testing of random number generators. *ACM Transactions on Mathematical Software (TOMS)*, 33(4):22, 2007.

[188] Deepak Dhar. Self-organized critical state of sandpile automaton models. *Physical Review Letters*, 64(14):1613, 1990.

[189] Stéphane Mahieu and Philippe Ruelle. Scaling fields in the two-dimensional abelian sandpile model. *Physical Review E*, 64(6):066130, 2001.

[190] VS Poghosyan, VB Priezzhev, and Philippe Ruelle. Jamming probabilities for a vacancy in the dimer model. *Physical Review E*, 77(4):041130, 2008.

[191] Vyatcheslav B Priezzhev and Philippe Ruelle. Boundary monomers in the dimer model. *Physical Review E*, 77(6):061126, 2008.

[192] Vahagn S Poghosyan, SY Grigorev, Vyatcheslav B Priezzhev, and Philippe Ruelle. Logarithmic two-point correlators in the abelian sandpile model. *Journal of Statistical Mechanics: Theory and Experiment*, 2010(07):P07025, 2010.

[193] Vahagn S Poghosyan and Vyatcheslav B Priezzhev. The problem of predecessors on spanning trees. *Acta Polytechnica*, 51(02), 2011.

[194] P Bak. *How nature works : the science of self-organized criticality*. Copernicus, New York, NY, USA, 1999.

[195] Vyatcheslav B Priezzhev. Structure of two-dimensional sandpile. i. height probabilities. *Journal of statistical physics*, 74(5-6):955–979, 1994.

[196] David Bruce Wilson. Generating random spanning trees more quickly than the cover time. In *Proceedings of the twenty-eighth annual ACM symposium on Theory of computing*, pages 296–303. ACM, 1996.

[197] Gregory F Lawler et al. A self-avoiding random walk. *Duke Mathematical Journal*, 47(3):655–693, 1980.